Michael Koch

Cake filtration modeling – Analytical cake filtration model and filter medium characterization

Michael Koch

Cake filtration modeling
Analytical cake filtration model and filter medium characterization

Thesis for the degree of philosophiae doctor

Trondheim, May 2008

Norwegian University of
Science and Technology

Faculty of Engineering Science and Technology
Department of Energy and Process Engineering

NTNU
Norwegian University of
Science and Technology

Preface

This thesis is submitted in partial fulfillment of the requirements for the degree philosophiae doctor (PhD) at the Norwegian University of Science and Technology, Trondheim.

The work was mainly carried out at the Department of Energy and Process Engineering at the Faculty Engineering Science and Technology with Professor Gernot Krammer as academic advisor.

Sammendrag

Kakefiltrering er brukt til å adskille faste partiklene fra et strømmende fluid. Partiklene avsettes på overflaten av et porøst *filtermedium* mens fluidet passerer gjennom filterporene pga. en trykkdifferanse over filteret. Under filtrasjonen dekkes filtermediet med partikler og en filterkake dannes. Etter hvert overtar kaken funksjonen for å tilbakeholde nye partikler fra filtermediet. Dannelsen av en filterkake er forbundet med en reduksjon av filterets permeabilitet, som fører til en mindre fluidvolumstrøm og/eller et økt trykktap.

Den klassiske filtrasjonsteorien forutsier en lineær økning av tykktapet over tid på homogene filtermedier når kakeoppbygningen foregår ved konstant volumstrøm. Publiserte simulasjoner av strømningen i inhomogene filtre, indikerer ikke lineære trykktapsøkninger ved kakeoppbygning. Litteraturen viser at inhomogene filtermedier har hurtigere trykktapsøkning i begynnelsen av filtreringen enn homogene filtermedier, og at for de inhomogene filtermedier vil trykktapsøkningen flate ut i løpet av filtrasjonen. Sammenligner man filtrasjonen på inhomogene filtermedier med den klaskiske teorien viser det seg at inhomogene filtre har en lavere integrert permeabilitet når den samme partikkelmassen er avskilt i filterkaken.

Filterkaken må fjernes periodisk fra industrielle gassfilter, for å kunne opprettholde semi-kontinuerlig drift. Hvis regenereringen ikke er fullstendig, men filterkaken fjernes bare delvis, vil trykktapsprofilen ligne på profilen til filtrasjon på inhomogene filtermedier. Delvis rensning av filterkaken kan skyldes både utilstrekkelige rensingstiltak og segmentert rensing av filteret. Den ufullstendige regenereringen fører til en filterkakefordeling, såkalte kakegenerasjoner oppstår, og filterarealer som fortsatt bærer kake etter rensingen har en mindre permeabilitet enn kakefrie arealer. Dermed dannes det igjen en såkalt permeabilitetsfordeling (PF). Trykk og hastighets profilene til ufullstendig rensa filter blir modellert med enkle strømningsmodeller (Darcys lov endimensjonal) i litteraturen.

I denne avhandlingen er det utviklet en filtermodell for inkompressible filterkaker, som beskriver sammenhenget mellom trykktapet og fluidvolumenstrømmen. Modellen er basert på Darcys lov i en dimensjon som strømningsmodell og den kan beskrive inhomogene filtermedier gjennom en kontinuerlig PF. PF'en ved begynnelsen av filtrasjonen kan innfatte både bidrag fra et inhomogent filtermedium og en gjenværende kakefordeling. Tidsintegrasjonen av modellen kan løses analytisk.

Modellen har matematisk formen av en generalisert Stieltjes integraltransformasjon og det kan bevises, at en trykktapsprofil for en konstant fluidvolumenstrøm tilsvarer akkurat en bestemt PF. En matematisk metode, *PF-metode*, er utviklet. Metoden inverterer filtermodellen for å identifisere PF'en fra en målt trykktapsprofil i et filter. Inversjonen kan bli utført ved hjelp av en global optimaliseringsalgoritme. Alternativt kan filtermodellen omskrives til et konvolusjonsintegral. Derved blir PF-methoden et dekonvolusjonsproblem, som tillater en vurdering av feilen som påvirker PF'en. Optimaliseringsløsningen er relativt enkelt å omsette og har derfor praktiske fordeler ved å beregne en PF. Dekonvolusjonen brukes for en vurdering av feilen i PF'en.

PF-metode'en er anvendt på eksperimentelle trykktapsforløp i gassfiltre med tekstile filtermedier. PF'er er bestemt for trykktapsdata av filtermedier i testanlegg, laboratorium-posefilteranlegg, pilotanlegg og industrielle anlegg. Selv for filtrasjon på tidligere ubrukte filtermedier finner man det en tydelig PF, dvs. de undersøkte filtermediene er generelt inhomogene. Den kontinuerlige analysen av filtermediene i kondisjoneringsfasen viser gradsvise endringer av den tilsvarende PF'en. Sammenlignet med vanligvis dokumenterte parameter av en filtertest, som f.eks. permeabiliteten for luft ved 200 Pa, gir en PF mer inngående informasjon om trykktapsøkningen.

Den utviklede modellen inneslutter fullstendig alle kjente kakegenerasjonsmodeller, hvis man ser bort fra kakekompresjonseffekter. Kakegenerasjonsmodellene må som regel bestemme en eller flere parameter fra en sammenligning av eksperimentelle og simulerte trykktapskurver. Alle de undersøke filtermedier i denne avhandlingen har en PF selv. Dette er ikke tatt hensyn til i de kjente filtermodellene fra litteraturen og dermed foregår bestemmelsen av parameterne i disser modeller under brutte modellantagelser. Dessuten vises det at feilen ved å bestemme en PF fra trykktapsprofiler er betydelig, slik at ikke mer en det to yngste kakegenerasjoner kan identifiseres. De numeriske egenskapene er universelt overførbar fra PF-metoden på kakegenerasjonsmodeller, fordi den underliggende modellstrukturen er den sammen. Dermed er en parametertilpasning eller en verifikasjon av mekanisktiske antakelser basert på en trykktapssammenlikning en tvilsom framgangsmåte.

PF-metoden krever en klar trykktapsøkning for å kunne bestemme en PF. Filterdriften i industrien foregår typisk semi-kontinuerlig, dvs. filteret renses periodisk og drives i sykluser. I målte trykktapsforløp kan syklusene neppe skjelnes fra hverandre og følgelig er en klar trykktapsøkning ikke tilgjengelig fra målt data. En rutine utvikles, som tar utgangspunktet i en antallfordeling av trykktapsmålinger og genererer en karateristisk filtrasjonssyklus, som kan analyseres ved hjelp av PF-methoden. PF'en bestemmes for et industrielt filter før og etter en bytting av alle filterposer. Siden filteret renses i segmenter er en PF et resultat av kombinasjonen av filtermediet med en gjenværende filterkake. Ikke desto mindre PF'ene er tydelig forskjellige, ikke bare med tanke på deres integral verdi, men også deres form.

Summary

Cake filtration is a unit operation to separate solids from fluids. The solid particles are retained at the surface of a porous *filter medium* whereas the fluid can pass though the pores. In the course of filtration, particles are not only retained by the filter medium itself, but a filter cake builds up. Since the flow is pressure driven, cake formation is accompanied by a reduction of the permeability of the combination filter cake and filter medium. This results in a reducing volume flow and/or an increasing pressure drop over the filter.

Classical filtration theory predicts a linear pressure drop increase for the build up of a cake on a homogeneous filter medium for a constant fluid volume flow. Flow simulation studies in literature show that an initially inhomogeneous filter medium permeability with a correspondingly inhomogeneous flow field entails a non-linear pressure drop increase. The pressure drop rise at the beginning of filtration is steeper than for a homogeneous medium and the pressure drop slope flattens in the course of filtration. For the same amount of solid deposited in the filter cake, this shape of the pressure drop profile leads to lower integral permeability values than one expects from the linear increase predicted by the classical theory.

A similar pressure drop pattern is observed in industrial gas filters, when they are regenerated partially. Filter regeneration is necessary to be able to operate the filtration process without interruption and it is achieved by periodically removing the filter cake from the filter medium. Partial regeneration occurs, when the filter cake is not entirely removed from the filter cloth due to an insufficient cleaning action and/or only partial exposure of the filter medium to the cleaning action. In literature, models accounting for partial regeneration are published, which are typically based upon a rather simple flow model (Darcy's law in one dimension). The result of partial regeneration is a distributed residual filter cake, i.e., several *cake generations* are present. Filter areas carrying older cake generations have a lower permeability than cake free areas. This situation represents an inhomogeneous distribution of the filter permeability.

A novel filter model describing the pressure drop - volume flow relation has been developed for incompressible filter cakes. The model is based on Darcy's law in one dimension to describe the fluid flow and can account for inhomogeneity of the filter with a continuous permeability distribution (PD). This initial PD can comprise both contributions: the filter medium and a residual filter cake distribution. The model can be solved analytically in the time domain.

The model has the form of a generalized Stieltjes integral transform and the relation between a pressure drop vs. time is unambiguously linked to the PD. A mathematical method, termed PD-method, is developed, which inverts the filter model to determine the PD from pressure drop data of the filter. The inversion is practically accomplished by either global optimization or the reformulation into a convolution transformation. The latter is also used to assess the error in the determination of a PD. The optimization approach to determine a PD is comparatively simple to implement. The most practical approach is therefore an optimization to determine the PD and the convolution formulation to estimate the error associated with the determination of the PD.

The PD-method is applied to a series of experimental pressure drop data of gas filters using fabric filter media. Pressure drop data from laboratory scale filter test-rigs, laboratory scale bag filter plants, pilot scale filter plants and industrial scale filter plants are used to determine corresponding PDs. It is shown that even virgin filter media examined in various laboratory scale facilities show a significant PD, i.e., the filter media are generally inhomogeneous. Continuous examination of a filter medium during its conditioning period shows a gradual change in its PD. It is demonstrated that the PD can provide more exhaustive information on the pressure drop performance of the filter medium, than commonly reported parameters such as the integral air permeability at 200 Pa pressure differential.

It is shown that cake generation models are fully covered by the model developed in this work, except for cake compression effects. These models determine one or more parameters from a comparison between experimental and simulated pressure drop curves. Every fabric filter medium investigated exhibits a PD itself. This is not accounted for by any known cake generation model, which all assume a homogeneous filter medium. Hence such parameter estimations are undertaken with violated model assumptions. In addition, the error in the determination of a PD from pressure drop data is significant (typically not more than the two newest cake generations are discernible) and the numerical properties are universal to both the literature cake generation models and the presented model. Hence, it is debatable practice to determine model parameters or even verify mechanistic assumptions from a comparison of simulated and measured pressure drop data.

The PD-method requires an unobscured pressure drop increase to be able to determine a PD. Industrially operating filters are typically operating semi-continuously in cycles, i.e., the filters are cleaned intermittently. In the measured pressure drop patterns the filtration cycles may hardly be discernible and hence a pressure drop increase is not available directly from measured data. A routine is developed based on the estimation of a pressure drop sample number distribution from individual measurements, which establishes a characteristic filter pressure drop cycle suitable as input for the PD-method. PDs are determined for an industrial filter unit before and after the change of filter bags. Since the filter is cleaned only partially the PD results as a combination of the filter cloth with a residual filter cake. Nevertheless, the resulting PDs show a clear difference, not only of the integral permeability, but also of the shape of the PD.

Zusammenfassung

Kuchenfiltration ist eine Möglichkeit zur Abtrennung einer festen von einer fluiden Phase. Die festen Partikel werden an der Oberfläche eines porösen *Filtermediums* zurückgehalten, während das Fluid aufgrund eines aufgeprägten Druckgefälles hindurch tritt. Im Zuge der Filtration wird das Filtermedium zusehends von Partikeln bedeckt, sodass die bereits angelagerten Partikel, der sogenannte *Filterkuchen*, die Funktion der Partikelabscheidung übernehmen. Der Aufbau des Filterkuchens geht mit einer Abnahme der Permeabilität des Filters einher, was einen verringerten Fluidvolumenstrom und/oder einen erhöhten Druckverlust nach sich zieht.

In der klassischen Filtrationstheorie ist während des Kuchenaufbaus für einen konstanten Fluidvolumenstrom ein linearer Druckverlustanstieg über die Zeit zu erwarten. Dir Literatur berichtet von Strömungssimulationen auf einem inhomogenen Filtermedium, die einen nichtlinearen Druckverlustverlauf zur Folge haben. Die Steigung des Druckverlustanstiegs zu Beginn er Filtration ist höher als für ein homogenes Filtermedium und flacht im Laufe der Filtration ab. Im Vergleich zu dem klassischen Fall der Filtration auf einem homogenen Medium ergibt sich hier eine geringere integrale Permeabilität des Filters für die gleiche abgeschiedene Feststoffmasse im Kuchen.

Der Filterkuchen muss von Gasfiltern im industriellen Einsatz periodisch entfernt werden, um einen semikontinuierlichen Betrieb zu ermöglichen. Falls dabei die Regenerierung nicht vollständig ist, sondern nur ein teilweises Abreinigen des Kuchens aufgrund unzulänglicher Abreinigungsmaßnahmen und/oder bewusst segmentierter Abreinigung erfolgt, so wird ein ähnlicher Druckverlustverlauf wie auf inhomogenen Filtermedien beobachtet. In der einschlägigen Literatur findet man Modelle, die unvollständige Abreinigung beschreiben und oftmals auf einem einfachen Strömungsmodell basieren (eindimensionales Darcy-Gesetz). Die unvollständige Regenerierung führt zu einer Verteilung des Restfilterkuchens, so genannte Kuchengenerationen entstehen, und jene Bereiche des Filters, die noch Kuchen tragen, habe eine geringere Permeabilität als kuchenfreie Teile, wodurch wiederum eine Permeabilitätsverteilung (PV) entsteht.

In dieser Arbeit wird ein Filtermodell für inkompressible Filterkuchen entwickelt, das den Zusammenhang zwischen Druckverlust und Fluidvolumenstrom beschreibt. Das Model zieht das Darcy-Gesetz zur Beschreibung der Fluidströmung in einer Dimension heran und kann Inhomogenität im Filtermedium über eine kontinuierliche PV beschrieben. Die PV zu Beginn der Filtration kann sowohl Beiträge eines inhomogenen Filtermediums als auch einer eventuellen Restkuchenverteilung beinhalten. Für die Zeitintegration des Filtermodells wird eine analytische Lösung beschrieben.

Das Modell hat mathematisch die Form der generalisierten Stieltjes Integraltransformation und es kann gezeigt werden, dass ein Druckverlustprofil für einen konstanten Fluidvolumenstrom eindeutig einer bestimmten PV entspricht. Durch Invertierung des Filtermodels wird die so genannte *PV-Methode* erhalten, die die PV aus dem gemessenen Druckverlustverlauf des Filters berechnet. In der Praxis wird diese Invertierung von einem globalen Optimierungsalgorithmus bewerkstelligt. Alternativ kann das Filtermodell in ein Faltungsintegral umge-

schrieben werden, wodurch die PV-Methode als Entfaltungsproblem betrachtet werden kann. Dieser Zugang erlaubt eine Fehlerabschätzung bei der Entfaltung und somit bei der Bestimmung der PV. In der Praxis hat sich die Optimierungsvariante aufgrund ihrer einfachen Umsetzung bewährt und die Entfaltung wird bei Bedarf zur Fehlerabschätzung herangezogen.

Die PV-Methode wird auf experimentelle Druckverlustdaten von Gasfiltern angewandt, die auf Filtertestständen, Laborschlauchfiltern, Pilotfilteranlagen und industriellen Filteranlagen gewonnen werden. Es werden textile Filtermedien untersucht. Selbst zuvor unbestaubte Medien, die in verschieden Laboranlagen untersucht wurden, weisen eine deutliche PV auf, d.h. die untersuchten Filtermedien sind im Allgemeinen inhomogen. Die fortlaufende Untersuchung von Filtermedien während der Konditionierungsphase zeigt eine schrittweise Änderung in der zugehörigen PV. Verglichen mit üblicherweise dokumentierten Parametern ist eine PV bezüglich des Druckverlustverlaufs eines Filtermediums aussagkräftiger.

Wenn man von Kuchenkompressionseffekten absieht, kann gezeigt werden, dass das hier vorgestellte Modell früher entwickelte Kuchengenerationsmodelle vollständig beinhaltet. Diese Modelle ziehen oftmals einen Vergleich zwischen simuliertem und experimentellem Druckverlustverlauf heran, um einen oder mehrere Modellparameter zu bestimmen. In keinem der mir bekannten Generationenmodelle wird ein eventuell inhomogenes Filtertuch berücksichtigt, obwohl alle untersuchten Tücher eine solche Inhomogenität aufweisen und die Parameterbestimmung somit unter Verletzung der Modellannahmen erfolgt. Weiters zeigt sich, dass bei der Bestimmung einer PV von Druckverlustdaten kaum mehr als die zwei jüngsten Kuchengeneration identifizierbar sind, d.h. der Fehler während der Entfaltung beachtlich ist; die numerischen Eigenschaften sind aufgrund der gleichen Modellstruktur universell von der PV-Methode auf die Kuchengenerationenmodelle übertragbar und somit sind die Parameterbestimmung oder gar die Verifikation von mechanistischen Annahmen über den Vergleich mit Druckverlustdaten eine zweifelhafte Vorgehensweise.

Die PV-Methode benötigt einen klaren Druckverlustanstieg um eine PV bestimmen zu können. Industrieller Filterbetrieb erfolgt typischerweise semikontinuierlich in Filterzyklen, d.h. der Filter wird periodisch abgereinigt. Diese Filterzyklen sind in gemessenen Druckverlustprofilen oftmals kaum erkennbar und folglich steht ein klarer Druckverlustanstieg aus gemessen Daten nicht direkt zur Verfügung. Es wird eine Routine entwickelt, die ausgehend von der Schätzung einer Anzahlverteilung der Druckverlustmesswerte einen charakteristischen Filtrationszyklus, der für die Auswertung mittels der PV-Methode geeignet ist, bestimmt. Für Druckverlustmessdaten eines semikontinuierlich arbeitenden Filters werden PVen vor und nach dem Austausch der gesamten Filterschläuche bestimmt. Da der Filter im Betrieb nur teilweise abgereinigt wird, sind die somit erhaltenen PVen ein Resultat der Kombination des Filtertuchs und des Restfilterkuchens. Dennoch weisen die PVen deutliche Unterschiede in sowohl der Lage als auch der Verteilungsform auf.

Contents

Nomenclature

Latin symbols

A	location on the filter, m^2
A	unitary pre-factor for the exponential change of variables, $1 \cdot \mathrm{m}^{-2}$
$\mathrm{A}_{\mathrm{tot}}$	total filter area, m^2
B	Wiener filter function
$\bar{c}_{\mathrm{sol}}$	mean solid concentration in the raw gas, $\mathrm{kg} \cdot \mathrm{m}^{-3}$
$\mathrm{c}_{\mathrm{sol}}$	solid concentration in the raw gas, $\mathrm{kg} \cdot \mathrm{m}^{-3}$
E_k	cumulative amplitude error in Φ', m
E_s	cumulative amplitude error in Φ, m^{-2}
f	cleaning function - patchy cleaning
f	frequency based on σ, $-$
f_k	cut-off frequency of the Wiener filter in the k-domain, m^{-1}
f_s	cut-off frequency of the Wiener filter in the s-domain, m^2
f_σ	cut-off frequency of the Wiener filter in the σ-domain
G	transformed pressure drop function, $\mathrm{m}^{\frac{1}{2}}$
h	convolution kernel function
i	PD discretization running variable
j	index denoting filter segment
j	measurements running variable
k	running variable of nodes in the frequency domain
k	total filter permeability, m
k_0	initial filter permeability, m
k_{c}	filter cake permeability, m
L	filter medium thickness, m
m	PD number of nodes
N	number of nodes
n	number of measurements
n	running variable of nodes in the σ-domain
P	power spectral density, dB
p	number of filter segments
p_{c}	prefactor of the pressure drop transformation, $\mathrm{Pa} \cdot \mathrm{m}$
$q_{\Delta p}$	density of the sample pressure drop number distribution, Pa^{-1}
$\hat{q}_{\Delta p}$	corrected density $q_{\Delta p}$, Pa^{-1}
$Q_{\Delta p}$	cumulative sample pressure drop number distribution, $-$

q_t	density of sample time number distribution, s^{-1}
s	filter state, m^{-2}
s_{cyc}	filter state change per cycle, m^{-2}
t	time, s
$\mathrm{t_c}$	prefactor of the time transformation, $\mathrm{s \cdot m}$
t_{cyc}	(mean) filtration cycle duration, s
u	PD variable, abbreviation for k_0^{-2}, m^{-2}
$\dot{V}$	gas volume flow, $\mathrm{m}^3 \cdot \mathrm{s}^{-1}$
v	filtration velocity, $\mathrm{m \cdot s}^{-1}$
X	Fourier transform of function x in the frequency domain
x	arbitrary function in the σ-domain
x	local coordinate perpendicular to the filter area, m
z	filter cake mass area load, $\mathrm{kg \cdot m}^{-2}$
z_{50}	parameter of the logarithmic normal distribution cake detachment function, $\mathrm{kg \cdot m}^{-2}$

Greek Symbols

α	solid distribution coefficient for a two area model, $-$
α_{m}	mass related specific filter cake resistance, $\mathrm{m \cdot kg}^{-1}$
β	area distribution coefficient for a two area model, $-$
δ	Dirac Delta function
Δp	filter pressure drop, Pa
$\Delta \Phi$	permeability frequency distribution
Δp_{high}	highest recorded pressure drop value, Pa
Δp_{low}	lowest recorded pressure drop value, Pa
$\Delta \tilde{\mathrm{p}}_0$	ordinate offset of Δp asymptote, Pa
ε_k	amplitude error in the density φ', m
ε_s	amplitude error in the density φ, m^{-2}
ε_σ	amplitude error in the transformed density $\tilde{\varphi}$, $\mathrm{m}^{\frac{1}{2}}$
η_{g}	dynamic gas viscosity, $\mathrm{Pa \cdot s}$
γ	asymptotic pressure drop correction factor (solid distribution), $-$
κ	intrinsic permeability, m^2
κ_{s}	initial pressure drop slope multiplier, $-$
μ_r	r^{th} moment of PD, m^r
Φ	cumulative PD function depending on u, $-$
$\varphi'_{\mathrm{cloth}}$	PD density φ' of the filter cloth, m^{-1}
Φ'	cumulative PD function depending on k_0, $-$
φ'	PD density function depending on k_0, m^{-1}
$\tilde{\varphi}$	transformed φ-function, $\mathrm{m}^{\frac{1}{2}}$
φ	PD density function depending on u, m^2
Ψ	cumulative solid distribution function, $-$
ψ	solid distribution density function, $-$
ρ_{c}	filter cake density, $\mathrm{kg \cdot m}^{-3}$
σ	exponentially changed variable s, $-$

σ_{LN}	parameter of the logarithmic normal distribution cake detachment function
Θ_{max}	cumulative number distribution of the pressure drop maxima, $-$
Θ_{min}	cumulative number distribution of the pressure drop minima, $-$
ξ	exponentially changed variable u, $-$
ξ	mass flow correction factor for a solid distribution, $-$
ζ	solid distribution parameter, $-$

Indices

| cycle | referenced to one filter cycle, i.e., from after cleaning to the next pulse |
| noise | noise model |

Acronyms

DFT	Discrete Fourier Transform
FFT	Fast Fourier Transform
PD	Permeability Distribution

Chapter 1

Introduction

1.1 Filtration principles

Filtration is a mechanical separation process used to separate a disperse phase from a continuous fluid phase [1, p. 18-74]. The fluid passes through a porous barrier, termed filter medium, which retains most of the disperse phase. This work is restricted to the filtration of solid particles.

Filtration can be further classified according to the particle deposition mechanism [2]: The separation by the capturing of particles inside the porous filter medium is termed *depth filtration* and the separation at the filter medium's surface is termed *surface filtration*. When particles deposit on to already deposited particles the resulting particle agglomerate is termed *filter cake* and the corresponding filtration mechanism is *cake filtration*. Cake filtration is preceded by surface filtration. This work deals with cake filtration only.

As a consequence of the cake build up filtration is locally, i.e., on a certain filter medium part, an intrinsically discontinuous process, since the cake amount is changing as filtration proceeds. This intrinsic discontinuous element in filtration makes it an especially challenging unit operation to describe. However, intrinsic discontinuous operation must not be confused with filtration equipment that can operate continuously, e.g. rotary drum filters [1, p. 18-96] operate continuously, but the filtration itself is still discontinuous with a cake building up on a localized part of the filter media.

The driving force for filtration is a pressure difference applied to the fluid, that drives the fluid through a possibly present filter cake and the filter medium.

1.2 Fluid mechanics

The flow in a filter can be divided into flow towards to the filter medium and from the filter medium within, e.g. a filter housing. This fluid flow upstream of the filter medium contains particles. The flow regime here is typically governed by momentum, turbulence, and pressure. The pressure drop in this flow region

is for cake filters typically small compared to the flow through the filter cake
and media. The fluid mechanics in the filter are an issue in the design process
of a filter plant but are not looked at in this work.

The fluid mechanics of the flow through a filter are characterized by laminar
flow in pores. The pores in the filter medium and in the filter cake are often
treated as a quasi continuous momentum sink. Since the flow velocities through
the filter are generally low the momentum in the flow is negligible and the flow
is exclusively pressure driven.

1.2.1   One-dimensional flow

The flow regime through the filter cake and filter medium is governed by Darcy's
law, which is given one-dimensionally in its differential form per unit filter area
by equ. (1.1)[1].

$$v = -\frac{\kappa}{\eta}\frac{\mathrm{d}p}{\mathrm{d}x} \tag{1.1}$$

In this equation the superficial flow velocity, i.e., the fluid velocity perpen-
dicular to the filter area is denoted v. On the right hand side stands the pressure
gradient over the local coordinate x perpendicular to the filter area. The pro-
portionality factor is the *intrinsic permeability* κ, which is specific to the porous
medium [4]. The fluid viscosity is denoted η. In the context of filtration Darcy's
law can be applied to both the filter medium and the filter cake with respective
permeability values.

Typically, i.e., because more detailed information is not available, the intrin-
sic permeability is assumed constant for the filter medium. When considering a
filter medium of a certain thickness L one obtains by integration of equ. (1.1)
via separation of variables:

$$v \int_0^L \mathrm{d}x = -\frac{\kappa_{\mathrm{medium}}}{\eta} \int_{P_1}^{P_2} \mathrm{d}p \tag{1.2}$$

$$v = \frac{\kappa_{\mathrm{medium}}}{L\eta}(P_1 - P_2) \tag{1.3}$$

Typically the pressure drop $(P_1 - P_2)$ is abbreviated Δp and the filter medium
permeability k_0 is introduced, which relates to the intrinsic permeability via:

$$k_0 = \frac{\kappa_{\mathrm{medium}}}{L} \tag{1.4}$$

This notation has the advantage that only one variable, i.e., the medium per-
meability k_0, is needed to characterize the filter medium.

Analogously the filter cake can be treated. But not a single filter cake
permeability is defined, since the filter cake is growing over time. Traditionally

---

[1]In the original publication of Henry Darcy only an integral version of this equation is
stated [3].

a specific filter cake resistance value α_m is used [5], which relates to the intrinsic cake permeabiltiy κ_c via:

$$\alpha_m = \frac{1}{\kappa_c \cdot \rho_c} \tag{1.5}$$

This defines the cake resistance based on cake mass with the cake density termed ρ_c. This formulation is used in this work.

Analytical models exist to calculate the (intrinsic) permeability of a porous medium, which are based again on homogenization of the intrinsically inhomogeneous structure to model a representative momentum sink. The best know approach stems from Carman and Kozeny [6] and a number of extensions to this concept are available [5, p.46]. However, the predictive capabilities of these approaches are highly limited, mainly because the idealized conditions underlying these concepts are rarely satisfied. In practical applications one often has to resort to the experimental determination of these parameters.

1.2.2 Higher dimensional flow phenomena

The application of the flow model concept outlined hitherto is straightforward, because of its analyticity and one-dimensionality. Darcy's law equ. (1.1) can be given in the generalized form:

$$\vec{v} = -\frac{\kappa}{\eta}\nabla p \tag{1.6}$$

Thereby flow situations in more than one-dimension can be described. This method is used by Dittler and Kasper [7] to simulate the flow field and filter cake build up in two dimensions for patchily regenerated filters. Thereby, residual filter cake is still present on the filter in discrete patches (see section 1.4), and thus the assumption of strictly one-dimensional flow perpendicular to the filter medium is not necessarily justified.

In a similar manner Dufrêche et al. [8] simulate the cake build up on a nonuniform filter medium. They assume the filter medium to be a highly idealized porous layer. The model geometry considered is an even sieve with regular perforations. Fluid can only pass through the actual perforation. The stream lines are correspondingly deflected upstream of the sieve and are concentrated through the perforation. Cake build up simulations with a Lagrangian-type particle tracking, neglecting any slip between the fluid and particles, yields a preferential cake build up upon or close to the perforation, since particles follow the streamlines. The deposited cake is treated as continuous porous solid with fixed, isotropic flow resistance properties, i.e., a constant intrinsic permeability. Its hydrodynamics can be described by Darcy's law. Subsequently an altered flow field is calculated with a filter cake present, and further cake build up can be simulated. Thus an inhomogeneous filter cake around the perforation evolves. An apparent permeability of the growing filter cake is calculated and for thin cakes the apparent permeability of the inhomogeneous filter cake is significantly lower than the corresponding permeability of a homogeneous cake with the same mean thickness. The apparent permeability approaches the mean

value as cake growth proceeds. This again implies that at a constant flow rate and constant upstream solid concentration, i.e., time-linear mean cake growth, the pressure drop is initially increasing faster, since the pressure drop and the permeability are inversely proportional. Here the inhomogeneity of the filter cake is not exclusively attributed to the pore structure of the medium, but also to the upstream flow. The even model sieve with the combination perforation - impermeable plate is, however, not directly applicable fabric filter media, and [8] rightfully mention their main application in membrane filtration.

1.2.3   Internally inhomogeneous filter cake

The assumption of a constant intrinsic permeability as stated above is certainly not always justified. Experimental findings show that the apparent intrinsic permeability of the filter cake may increase when pressure is applied to the filter cake. This phenomenon is termed cake compression or compaction and it is attributed to a further consolidation of the porous filter cake under the external influence of pressure, thereby reducing its permeability.

Experimentally this effect leads to an increasing pressure drop slope as cake build up proceeds, since a higher pressure drop entails higher stresses on the cake and therefore consolidation of the cake. The effects of cake compression are most pronounced in the field of liquid filtration [2]. Schmidt ([9], [10]) studies cake compression for dust filtration.

Another effect, that leads to an apparent similar effect is depth filtration, which precedes cake build up. Particles reaching a clean filter surface may to some extent penetrate inside the filter media and thereby do not participate in the formation of a filter cake. Hence the filter cake forms more slowly than one would expect given the solid mass reaching the filter and decrease in permeability is not as pronounced [11].

1.3   Filter media

The filter medium and its hydrodynamic properties are partly discussed above. The selection of filter media is a highly complex and empirical process and an overview on this issue for cleanable textile filter media for gas cleaning is given by e.g. [5, chapter 2]. Here only an introduction to some filter medium characterization methods is given, which moreover is restricted to the main type application discussed further in this work: The gas cleaning with cleanable textile filter media.

The fiber material in state of the art filter media can be a polymer, e.g. polyamides or polytetrafluoroethylene, or of mineral origin, such as glass wool. Occasionally metal fibers are used. The actual choice of the fibers depends on the challenges in filter operation, such as temperature and chemical attack. The filter media is made from separate fibers that are processed into a cloth like form as either woven or needle felt. The latter has frequently a supporting scrim, which is actually woven and used as basis to produce the needle felt. Such

a needle felt combins the mechanical strength and air permeability of a woven material, and the good dust separation characteristics of a felt [5]. Generally fabric filter media are inhomogeneous with respect to both, inner structure and surface characteristics.

Characterization of filter media is important to determine the suitability of a medium for a certain application. Moreover the results are used to compare the performance of different filter media for a certain application in terms of pressure drop and solid emissions. A series of industry standards are available which standardize filter media testing procedures.

On the one hand there are methods available that aim towards characterizing the filter media by objective parameters such as air permeability (EN ISO 9237 is reporting gas flow at $20\,\text{mm}$ water gauge pressure difference) or mechanical properties (area weight, thickness, strength in EN 29073) without actually doing filtration tests.

On the other hand test standards exist that are designed to assess the performance of the filter media for filtration as the VDI-guideline 3926 [12]. Thereby an actual sample of the filter cloth is exposed to dust and the pressure drop is recorded over time, eventually the filter is regenerated by a jet pulse. The standards also give guidelines for evaluating the experiments concerning the filtration cycle duration between jet pulses and the pressure drop level. In addition, the clean gas concentration after the filter medium can be measured, which is important for meeting the environmental standards.

Some studies indicate that the filtration characteristics are influenced by the structure of the filter medium. Chen et al. [13] present a detailed experimental study of the pressure drop behavior of three cleanable needle felt filter media when challenged with monodisperse dust. They find a rather fast pressure drop increase after the filtration start, which reduces in the course of filtration. This effect is observed on all filter media with three different particles sizes of 5, 10 and $20\,\mu\text{m}$. The smallest particles, however, show initially a slightly lower slope of the pressure drop increase, which indicates depth filtration. This is feasible, since the smallest particles might be able to advance deeper into the filter media than bigger particles which are retained closer to the surface. The phenomenon of a fast pressure drop increase at the beginning of filtration is ascribed to an initially inhomogeneous particle deposition filling up the pores on the filter media's surface, before a more homogeneous cake build up evolves. For the case of the monodisperse dusts with 10 and $20\mu m$ this phenomenon is discussed using the hypothesis of a two-stage cake build up within and on top of the pores. They observed that stage one, i.e., pore filtering, is finished with the same amount of particles mass irrespective of the particle size. Stage two is homogeneous filter cake build up on the entire filter media area. The experimental findings in [13] suggest an initially inhomogeneous cake build up due to the pore structure, but no quantitative treatment of these findings is given.

1.4   Gas filtration in industry

In this section the main application referred to in this work is presented: Dust removal from industrial gas streams in bag filters. This unit operation is described in detail by Löffler et al. [5]; here only a brief overview of the most commonly applied operation principle is given. Cylindrical filter bags are pervaded by the process gas, whereby the dust is retained on the filter bag's surface. The filter bags are pervaded by the gas from the outside and are mounted on wire cages to prevent them from collapsing. Inside the filter bag the clean gas moves towards the clean gas chamber where it is collected.

The filter bags are typically cleanable. The dust cake removal by e.g. reverse jet pulses is described in detail by e.g. [14] and [15]. The movement of the filter bag and the reverse flow against the filtration flow direction liberate the filter cake from the bag. The torn-off filter cake settles and is collected in a dust hopper at the bottom of the filter. A basic filtration plant is displayed in the flowchart Figure 1.1. The induced draft fan is used to overcome the flow
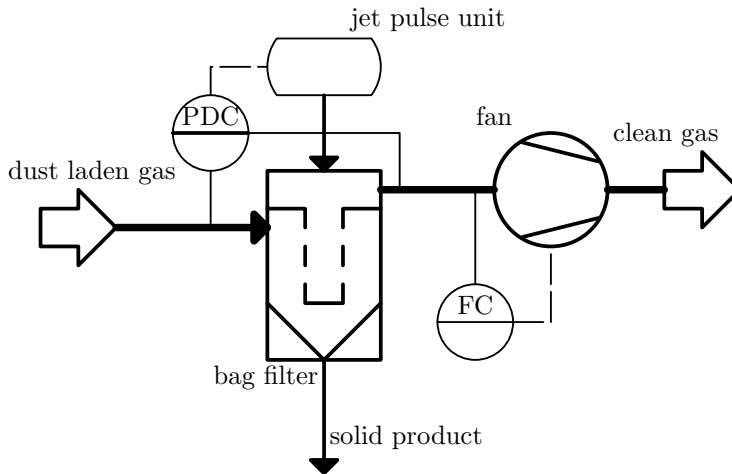
Figure 1.1: Basic flowchart of a bag filter plant with crucial control circuits and measurements.

resistance of the filter. During filtration this resistance is increasing which either leads to a decreased volume flow while the pressure drop over the filter remains constant or the flow is kept constant while the pressure drop rises. Eventually the filter is cleaned after a certain time interval and/or at a certain pressure drop level. Löffler et al. [5] provide a basic overview about the possible cleaning modes.

Filter cleaning is not necessarily complete, i.e., residual dust cake is left on parts of the filter. Incomplete regneration can be intended by cleaning only a part of a filter that is divided into compartment, which can be cleaned separately. Insufficient regneration as described by [16] leaves parts of the filter cake, termed

patches, unchanged on the filter medium, although these patches were exposed to some cleaning action. Thereby a spatially distributed cake arises.

This incomplete regneration mechanism is the basis of several filter modeling studies that make use of mechanistic assumptions to describe the pressure drop - flow relation in cleanable filters ([17], [18], [19], [20]). These models use one-dimensional Darcy equations which are solved numerically to describe the pressure drop vs. volume flow through the filter media and filter cake. The filter medium and cake are considered as a uniform flow resistances, respectively. After cleaning cake patches cover some parts of the filter area, while other parts are not carrying any cake. Hence, the permeabilty over the filter in the cake-free areas is higher and filtration will take place preferentially in these areas. Thereby the initially distributed cake will be evened out towards a homogeneous cake coverage. Typically, experimental pressure drop data is used to fit model parameters, which describe the cake regeneration efficiency. These models focus on the filter cake regeneration, the subsequent distribution on filter cake, and the implications on the pressure drop - volume flow relation of the filter. They, however, do not consider any inhomogeneity in the filter medium itself.

1.5 Scope

Attempts at filter modelling take their starting point in Darcy's law as the governing equation of fluid mechanics. On the one hand studies employing a one-dimensional approach were conducted for the simulation of industrial filter operation assuming a discrete distribution of residual filter cake. On the other hand simulations of the cake build up in two (or more) dimensions were carried out to study the influence of the flow field on cake build up. In the latter studies the inhomogeneity considered is caused by either a distributed residual cake [7] or an inhomogeneous filter medium [8].

An experimental study [13] of fabric filter media's structure suggests local inhomogeneities, which must be attributed to the pore structure of the media. The effect of any inhomogeneity of the filter at the beginning on the pressure drop curve is similar, i.e., the initial decrease in the integral permeability is relatively fast compared to the cake mass increase. This is found by both, experimental and theoretical studies.

In this work a filter model describing the pressure drop - volume flow relation is developed, which can account for inhomogeneity of the permeability in the filter medium. The inhomogeneity is described by a continuous distribution of the initial permeability of the filter medium, which may also include contributions of residual filter cake. It is shown that pressure drop - volume flow relations and the distribution of filter permeability are unambiguously linked. It is demonstrated that a permeability distribution can be quantitatively extracted from filter pressure drop data for constant flow filtration.

A convolution transformation formulation of the filter model is developed and used to estimate the error for the determination of a permeability distribu-

tion. The developed method is applied to various experimental pressure drop data from cleanable gas filters with fabric filter media.

The application of the developed filter model to the simulation of industrial filter operation is discussed. A specialized routine is developed to be able to apply the developed method to semi-continuously operating filter plants.

In a separate chapter a simulation study on the assumption of a solid concentration distribution upstream the filter media is presented. Typically a constant solid distribution is used as model assumption. This section shows the influence of the violation of this seldom questioned assumption.

Chapter 2

Cake filter model

2.1 Model structure and assumptions

A cake filter model is developed for filter media with a distributed permeability. Starting from an illustration of the cake filtration on an inhomogeneous filter media, the required mathematical framework is derived. Hereafter *homogeneous* refers to a property that is independent of the location on the filter, whereas *inhomogeneous* can vary with filter location.

In Fig. 2.1 the plain filter media is displayed schematically. The filter media is illustrated by vertical lines depicting pores penetrating the filter media vertically. The pore size varies and thereby symbolizes the local permeability of the filter media, i.e., small pores (dense lines) have a higher flow resistance, than the wider pores. The filter model assumes Darcy flow [3] through the filter media and thus the relation of flow velocity and pressure drop is linear:

$$v(t = 0, A) = k_0(A)\frac{\Delta p(t)}{\eta_\mathrm{g}} \tag{2.1}$$

Equ. (2.1) is the proportional relation between the pressure drop and the flow velocity across the filter media. It is given at time $t = 0$, which henceforth refers to the beginning of filtration. The proportionality factor is the ratio of the permeability k_0 of the filter media and the dynamic gas viscosity η_g. The velocity profile in Fig. 2.1 illustrates the effect of the inhomogeneous permeability of the filter media: At locations with a lower permeability also the flow velocity is lower, and according to equ. (2.1) this is a directly proportional relation. The depicted flow velocity is taken directly after or even within the filter cloth. Downstream of the filter viscosity effects will equalize the velocity profile rapidly. The superficial flow, i.e., the flow velocities in or through filter media, encountered in filtration is perpendicular to the filter medium.

It must be noted that, although one-dimensional cake build up is assumed, flow is not restricted to be perfectly perpendicular to the filter medium, rather than the cake build up is sufficiently well described one-dimensionally along the
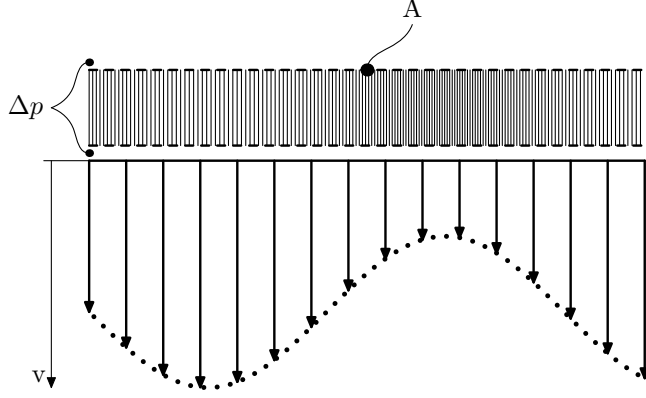
Figure 2.1: Scheme of a cross section of a filter medium with inhomogeneous permeability and the corresponding flow field.

streamlines. Filtration takes place when the fluid upstream contains particles. The particles are retained by the filter media. During cake filtration the particles deposit onto the filter media and subsequently onto already deposited particles, thereby forming a filter cake. In Fig. 2.2 the idealized cake formation is depicted. A filter cake is formed on the filter media. Since the flow field for the filter media is inhomogeneous due to a distributed permeability, also cake formation is hereby affected. Cake forms faster in areas with an initially high flow velocity, since more particles are deposited on these areas. This is reflected by the filter cake thickness in Fig. 2.2, which is higher at areas with a higher permeability of the filter medium and thus a higher initial flow velocity. However, the filter cake itself represents a flow resistance, too. Under the assumption of an *internally homogeneous* cake, i.e., a cake that has a constant specific flow resistance at a Darcy scale (cf. [8]), the flow resistance is proportional to the filter cake thickness. Mathematically this fact can be captured by equ. (2.2). Here the left hand side (LHS) is the reciprocal value of the filter cake permeability, i.e., the filter cake resistance. On right hand side (RHS) stands the solid area load, which under the assumption of an internally homogeneous cake corresponds to a certain cake thickness. The proportionality factor is the specific cake resistance α_{m}.

$$\frac{1}{k_{\mathrm{c}}(t, A)} = \alpha_{\mathrm{m}} \cdot z(t, A) \tag{2.2}$$

When a filter cake is present, the fluid flow is determined by the combined flow resistances of filter medium and filter cake. The flow resistances of filter medium $k^{-1}(A)$ and filter cake $k_{\mathrm{c}}^{-1}(t, A)$ are in series and thus add linearly:

$$\frac{1}{k(t, A)} = \frac{1}{k_{\mathrm{c}}(t, A)} + \frac{1}{k_0(A)} \tag{2.3}$$
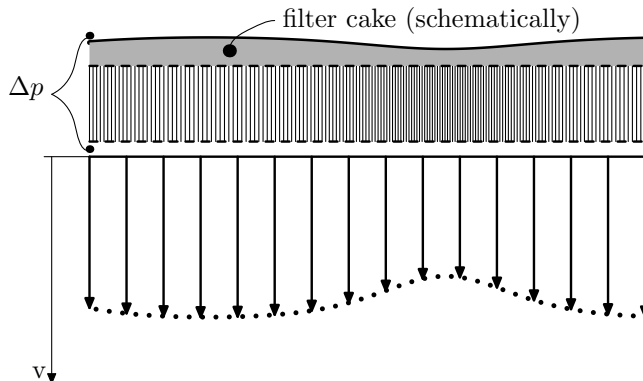
Figure 2.2: Scheme of a cross section of a filter medium carrying filter cake. The correspondingly altered flow field is also displayed.

When cake is present the fluid flow is determined by a linear relation similar to equ. (2.1), but with the combined permeability k instead of just k_0:

$$v(t, A) = k(t, A) \frac{\Delta p(t)}{\eta_\mathrm{g}} \qquad (2.4)$$

The permeability depends on both, the location on the filter A, and the filtration time t. The latter dependency is describing the evolution of the permeability as cake build up proceeds. The mechanistic cake build up is described by solid continuity. In cake filters almost the entire amount of dust, which is transported to the filter, is retained on the filter and thereby forming a cake. Here it is assumed that the upstream solid concentration is constant and thereby the filter cake mass balance reads:

$$\frac{\mathrm{d}z(t, A)}{\mathrm{d}t} = c_\mathrm{sol} \cdot v(t, A) \qquad (2.5)$$

From equ. (2.5) the direct proportionality between cake build up flow velocity can be seen.

The filter cake depicted in Fig. 2.2 causes, as stated, additional flow resistance. To overcome that increased resistance and keep the total volume flow constant (constant flow filtration) the pressure drop augments. In classical filtration theory a homogeneous filter medium and a homogeneous filter cake build up give a linear pressure drop increase [5]. However, if the filter medium is inhomogeneous but an internally homogeneous cake builds up the pressure drop increases non-linearly and always concave. Of course, if the filter medium is homogeneous but the cake builds up inhomogeneously the pressure drop may also increase non-linearly. Such a case is e.g. described in chapter 7.

2.2   Mathematical model development

In this section a mathematical pressure drop model is developed for a filter that leads to a characteristic function of the permeability of the filter media. This pressure drop model is solely based on the equations that comprise of the cake filter model (chapter 2.1) and the respective assumptions.

The time derivative of equ. (2.2) is

$$\frac{\mathrm{d}\frac{1}{k_c(t,A)}}{\mathrm{d}t} = \alpha_\mathrm{m} \cdot \frac{\mathrm{d}z(t,A)}{\mathrm{d}t} \tag{2.6}$$

and the time derivative of equ. (2.3) is:

$$\frac{\mathrm{d}\frac{1}{k(t,A)}}{\mathrm{d}t} = \frac{\mathrm{d}\frac{1}{k_c(t,A)}}{\mathrm{d}t} \tag{2.7}$$

Expressing the solid area load term in equ. (2.6) by equ. (2.5) and subsequently by using equ. (2.7) gives:

$$\frac{\mathrm{d}\frac{1}{k(t,A)}}{\mathrm{d}t} = \alpha_\mathrm{m} \cdot c_\mathrm{sol} \cdot v(t,A) \tag{2.8}$$

Here the filtration velocity $v(t,A)$ can be expressed by equ. (2.4) which reads:

$$\frac{\mathrm{d}\frac{1}{k(t,A)}}{\mathrm{d}t} = \frac{\alpha_\mathrm{m} \cdot c_\mathrm{sol}}{\eta_\mathrm{g}} \cdot k(t,A) \cdot \Delta p(t) \tag{2.9}$$

In this equation the permeability and the pressure drop are time dependent. However, equ. (2.8) can be rearranged by separating variables. Thereby evaluating the derivative on the LHS of equ. (2.9) gives:

$$-\frac{\mathrm{d}k(t,A)}{k^3(t,A)} = \frac{\alpha_\mathrm{m} \cdot c_\mathrm{sol}}{\eta_\mathrm{g}} \cdot \Delta p(t) \cdot \mathrm{d}t \tag{2.10}$$

Equ. (2.10) is a differential equation with separated variables $k(t,A)$ and t, respectively. Integrating from time zero to t on the RHS and the corresponding permeabilities on the LHS gives:

$$\frac{1}{k^2(t,A)} - \frac{1}{k_0^2(A)} = 2 \cdot \frac{\alpha_\mathrm{m} \cdot c_\mathrm{sol}}{\eta_\mathrm{g}} \cdot \int_0^t \Delta p(t) \cdot \mathrm{d}t \tag{2.11}$$

Hereby, the relation $k(t=0,A) \equiv k_0(A)$ is used, reflecting that at time $t=0$ the permeability relates only to the filter medium's permeability (cf. equ. (2.1)). In equ. (2.11) the RHS is only time dependent, i.e., it does not show any dependency of the filter area. That implies that the evolution of the permeability with the distributed initial value $k_0(A)$ is related by only one scalar value which shall be abbreviated $s(t)$, hence termed filter state.

$$s(t) \equiv 2 \cdot \frac{\alpha_\mathrm{m} \cdot c_\mathrm{sol}}{\eta_\mathrm{g}} \cdot \int_0^t \Delta p(t) \cdot \mathrm{d}t \tag{2.12}$$

The physical meaning of equ. (2.11) is that the evolution of the permeability at any location A on the filter is solely determined by the evolution of the pressure drop over time. This is because the build up of the filter cake is the reason for a changing permeability which in turn is merely determined by the filtration velocity and thus the pressure difference over the filter.

Equs. (2.11) and (2.12) lead to an additive relation that describes the permeability by two contributors, the initial permeability $k_0^{-2}(A)$ only depending on the filter location and the filter state $s(t)$ only depending on time. Thus a separation of variables is accomplished in the integrated form, too.

$$k^{-2}(t, A) - k_0^{-2}(A) = s(t) \tag{2.13}$$

In other words the flow situation of the unloaded filter media (Fig. 2.1) depends only upon the spatial domain. Based on that, the subsequent filter cake build up is only determined by the scalar filter state $s(t)$, which is only time dependent.

Hitherto the filter is looked at a scale resolving the inhomogeneities on the filter location A. However, to describe a filter by a pressure drop model the entire filter must be considered. By integrating over all filter locations A, i.e. the entire filter area A_{tot}, in equ. (2.4) one obtains:

$$\int_{A=0}^{A_{\text{tot}}} v(t, A)\mathrm{d}A = \frac{\Delta p(t)}{\eta_{\text{g}}} \int_{A=0}^{A_{\text{tot}}} k(t, A)\mathrm{d}A \tag{2.14}$$

The LHS represents the volume flow through the entire filter $\dot{V}(t)$. Rearranging equ. (2.14) and expressing the permeability by equ. (2.13) yields:

$$\frac{\eta_{\text{g}} \cdot \dot{V}(t)}{\Delta p(t)} = \int_{A=0}^{A_{\text{tot}}} \left[k_0^{-2}(A) + s(t)\right]^{-\frac{1}{2}} \mathrm{d}A \tag{2.15}$$

Equ. (2.15) represents a direct relation between the time dependent pressure drop $\Delta p(t)$ and volume flow $\dot{V}(t)$ on the LHS and the initial permeability function $k_0(A)$ on the RHS. For simplifying the representation of this relation slightly and with respect to further mathematical treatment it is advisable to introduce the abbreviation:

$$u \equiv k_0^{-2}(A) \tag{2.16}$$

The filter location A is barely used to identify an area of the filter to its permeability value. The permeability is not resolved locally. Thus the relation between area A and permeability, i.e., k_0 or u, can be inverted, leading to an area distribution function. This distribution function can be introduced in dimensionless form by:

$$\Phi(u) \equiv \frac{A}{A_{\text{tot}}} \tag{2.17}$$

Here A_{tot} is the constant total filter area and $\Phi(u)$ is the cumulative permeability area distribution function. Since u is unambiguously linked to k_0 (equ. (2.16)),

$\Phi(u)$ will be referred to as permeability distribution (PD). The limits of integration of equ. (2.15) are changed accordingly to account for the substitution of the variable of integration by equ. (2.17):

$$\frac{\eta_{\mathrm{g}} \cdot \dot{V}(t)}{A_{\mathrm{tot}} \cdot \Delta p(t)} = \int_{u=0}^{\infty} [u + s(t)]^{-\frac{1}{2}} \, \mathrm{d}\Phi(u) \tag{2.18}$$

The form of equ. (2.18) with a function as variable of integration is called Riemann-Stieltjes integral. In this equation both, the LHS (namely Δp and $\dot{V}$) and s appear depending on time t. It is shown below that the filter state s is treated as a parameter and therefore the explicit time dependency will be omitted:

$$\frac{\eta_{\mathrm{g}} \cdot \dot{V}}{A_{\mathrm{tot}} \cdot \Delta p} = \int_{u=0}^{\infty} (u + s)^{-\frac{1}{2}} \, \mathrm{d}\Phi(u) \tag{2.19}$$

Equ. (2.19) is the mathematical representation of the cake filter model used further on. The LHS only contains integral, measurable filter parameters, while the RHS depends on the PD and the filter state s. The filter state is defined by equ. (2.12).

For the application of the filter model two main cases for filter operation:

- constant pressure
- constant volume flow

are considered, and the respective formulations are derived in the sections below.

2.3   Constant pressure filtration

Filtration with a time-constant overall pressure difference leads to a simple relation of filter state s and time t since equ. (2.12) can be integrated analytically giving a direct proportionality:

$$s = \frac{2 \cdot \alpha_{\mathrm{m}} \cdot c_{\mathrm{sol}} \cdot \Delta p}{\eta_{\mathrm{g}}} \cdot t \tag{2.20}$$

Thus equ. (2.19) made explicit for the volume flow $\dot{V}$ reads:

$$\dot{V} = \frac{A_{\mathrm{tot}} \cdot \Delta p}{\eta_{\mathrm{g}}} \int_{u=0}^{\infty} \left(u + \frac{2 \cdot \alpha_{\mathrm{m}} \cdot c_{\mathrm{sol}} \cdot \Delta p}{\eta_{\mathrm{g}}} \cdot t \right)^{-\frac{1}{2}} \mathrm{d}\Phi(u) \tag{2.21}$$

2.4   Constant flow filtration

The case of a constant volume flow $\dot{V}$ requires a slightly more extensive mathematical treatment, since the filter state is not so readily obtained from integration of equ. (2.12). Instead a parametric model for the relation of pressure drop Δp and time t is developed with filter state s being the parameter.

Two abbreviations of constants are introduced for a simpler model representation:

$$p_c \equiv \frac{\dot{V} \cdot \eta_g}{A_{tot}} \tag{2.22}$$

and

$$t_c \equiv \frac{A_{tot}}{\alpha_m \cdot c_{sol} \cdot \dot{V}} \tag{2.23}$$

The pressure drop is obtained by rearranging equ. (2.19) and using the constant p_c defined:

$$\frac{1}{\Delta p} = \frac{1}{p_c} \cdot \int_{u=0}^{\infty} (u+s)^{-\frac{1}{2}} \, d\Phi(u) \tag{2.24}$$

Equ. (2.24) contains s which depends upon the pressure drop Δp and time t according to the definition by equ. (2.12). Equ. (2.12) shall be manipulated mathematically to explicitly obtain time t as a function of filter state s and the PD $\Phi(u)$.

Rewriting equ. (2.12) by using the abbreviations introduced by equs. (2.22) and (2.23) gives:

$$s = \frac{2}{t_c \cdot p_c} \int_0^t \Delta p \, dt \tag{2.25}$$

Derivation with respect to time yields:

$$\frac{ds}{dt} = \frac{2}{t_c \cdot p_c} \Delta p \tag{2.26}$$

Rearranging equ. (2.26) and expressing the pressure drop Δp by equ. (2.24) yields:

$$\frac{t_c}{2} \int_{u=0}^{\infty} (u+s)^{-\frac{1}{2}} \, d\Phi(u) = \frac{dt}{ds} \tag{2.27}$$

Integration of both sides via s from 0 to s yields:

$$\frac{t_c}{2} \int_{s=0}^{s} \int_{u=0}^{\infty} (u+s)^{-\frac{1}{2}} \, d\Phi(u) ds = \int_{s=0}^{s} \frac{dt}{ds} ds \tag{2.28}$$

Changing the order of integration on the LHS and evaluating the RHS gives:

$$\frac{t_c}{2} \int_{u=0}^{\infty} \int_{s=0}^{s} (u+s)^{-\frac{1}{2}} \, ds \, d\Phi(u) = t \tag{2.29}$$

Evaluating the definite inner integral on the LHS yields:

$$\frac{t_c}{2} \int_{u=0}^{\infty} 2 \left[(u+s)^{\frac{1}{2}} - (u+0)^{\frac{1}{2}} \right] d\Phi(u) = t \tag{2.30}$$

Thus another integral transformation similar to equ. (2.24) is obtained for the time t:

$$t = \mathrm{t_c} \int\limits_{u=0}^{\infty} \left[(u+s)^{\frac{1}{2}} - u^{\frac{1}{2}} \right] \mathrm{d}\Phi(u) \qquad (2.31)$$

Equs. (2.24) and (2.31) together represent a parametric filter model for the constant volume flow case with filter state s being the parameter.

Chapter 3

Properties of the constant flow cake filter model

This chapter discusses selected properties of the filter model for constant flow filtration presented in section 2.4. An overview over the relation of the filter model is given. In addition characteristic values of a PD are reported. For reasons of clarity the two integral transformations used in this section are repeated:

$$\frac{1}{\Delta p} = \frac{1}{\mathrm{p_c}} \cdot \int\limits_{u=0}^{\infty} (u+s)^{-\frac{1}{2}} \, \mathrm{d}\Phi(u) \qquad\qquad [2.24]$$

$$t = \mathrm{t_c} \int\limits_{u=0}^{\infty} \left[(u+s)^{\frac{1}{2}} - u^{\frac{1}{2}} \right] \mathrm{d}\Phi(u) \qquad\qquad [2.31]$$

3.1 Test data

In order to illustrate this cake filter model, an analytically generated PD is used. This PD is generated by the cake generation model from Kavouras and Krammer [20]. The connection between this model and the PD is discussed in depth in section 6.2. For the time being it, however, suffices to simply generate a PD by this very model.

The operation chosen to generate the PD uses a cycle time for cleaning one row at a time of $\mathrm{t_{cycle}} = 300\,\mathrm{s}$ and cleaning function parameters used are $\ln(z_{50}) = -0.15$ and $\sigma_{\mathrm{LN}} = 1.1$[1]. All other filter parameters are taken unaltered from [20]. The quite large σ_{LN} parameter is chosen to obtain a significant PD also in cakes of generation 2 and older. The resulting PD is displayed in

---

[1]The broadness parameter of the cleaning function is originally referred to as barely σ, but in this work the cleaning function broadness is referred to as σ_{LN} to account for the Logarithmic Normal distribution and to avoid confusion with the integral transformation parameter introduced in section 5.2.

Figure 3.1 as the cumulative distribution function Φ' versus the permeability k. This distribution depending upon the permeability is derived from the mathematically introduced distribution $\Phi(u)$ (see appendix A.1 for the conversion between the two). Although $\Phi(u)$ is advantageous for mathematical manipulation $\Phi'(k)$ is usually displayed.
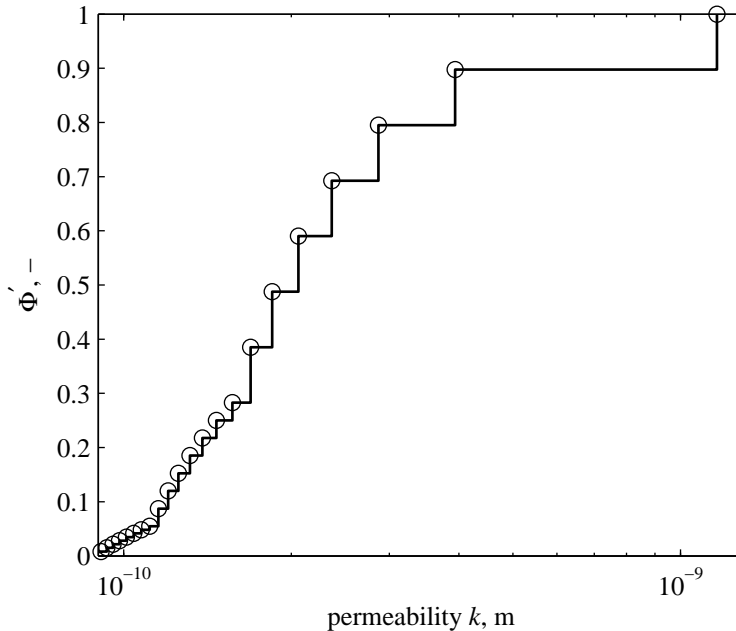
Figure 3.1: PD generated by the cake generation model used for theoretical studies.

In Figure 3.2 the pressure drop curve is displayed resulting from this PD for time t ranging from 0 to 700 s. This time range is used as input data for deconvolution. Although the transient pressure drop evolution is displayed beyond the actual cycle time t_{cycle}, the cycle time is used for the PD generation. The displayed Δp curve over 700 s corresponds to continued filtration without cleaning after a stable periodic operation was established.

From the pressure drop curve over time one can directly calculate the values of filter state s over time via integration of equ. (2.25), left aside the knowledge of a PD. In Fig. 3.2 the shaded area under the pressure drop curve is displayed to illustrate the filter state s at a time $t = t_{\mathrm{cycle}}$, which is proportional to that area according to equ. (2.25). Alternatively s can be obtained from a known PD directly using equ. (2.31).
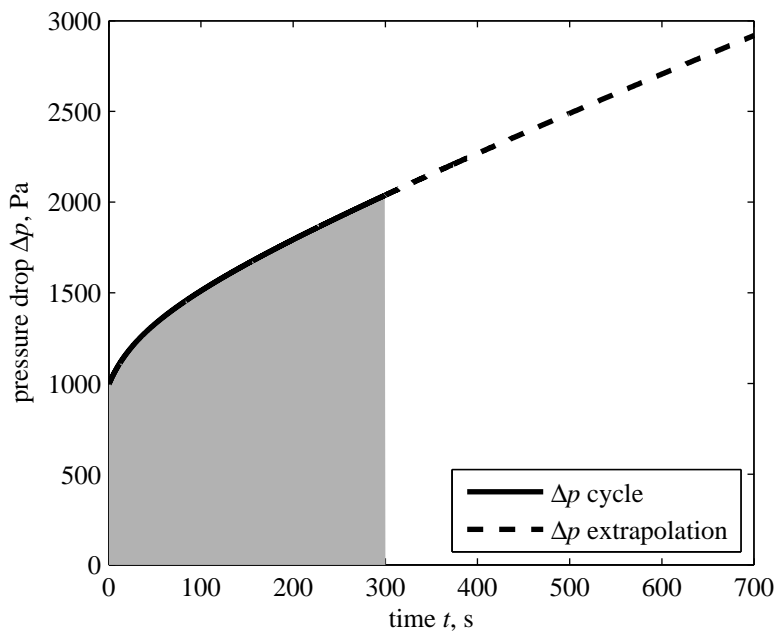
Figure 3.2: Pressure drop curve generated by the cake generation model. The solid line is the pressure drop during semi-continuous operation and the dashed line is the extrapolation to 700 s. The shaded area corresponds to the filter state s.

3.2   Pressure drop characteristic of a PD

In Fig. 3.3 a pressure drop increase over time is displayed, which has the typical curvature for a filtration on an inhomogeneous cloth. Together with the bold pressure drop curve the asymptote for $t \to \infty$ is displayed as a dashed line. For long filtration time, any initial PD is leveled out and the slope of the pressure drop curve is equal to the slope of a homogeneous filter $\frac{p_c}{t_c}$. The ordinate offset is termed $\Delta\tilde{p}_0$ and can be seen as a hypothetical initial pressure drop of a homogeneous filter that is having the asymptote as its pressure drop curve. When the actual inhomogeneous filter is operated until the linear part of the curve is nearly (i.e. asymptotically) reached, it will give the same performance in terms of cycle time, pressure drop at cleaning as this homogeneous reference filter.

Moreover the initial tangent at $t = 0$ to the Δp-curve is shown. The ordinate offset here is the initial pressure drop value of the filter Δp_0. For an inhomogeneous filter medium the slope of the initial tangent is always higher than the asymptotic slope. This increase is captured by a factor κ_s.

These four characteristic values define the two linear functions and thereby reflect the basic shape of the actual Δp-curve, too. Below mathematical derivations are given to calculate the mentioned values directly from a the filter model. It can be shown that only three moments of a PD relate to these characteristic values.

3.2.1   Initial pressure drop

At the beginning of the filtration both time and filter state are zero. The initial pressure drop is thus straightforwardly calculated from equ. (2.24):

$$\frac{1}{\Delta p_0} = \frac{1}{p_c} \cdot \int_{u=0}^{\infty} u^{-\frac{1}{2}} \mathrm{d}\Phi(u) \tag{3.1}$$

and thus

$$\Delta p_0 = p_c \cdot \frac{1}{\displaystyle\int_{u=0}^{\infty} u^{-\frac{1}{2}} \mathrm{d}\Phi(u)} \tag{3.2}$$

In equ. (3.2) the value Δp_0 only depends upon the parameter p_c and the PD. By introducing the notation of moments

$$\mu_r \equiv \int_0^{\infty} u^{-\frac{r}{2}} \mathrm{d}\Phi(u) \tag{3.3}$$

one obtains:

$$\Delta p_0 = p_c \cdot \mu_1^{-1} \tag{3.4}$$

The scaling of the exponent for the moment in equ. (3.3) is outlined in more detail in appendix A.2.
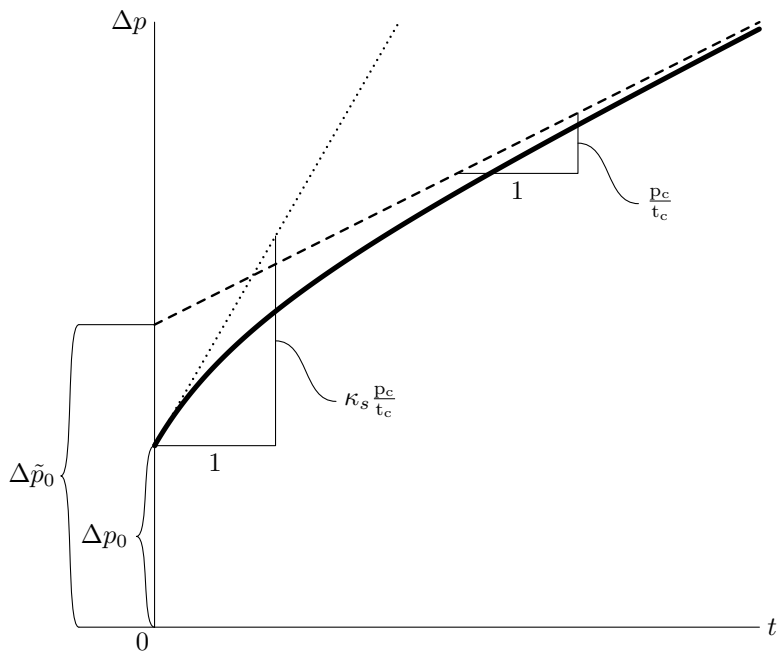
Figure 3.3: Schematic pressure drop increase together with its initial tangent and asymptote

The moment μ_1 is the arithmetic mean of the permeability distribution $\Phi'(k)$. The pressure drop at the beginning of filtration corresponds, of course, to the mean permeability of the filter medium. As such the result is almost trivial. However, for a stringent deduction of the characteristic values from the model equations it is mentioned.

3.2.2   Slope of the pressure drop increase

The pressure drop increase can be calculated via a derivative of Δp over time t. Expressing this derivative via the chain rule one obtains

$$\frac{\mathrm{d}\Delta p}{\mathrm{d}t} = \frac{\mathrm{d}\Delta p}{\mathrm{d}s} \cdot \frac{\mathrm{d}s}{\mathrm{d}t} \tag{3.5}$$

Expanding the first factor and rewriting the second one gives:

$$\frac{\mathrm{d}\Delta p}{\mathrm{d}t} = -\frac{\frac{\mathrm{d}\left(\frac{1}{\Delta p}\right)}{\mathrm{d}s}}{\left(\frac{1}{\Delta p}\right)^2} \cdot \frac{1}{\frac{\mathrm{d}t}{\mathrm{d}s}} \tag{3.6}$$

The pressure drop appearing in the first factor is expressed by equ. (2.24) and the derivative via s is determined. The derivative in the second factor appeared already in equ. (2.27) and the respective result can be used directly.

$$\frac{\mathrm{d}\Delta p}{\mathrm{d}t} = \frac{-p_c \int\limits_0^\infty -\frac{1}{2}(u+s)^{-\frac{3}{2}} \, \mathrm{d}\Phi(u)}{\left[\int\limits_0^\infty (u+s)^{-\frac{1}{2}} \, \mathrm{d}\Phi(u)\right]^2} \cdot \frac{2}{t_c \int\limits_0^\infty (u+s)^{-\frac{1}{2}} \, \mathrm{d}\Phi(u)} \tag{3.7}$$

Simplifying this result gives:

$$\frac{\mathrm{d}\Delta p}{\mathrm{d}t} = \frac{p_c}{t_c} \cdot \frac{\int\limits_0^\infty (u+s)^{-\frac{3}{2}} \, \mathrm{d}\Phi(u)}{\left[\int\limits_0^\infty (u+s)^{-\frac{1}{2}} \, \mathrm{d}\Phi(u)\right]^3} \tag{3.8}$$

To obtain the asymptotic slope of the pressure drop curve, one needs to calculate the limit of equ. (3.8) for filter state s approaching infinity:

$$\lim_{s\to\infty} \frac{\mathrm{d}\Delta p}{\mathrm{d}t} = \frac{p_c}{t_c} \frac{s^{-\frac{3}{2}} \int\limits_0^\infty \mathrm{d}\Phi(u)}{\left[s^{-\frac{1}{2}} \int\limits_0^\infty \mathrm{d}\Phi(u)\right]^3} \tag{3.9}$$

By using the property of a distribution $\int\limits_0^\infty \mathrm{d}\Phi(u) \equiv 1$ this limit evaluates to:

$$\lim_{s\to\infty} \frac{\mathrm{d}\Delta p}{\mathrm{d}t} = \frac{p_c}{t_c} \tag{3.10}$$

It must be emphasized that also this result refers to a trivial situation, because it represents the pressure drop increase of a filter with an equalized permeability profile. Thus the slope is identical to the slope of an homogeneous filter.

The slope of the initial tangent is obtained by evaluating equ. (3.8) at $s = 0$:

$$\left.\frac{\mathrm{d}\Delta p}{\mathrm{d}t}\right|_{s=0} = \frac{p_c}{t_c} \cdot \frac{\int\limits_0^\infty u^{-\frac{3}{2}} \mathrm{d}\Phi(u)}{\left[\int\limits_0^\infty u^{-\frac{1}{2}} \mathrm{d}\Phi(u)\right]^3} \tag{3.11}$$

Thus a multiplying factor depending on moments of the PD is the quotient between equs. (3.9) and (3.11). This factor is a measure for the augmented pressure drop increase at the beginning of filtration due to an inhomogeneous PD.

$$\kappa_s = \frac{\int\limits_0^\infty u^{-\frac{3}{2}} \mathrm{d}\Phi(u)}{\left[\int\limits_0^\infty u^{-\frac{1}{2}} \mathrm{d}\Phi(u)\right]^3} \tag{3.12}$$

Using again the notation of moments introduced by equ. (3.3) one can rewrite equ. (3.12) as:

$$\kappa_s = \frac{\mu_3}{\mu_1^3} \tag{3.13}$$

3.2.3 Asymptote of the pressure drop curve

The slope of that asymptote is equal to the slope of a completely homogeneous filter and given by equ. (3.9). A more interesting feature of this asymptote is the ordinate offset $\Delta\tilde{p}_0$, i.e. the pressure drop value at which the asymptote intersects the ordinate axis.

The asymptote of $\Delta p(t)$-curve is given by equ. (3.14).

$$\Delta p = \frac{p_c}{t_c} \cdot t + \Delta\tilde{p}_0 \tag{3.14}$$

The parameter $\Delta\tilde{p}_0$ can be calculated from equ. (3.15):

$$\Delta\tilde{p}_0 = \lim_{t\to\infty} \left(\Delta p - \frac{p_c}{t_c} \cdot t\right) \tag{3.15}$$

Since a closed form expression for Δp depending on time t is not available, the limit variable is changed to a limit for $s \to \infty$. Here the pressure drop Δp can be expressed by equ. (2.24) while the time t is given by equ. (2.31). The resulting limit reads:

$$\frac{\Delta\tilde{p}_0}{p_c} = \lim_{s\to\infty} \left\{ \frac{1}{\int\limits_0^\infty (s+u)^{-\frac{1}{2}} \mathrm{d}\Phi(u)} - \frac{1}{t_c} \int\limits_0^\infty \left[(s+u)^{\frac{1}{2}} - u^{\frac{1}{2}}\right] \mathrm{d}\Phi(u) \right\}$$

For the consideration of the orders of magnitude in this limit calculation the orders of magnitude of s and u should be considered.

$$\frac{\Delta\tilde{p}_0}{p_c} = \lim_{s\to\infty} \left[\frac{1}{\int_0^\infty (s+u)^{-\frac{1}{2}}\,d\Phi(u)} - \int_0^\infty \left[(s+u)^{\frac{1}{2}} - u^{\frac{1}{2}} \right] d\Phi(u) \right]$$

Filter state s is going towards infinity, whereas u remains limited, since the PD's contribution to the integral is only significant when the cumulative distribution function $\Phi(u)$ is actually changing. Hence the comparison of orders of magnitude $s \gg u$ applies to the inner parentheses. Thus the first integral is reduced to $s^{\frac{1}{2}}$ while the second integral can be separated into contributions depending on s and u, respectively:

$$\frac{\Delta\tilde{p}_0}{p_c} = \lim_{s\to\infty} \left[\frac{1}{s^{-\frac{1}{2}} \cdot 1} - s^{\frac{1}{2}} \cdot 1 + \int_0^\infty u^{\frac{1}{2}}\,d\Phi(u) \right]$$

The result is independent on s and reads:

$$\frac{\Delta\tilde{p}_0}{p_c} = \int_0^\infty u^{\frac{1}{2}}\,d\Phi(u) \tag{3.16}$$

Obviously, also this result can be expressed as a moment equ. (3.3):

$$\frac{\Delta\tilde{p}_0}{p_c} = \mu_{(-1)} \tag{3.17}$$

3.2.4   Relation time t - filter state s

In Fig. 3.4 the relation between filter state s and time t is displayed. The time scale here ranges over an unrealistically wide range, that cannot be measured practically. Interestingly the curve has two finite asymptotes in this double-logarithmic plot.

Closer examination of the slopes on the straight sections reveals, that for small values the slope is equal to one, whereas right of the transition it is equal to two. The linear relation between t and s for small values, i.e. at the left hand side of the bend, and a quadratic relation for big values. From the integral time transformation equ. (2.31) the mathematical basis of these observations can be derived. For small values of s as compared to u one can develop the integral transform into a first order Taylor series for s around zero:

$$t(s \ll u) \approx t(s=0) + \left.\frac{dt}{ds}\right|_{s=0} (s-0) = t_c s \int_0^\infty \frac{1}{2\sqrt{u}}\,d\Phi(u) \tag{3.18}$$

For big values of filter state s compared to u, i.e., $s \gg u$ applies, one obtains an analogous relation directly from equ. (2.31). As an additional simplification $\sqrt{s} \gg \sqrt{u}$ can be applied.

$$t(s \gg u) \approx t_c \int\limits_0^\infty \sqrt{s}\,\mathrm{d}\Phi(u) = t_c \sqrt{s} \underbrace{\int\limits_0^\infty \mathrm{d}\Phi(u)}_{=1} = t_c \sqrt{s} \qquad (3.19)$$

In section 3.2.3 the simplification $\sqrt{s} \gg \sqrt{u}$ cannot be applied, since there the limit transition for $s \to \infty$ is used for an extrapolation back to filter state s zero. The goal there was to calculated the asymptotic pressure drop offset. But allowing $\sqrt{s} \gg \sqrt{u}$ would erroneously give an asymptote through the origin.

The relationships developed here can be used for extrapolation of filter state s from measured points to practically not measurable ones at small and big t values. The results of the analytical expressions equs. (3.18) and (3.19) are displayed in Figure 3.4, too.
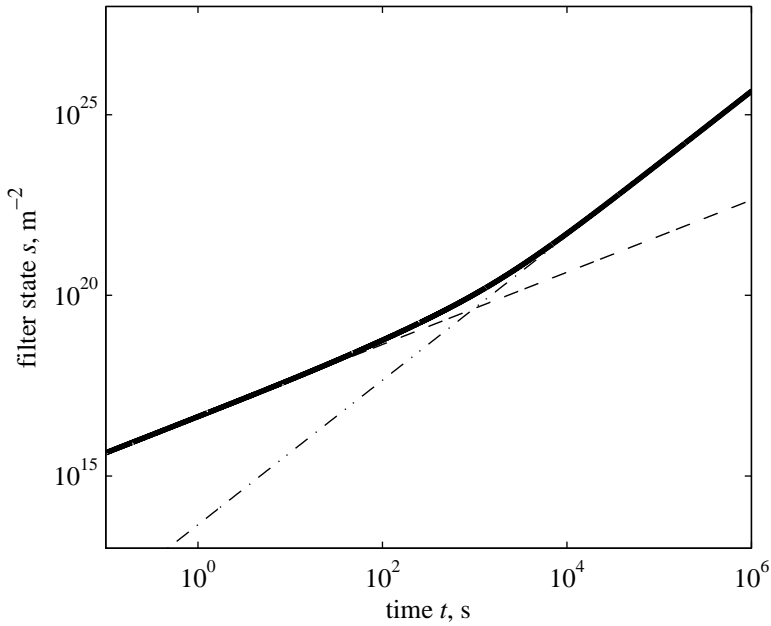
Figure 3.4: Relation between time t and filter state s in a double logarithmic diagram. The asymptotes of the curve are also displayed.

The asymptotical relations can, of course, be related to filter operation via the definition of filter state s equ. (2.12). For small values of t the pressure drop Δp remains virtually constant, since it does not change measurably within a short time, which leads directly to a linear relation after integration. For

big t-values the pressure drop will increase linearly, thus yielding a quadratic relation after integration, which for big t-values is, of course, dominated by the quadratic term (neglecting the linear one).

It must be noted that the resulting equ. (3.18) is practically identical with equ. (2.20) for constant pressure filtration. The difference of these equations is only notation, since in the latter equation the parameters are not abbreviated and the pressure drop is explicitly included, whereas in equ. (3.18) the integral mean of the PD embodies the initial pressure drop value.

Chapter 4

The PD-method

In the chapters 2 and 3 a cake filter model is comprehensively developed and some of its properties are detailed for the case of constant flow filtration. However, this model requires a PD as input.

In this chapter the model is used to determine a PD from operational filter data. In general a pressure drop - volume flow relation must be available as input. However, the method is explicated only for the determination of a PD from filter pressure drop data and a constant volume flow. Moreover it is shown that this relation between a pressure drop curve and a PD is unambiguous and the uncertainty with the determination of the PD is assessed.

The PD-method represents the inversion of the filter model to obtain a PD from a filter pressure drop curve. The model assumptions must, of course, be fulfilled to properly carry out this inversion.

The completeness of the PD-method is based on 2 model properties:

i The relation between time t and filter state s is bijective for a certain pressure drop profile.

ii The integral pressure drop transformation equ. (2.24) is invertible.

The property (i) is required, since the pressure drop relation is only available as a function of filter state s, whereas the pressure drop is measured depending on time t. A bijective assignment between t and s ensures that the pressure drop curve can be unambiguously transformed into a corresponding function depending upon filter state s. From equ. (2.12) one easily finds (i) verified, since the integrand Δp is always positive and thus the relation between t and s is strictly monotonic. In addition the relation $t - s$ relation is obviously continuous for a continuous $\Delta p(t)$ and thus the $t - s$ relation is bijective.

The inversion of equ. (2.24) is subsequently used to determine the actual PD from the LHS via an inversion of the integral transformation. The type of this integral transformation is known in mathematics and termed generalized Stieltjes transform (not to be confused with the notation as Riemann-Stieltjes integral). Hirschman and Widder [21, p. 78 f.] tackle that very transformation

and outline a theory for its inversion based on uniqueness. The inversion formula given is highly abstract and makes use of high order derivatives, that cannot be accurately supplied by experimental data. However, the integral transformation equ. (2.24) is uniquely invertible in theory[1] thereby constituting property (ii).

Of course the combination of (i) and (ii) also establishes a bijective $t - s$ relation being derived from equ. (2.31). A certain pressure drop profile gives both, a unique $t-s$ relation and subsequently an unambiguous PD. In equ. (2.31) a PD is used to calculate t from s, but explicitly no statement on the invertibility of equ. (2.31) is made.

4.1   Optimization approaches

Practically optimization methods can be used to determine a PD from pressure drop data. Such pressure drop data is typically availably as discrete measurements over time. The measurement couples should be identified as $\Delta p_{j,\mathrm{exp}}$ and t_j with n measurement points. In a first step the time values t_j is converted to filter state s_j via numerical integration of equ. (2.12), whereas the experimental pressure drop is used in the integrand.

The PD is discretized into u_i and Φ_i values. A discretization of the PD on $m = 30$ nodes proves pratically suitable, when considering the trade off of computational time versus achievable resolution (see section 5.3.6 for attainable resolution). A simulated pressure drop value Δp_j for a certain filter state s_j is computed from equ. (2.24) again via numerical integration by the rectangle rule.

$$\frac{\mathrm{p_c}}{\Delta p_j} = \sum_{i=1}^{m} (s_j + u_i)^{-\frac{1}{2}} \, \Delta\Phi_i \tag{4.1}$$

Note that the equation was also multiplied by $\mathrm{p_c}$.

Alternatively to a single optimation run using a fixed discretization of the PD, several optimation runs can be carried out in succession and the discretization can be refined in between these steps. A simple rule for refining is to insert additional nodes where the preliminary determined PD has the biggest gradient. Such an adaptive grid method can be used when highly resolved pressure drop data is available and rather detailed PDs can be determined. The implementation of such a refining step is typically easy to accomplish by modifying the code using fixed a discretization. An example for the application of this extension to the optimisation approach is given in section 6.4.5.

---

[1] This fact can also be illustrated by considering the discretized form of the integral transformation. The inversion towards the discretized PD leads to a system of linear equations. That system is linearly independent and has no trivial solution. Hence the PD is unambiguously determined.

4.1.1 Permeability value variable

The easiest approach is to fix the discretization of the cumulative distribution function Φ linearly between 0 and 1:

$$\Phi_i = \frac{i}{m} \quad i = 0 \ldots m \tag{4.2}$$

Consequently the differences $\Delta\Phi_i$ are constant at $\frac{1}{m+1}$ for all m nodes. An initial guess for the PD is made. Commonly a non-distributed permeability is taken as initial guess, i.e., a constant value for all u_i's.

The pressure drop value Δp_j for a certain filter state s_j is computed from equ. (4.1). The goal function for the optimization algorithm is the sum of square errors between the measured pressure drop values and the simulated ones for each measurement point. Generally the measurement points are not weighted.

$$\sum_{j=1}^{m} (\Delta p_j - \Delta p_{j,\text{exp}})^2 \overset{!}{=} \min \tag{4.3}$$

The changing variables during the optimization are the permeability values at each of the m nodes. Note, that none of the nodes is distinguished from others because of integration via the rectangle rule and equidistant spacing of the Φ_i vector. Thus it depends largely on the optimization algorithm actually used which node assumes a certain value. However, the optimization result is eventually sorted to obtain a distribution function. The result is, of course, not affected. Assuming that a global optimum exists and that the optimization actually finds that optimum, the result is unambiguous.

The implementation of the problem described was attempted on various platforms with different algorithms for nonlinear, unconstrained optimization problems. Only absolute values of the optimization variables are used, thereby avoiding unphysical negative permeability during the optimization run. This is easily implemented in the calculation of equ. (4.1) itself. Alternatively, one could add constraints to the optimization problem, which is, however, increasing the size of the problem and hence the complexity. Additionally the optimization variables are scaled. Permeability values are typically in the order of $10^{-8} - 10^{-10}$ m and were therefore scaled by a factor of 10^8, which greatly improved the convergence of the optimization algorithms.

The determination of a PD via optimization is chosen because of its straight forward implementation (only two numerical integrations required) and the simplicity of the application of optimization methods.

4.1.2 Distribution function variable

An alternative way of discretizing a PD is by fixing the permeability discretization u_i and using the corresponding values of the distribution function Φ_i as variables.

Obviously equ. (4.1) makes up a system of n linear equations for the variables $\Delta\Phi_i$ with the coefficient matrix:

$$A_{j,i} = (s_j + u_i)^{-\frac{1}{2}} \quad i = 1 \ldots m, \ j = 1 \ldots n \tag{4.4}$$

To obtain a non-parametric solutions of the system of equations at least as many measurement points n as PD nodes m are required. This system is usually overdetermined, since the number of available measurements n is larger than the number of nodes of the discretization of the PD m. Hence the system has in general no solution, however, similar to the optimization approach, the least sum of square error solution is sought after.

The system is ill conditioned, although the coefficient matrix $A_{j,i}$ is full in rank[2]. The numerical properties of this linear system are not discussed in detail. The error stemming from the inversion of the underying integral transform is discussed in this thesis in section 5.3.6 with the help of a convolution transform formulation of the problem.

Attempting the solution of the linear square system via the pseudoinverse $(A^T A)^{-1} A^T$ fails on even generated data, i.e., data having a solution with zero residual error. This must be attributed to the ill conditioning of the system. However, QR decomposition, where A is decomposed into an orthogonal matrix Q and a triangular matrix R, succeeds in solving the linear system to its least square solution for all attempted cases using artifiially generated input data [22, p. 112ff].

This way of determining a PD is numerically inexpensive, since it requires only one numerical integration to obtain the filter state values s_j. The solution of the linear least square problem is extremely fast.

However, there are several shortcomings of this direct approach when applied to experimental data, that is always affected by noise. Ideally the solution vector $\Delta\Phi_i$ must add up to one, since the sum must not exceed one. If this value is smaller than one, it just means that part of the filter has zero permeability, which is physically meaningful. If, however this sum exceeds one the solution is not physical. An even bigger problem is the possibility of negative solutions which must not appear in a frequency distribution.

However, constraints can be added to the linear least square problem to exclude unphysical solutions. For m variables $\Delta\Phi_i$ $m+1$ constraints are required:

$$\Delta\Phi_i \geq 0 \quad i = 1, \ldots, m \tag{4.5}$$

$$\sum_{i=1}^{m} \Delta\Phi_i \leq 1 \tag{4.6}$$

This turns the pure system of linear equations into an optimization problem. Contrary to the effectively unconstrained non-linear optimization carried out in section 4.1.1, this constrained problem can be tackled by specifically designed

---

[2]If the number of linearly independent rows in the coefficient matrix equals the total number of rows the rank of the matrix is termed *full*.

algorithms for linear least squares. The constrains are easily implemented and the convergence is quite fast because of its linearity.

The only remaining shortcoming known to the author is that the discretization for the permeability values is fixed. This entails the practical problem of how to choose the discretization for this domain. The discretization of the cumulative distribution is straightforward between zero and one, thereby coving the entire possible range at a certain resolution. The fixed discretization of the permeability values restricts these values to a certain range, although a wider spread of values could be required to determine the optimal PD in a least squares sense. In practice the method of adjusting the permeability values, rather than the distribution values proved more flexible and on an equal number of nodes generally better fits were obtained using the method proposed in section 4.1.1. However, in terms of computational time the linear approach has an advantage.

4.2 Uncertainties in parameters

In addition to the properties of the cake filter model outlined in chapter 3 the influence of uncertainties in the combined model parameters p_c and t_c is discussed here. The main focus when discussing variation in these parameters is the impact on a PD determined by the PD-method for a certain pressure drop curve. The property (ii), which is the invertibility of the pressure drop transform, introduced at the beginning of this chapter, is a prerequisite for this discussion.

The output of the PD-method obtained by two arbitrarily different sets of parameters is discussed. The parameters p_c and t_c are regarded as the true and hence correct parameters for a pressure drop curve corresponding to a certain PD Φ. Meanwhile the parameters $\hat{p}_c$ and $\hat{t}_c$ are the actually used and erroneous parameters with which a PD $\hat{\Phi}$ is obtained from the same pressure drop curve.

From equ. (2.25) it is clear that the filter state s will be altered when using different parameters and is henceforth termed $\hat{s}$. However, since the pressure drop curve remains the same, one can easily convert the filter states by equating the integral for the two sets of parameters:

$$s \cdot p_c \cdot t_c = \hat{s} \cdot \hat{p}_c \cdot \hat{t}_c \tag{4.7}$$

The pressure drop can be calculated from equ. (2.24) for both sets. Equating the pressure drops gives:

$$\frac{1}{p_c} \cdot \int_{u=0}^{\infty} (u + s)^{-\frac{1}{2}} \, d\Phi(u) = \frac{1}{\hat{p}_c} \cdot \int_{\hat{u}=0}^{\infty} (\hat{u} + \hat{s})^{-\frac{1}{2}} \, d\hat{\Phi}(\hat{u}) \tag{4.8}$$

The symbol of the integration variable is changed on the RHS to $\hat{u}$ to avoid confusion. The filter state $\hat{s}$ can be expressed via equ. (4.7) as a function of s. The entire equ. (4.8) is multiplied by $\mathrm{p_c}$.

$$\int\limits_{u=0}^{\infty} (u+s)^{-\frac{1}{2}}\, \mathrm{d}\Phi(u) = \frac{\mathrm{p_c}}{\hat{\mathrm{p}}_\mathrm{c}} \cdot \int\limits_{\hat{u}=0}^{\infty} \left(\hat{u} + \frac{\mathrm{p_c}\cdot\mathrm{t_c}}{\hat{\mathrm{p}}_\mathrm{c}\cdot\hat{\mathrm{t}}_\mathrm{c}}\cdot s\right)^{-\frac{1}{2}} \mathrm{d}\hat{\Phi}(\hat{u}) \qquad (4.9)$$

Subsequently $\hat{u}$ can be substituted by:

$$\hat{u} \equiv \frac{\mathrm{p_c}\cdot\mathrm{t_c}}{\hat{\mathrm{p}}_\mathrm{c}\cdot\hat{\mathrm{t}}_\mathrm{c}}\cdot u$$

Of course the integral boundaries are changed correspondingly and after simplification one obtains:

$$\int\limits_{u=0}^{\infty} (u+s)^{-\frac{1}{2}}\,\mathrm{d}\Phi(u) = \int\limits_{u=0}^{\infty} (u+s)^{-\frac{1}{2}}\,\mathrm{d}\left[\left(\frac{\mathrm{p_c}\cdot\hat{\mathrm{t}}_\mathrm{c}}{\hat{\mathrm{p}}_\mathrm{c}\cdot\mathrm{t_c}}\right)^{\frac{1}{2}}\cdot\hat{\Phi}(\frac{\mathrm{p_c}\cdot\mathrm{t_c}}{\hat{\mathrm{p}}_\mathrm{c}\cdot\hat{\mathrm{t}}_\mathrm{c}}\cdot u)\right] \quad (4.10)$$

The integral kernels on both sides are obviously identical. Since the Stieltjes transform is unambiguously invertible the functions in the differential must be necessarily identical too. Hence one can write:

$$\Phi(u) = \left(\frac{\mathrm{p_c}\cdot\hat{\mathrm{t}}_\mathrm{c}}{\hat{\mathrm{p}}_\mathrm{c}\cdot\mathrm{t_c}}\right)^{\frac{1}{2}}\cdot\hat{\Phi}\left(\frac{\mathrm{p_c}\cdot\mathrm{t_c}}{\hat{\mathrm{p}}_\mathrm{c}\cdot\hat{\mathrm{t}}_\mathrm{c}}\cdot u\right) \qquad (4.11)$$

Consequently variation in the model parameters $\mathrm{p_c}$ and $\mathrm{t_c}$ lead to a scaling and shifting of the resulting PD. Thus all information of the PD Φ is contained in the determined $\hat{\Phi}$. Nevertheless, such a variation in the parameters can make the determined PD appear physically impossible and thus impede its determination.

The effect of this shifting and scaling is illustrated by Figure 4.1. The original PD Φ from Figure 3.1 is displayed together with the corresponding PDs for an altered model parameter $\hat{\mathrm{t}}_\mathrm{c}$ whereby its value was doubled and halved, respectively. It must be noted that the resulting $\hat{\Phi}$ functions can be shifted vertically without altering the result, since the function only appears in the differential. Therefore the function for $\hat{\mathrm{t}}_\mathrm{c} = 2\,\mathrm{t_c}$ is shifted, so Φ' eventually reaches one for large permeability values. Since the cumulative distribution function spans less than one, as a result from the scaling equ. (4.11), the function value eventually levels out at a value higher than zero. That can be interpreted as a part of the total filter area not being used for filtration. That area has simply permeability zero, and is thus added at the left end of the distribution function. However, the other case with $\hat{\mathrm{t}}_\mathrm{c} = 0.5\,\mathrm{t_c}$ uses more than the total available filter area, since its cumulative distribution function exceeds one. To illustrate this, the dotted curve is shifted to start at zero permeability with zero cumulative area, and eventually exceeds one. This PD is physically not meaningful, although in the present case it arose due to an incorrect parameter value.
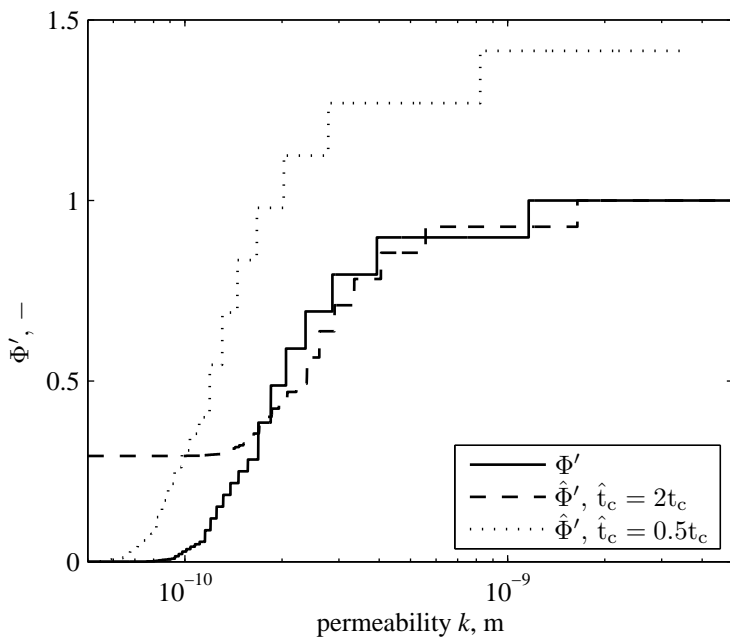
Figure 4.1: PDs leading to identical pressure drop profiles for a variation in the parameter t_c.

It is shown that altered parameter values only lead to a scaled and shifted PD, which, however, can be converted to the original one without loss of information. Nevertheless, certain parameter combinations lead to an apparently unphysical PD (cumulative area exceeding one), that cannot be identified by the methods described above. For a fixed discretization between zero and one on the distribution axis as used in section 4.1 the identification of such a PD is simply impossible and it also contravenes with the constraint equ. (4.6) in section 4.1.2. The latter could of course be waived in favor of detecting inconsistent variable values.

Practically one can derive guidelines for determining the model parameters t_c and p_c. Choosing a fairly large t_c and/or rather small p_c value ensures that a consistent PD can principally be estimated. The focus is usually put on t_c since this parameters contains the specific cake resistance, which is practically difficult to obtain. The remaining filter parameters are quite well known, with the exemption of perhaps the gas volume flow $\dot{V}$. The drawback of intentionally choosing the parameters as suggested, is a lower resolution of the PD with the same discretization, since the PD is compressed over a smaller range on the distribution axis. Additionally its comparability with PDs determined for other sets of parameters is, of course, reduced, since the absolute scaling is missing. Nevertheless the PD preserves its shape during the proposed transformation.

Chapter 5

Convolution transform formulation

5.1 Motivation

The optimization approaches outlined in section 4.1 are relatively easy to implement. However, the only measure of quality of the obtained fit is the agreement between the simulated and experimental pressure drop curve.

The achievable accuracy of a certain PD cannot be assessed independently by an analysis of the employed optimization algorithm. Sensitivity analysis of a single optimization variable on the optimal solution cannot account for a possible interdependency of the optimization variables. Such a dependency is, however, very likely to play an important role, since e.g. the integral value of a PD is usually known very accurately in the form of a filter media resistance. Thus changing only one value of a permeability node at a time is changing this integral value. A simultaneous compensation of one or more other node values would be required to keep ascertained information, i.e., the integral value, correct. Single data sensitivity analysis cannot deal with such additional information, which requires to change multiple variable values at a time to keep that ascertained information unchanged. Thus it is not suitable to assess the possible variation associated with a PD.

The scatter associated with the input data (pressure drop) affects the achievable quality of a PD. The optimization method does not allow for a quantification of the data quality's impact on the quality of the output PD either.

The determination of a PD by means of an optimization algorithm is thus intrinsically uncertain with respect to the accuracy of the output PD. Uncertainty in solutions caused by imperfections of the data cannot be identified and a measure of quality of the determined PD cannot be given.

The following sections outline the concept of using deconvolution for the implementation of the PD-method. In contrast to the identification based on a global optimization algorithm, that cannot guarantee more than a local opti-

mum, this method is deterministic and the accuracy of unambiguous identification of a PD can be ascertained. Also limitations of the PD-method concerning the identifiability of a PD can be shown.

5.2   Mathematical deduction

In this section the filter model derived in section 2.4 is rewritten to form a convolution integral. In the following subsections the Riemann integral notation will be used (cf. appendix A.3). The convolution transform notation is advantageous for further treatment since convolution transforms are extensively studied and error estimations methods are available.

The integral transform formulation of the PD-method consists in the equs. (2.24) and (2.31) which are here repeated in the Riemann notation:

$$\frac{1}{\Delta p(s)} = \frac{1}{\mathrm{p_c}} \int_0^\infty (u+s)^{-\frac{1}{2}} \varphi(u)\mathrm{d}u \tag{5.1}$$

$$t(s) = \mathrm{t_c} \cdot \int_0^\infty \left[(u+s)^{\frac{1}{2}} - u^{\frac{1}{2}}\right] \varphi(u)\mathrm{d}u \tag{5.2}$$

The pressure drop transform equ. (5.1) has, as noted previously, the form of a generalized Stieltjes transform. Following the exponential change of variables suggested by [21] one obtains the pressure drop transform as a convolution transform.

With the exponential change of variables

$$\mathrm{e}^\sigma \equiv s \tag{5.3}$$

and

$$\mathrm{e}^\xi \equiv u \tag{5.4}$$

equ. (5.1) can be rewritten as:

$$\frac{\mathrm{p_c}}{\Delta p(\mathrm{e}^\sigma)} = \int_{-\infty}^\infty \left(\mathrm{e}^\xi + \mathrm{e}^\sigma\right)^{-\frac{1}{2}} \varphi(\mathrm{e}^\xi)\mathrm{e}^\xi \mathrm{d}\xi \tag{5.5}$$

In addition the equation is multiplied by $\mathrm{p_c}$. Note that the integration bounds were transformed accordingly. Using the identity equ. (5.6)

$$\mathrm{e}^\xi + \mathrm{e}^\sigma \equiv \mathrm{e}^{\frac{\xi+\sigma}{2}} \left(\mathrm{e}^{\frac{\xi-\sigma}{2}} + \mathrm{e}^{-\frac{\xi-\sigma}{2}}\right) \tag{5.6}$$

one obtains:

$$\frac{\mathrm{p_c}}{\Delta p(\mathrm{e}^\sigma)} = \int_0^\infty \left(\mathrm{e}^{\frac{\xi-\sigma}{2}} + \mathrm{e}^{-\frac{\xi-\sigma}{2}}\right)^{-\frac{1}{2}} \mathrm{e}^{-\frac{\sigma}{4}} \mathrm{e}^{\frac{3}{4}\xi} \varphi(\mathrm{e}^\xi)\mathrm{d}\xi \tag{5.7}$$

Recalling the definition of the hyperbolic secans $\text{sech}(x) \equiv \frac{2}{e^x + e^{-x}}$ and using this function in equ.(5.7) gives:

$$\frac{\text{p}_\text{c}}{\Delta p(e^\sigma)} e^{\frac{\sigma}{4}} = \int\limits_0^\infty \frac{1}{\sqrt{2}} \text{sech}^{\frac{1}{2}} \left(\frac{\xi - \sigma}{2} \right) e^{\frac{3}{4}\xi} \varphi(e^\xi) d\xi \qquad (5.8)$$

By introducing the functions:

$$h(x) \equiv \frac{1}{\sqrt{2}} \text{sech}^{\frac{1}{2}} \left(\frac{x}{2} \right) \qquad (5.9)$$

$$G(\sigma) \equiv \frac{\text{p}_\text{c}}{\Delta p(e^\sigma)} e^{\frac{\sigma}{4}} \qquad (5.10)$$

$$\tilde{\varphi}(\xi) \equiv \varphi(e^\xi) e^{\frac{3}{4}\xi} \qquad (5.11)$$

one can rewrite equ. (5.8) as:

$$G(\sigma) = \int\limits_{-\infty}^\infty h(\xi - \sigma) \tilde{\varphi}(\xi) d\xi \qquad (5.12)$$

Equ. (5.12) has the form of a convolution transform, with $\tilde{\varphi}(\xi)$ being the permeability distribution density, that underwent an exponential change of variables. The term $h(\xi - \sigma)$ represents the convolution kernel. The function $G(\sigma)$ is pressure drop related and also underwent an exponential change of variables.

When the Fourier transformation $\mathcal{F}[\cdot](f)$, with f denoting the frequency, is applied to equ. (5.12) and the convolution theorem is used, one obtains:

$$\mathcal{F}[G](f) = \mathcal{F}[h](f) \cdot \mathcal{F}[\tilde{\varphi}](f) \qquad (5.13)$$

The convolution theorem states, that the convolution of two functions in the original variable domain can be expressed by the simple product of their Fourier transforms in the frequency domain. The usage of the Fourier transform is suitable for both, convolution and deconvolution, which are accomplished by pointwise multiplication and division of the Fourier-coefficients, respectively. The functions are discretized further on for computational purposes. When referring to the Fourier transform, the discrete Fourier transform (DFT)

$$\mathcal{F}[x(\sigma_n)](f_k) = X(f_k) = \sum_{n=0}^{N-1} x(\sigma_n) \exp\left(-2\pi i \sigma_n f_k\right) \quad k = 0, 1, 2, \ldots, N-1$$
$$(5.14)$$

with its inverse transform

$$\mathcal{F}^{-1}[X(f_k)](\sigma_n) = x(\sigma_n) = \frac{1}{N} \sum_{k=0}^{N-1} X(f_k) \exp\left(2\pi i \sigma_n f_k\right) \quad n = 0, 1, 2, \ldots, N-1$$
$$(5.15)$$

is addressed. The notation for the DFT is taken from signal processing, but the time is replaced with σ for the application at the PD-method.

5.3   Implementation and application

In this section the convolution notation of the filter model is used to demonstrate its ability for convolution, i.e., the calculation of a pressure drop profile from a PD, as well as deconvolution, i.e., the PD-method. Deconvolution from simulated and experimental data is shown together with error considerations.

5.3.1   Variable domains and discretization

To obtain the formulation of the filter model as a convolution integral the commonly used variable time t changes twice: The first change of t into filter state s is model inherent by the transformation equs. (2.31) or (2.12), respectively. The second exponential change of variables from s to σ (equ. (5.3)) is required to obtain a convolution transform formulation. The distribution variable u is according to the filter model (likely the major benefit from this formulation) also defined in the same domain as the filter state s, hence termed *s-domain*. Subsequently ξ, which stems from u, is defined for the same domain as σ, henceforth called *σ-domain*, too. The Fourier transform applied on the functions of the σ-domain yields an output depending on the frequency f in the *frequency domain*. The frequency f is not in the conventional sense a time based frequency, but naturally a σ-based frequency and only indirectly time based[1].

Here the Fast-Fourier-Transform FFT is used to compute the DFT. The use of the fast Fourier transformation (FFT) for computing a DFT is computationally favorable over the more expensive direct computation of the series equs. (5.14) and (5.15), respectively. But certain criteria must be considered, that are imposed by the features of the FFT. Most notably the FFT requires the input data to be available on equally spaced nodes on its input-domain. In addition a number of nodes being a power of 2 is speeding up computation significantly. Since the FFT inherently treats any input as period the input data must be padded with a sufficient number of zeros, so that the end of an input dataset is not reflected into its beginning. A more concise description of the FFT is given by e.g. [23, sec. 13].

Here the input data for the FFT is in the convolution case the transformed PD $\tilde{\varphi}$ which is calculated by equ. (5.11) on an equally spaced σ-domain. This implies a logarithmic spacing of the nodes in the s-domain. Here the σ-domain is divided into $N = 2^{15} = 32768$ nodes on a range $\sigma \in [-103, 103]$. This corresponds to a logarithmic spacing of s and u, respectively, in the interval $[10^{-45}, 10^{45}]\mathrm{m}^{-2}$. Notably, the initial point $s = 0$ is singular in the σ-domain. This range is found to be sufficient in both the required zero padding and accuracy of computation.

---

[1]Concerning the use of units one must note that in the exponential change of variables equs. (5.3) and (5.4) the unit of s-domain, i.e., m^{-2} in the SI system, cannot be consistently passed on to the exponential σ-domain. A comprehensive exchange of variables should read: $s = A \cdot \exp \sigma$ and $u = A \cdot \exp \xi$ with A being a prefactor containing the unit. For the sake of simplicity this factor shall be unity and will not be mentioned further on.

When applying the FFT to a function defined in the σ-domain with an equal spacing $\Delta\sigma$ the sampling frequency is $\frac{1}{\Delta\sigma}$. The maximum resolvable frequency from such a sample is according to the sampling theorem the Nyquist frequency:

$$f_{\mathrm{c}} = \frac{1}{2\,\Delta\sigma} \tag{5.16}$$

The FFT will give the discrete frequency values f_k whereby $k = 0$ corresponds to frequency $f_0 = 0$ and positive frequencies $0 < f < f_{\mathrm{c}}$ are corresponding to $1 \leq k \leq \frac{N}{2} - 1$. The negative frequencies are appended thereafter with $-f_{\mathrm{c}} < f < 0$ corresponding to $\frac{N}{2} + 1 \leq k \leq N - 1$. The Nyquist frequency $f = f_{\mathrm{c}}$ and $f = -f_{\mathrm{c}}$ corresponds to $\frac{N}{2}$ because of symmetry. An exhaustive explanation is given by [23, sec. 12.1].

$$f_k = \frac{k}{N\,\Delta\sigma} \quad k = 0,\,1,\,2,\,\ldots,\,N-1 \tag{5.17}$$

5.3.2 Convolution situation in the σ-domain

The cumulative distribution $\Phi(u)$ is analytically generated and can be obtained with high accuracy only limited by machine precision (cf. Figure 3.1). The required density $\varphi(u)$ is generated by taking the derivative of the stepped function $\Phi(u)$ and thus is analytically represented by a sum of appropriately scaled Dirac-Delta-functions. This information can also be represented by a series of finite peaks resulting from numerical differentiation on any discretized s-domain. The peaks' heights, however, depend on the chosen discretization of u in the s-domain and the discrete representation is naturally accompanied by a loss of information, because of discretization. The calculation of the actual values of $\tilde{\varphi}$ can be done pointwise by equ. (5.11) in the σ-domain.

The Δp-values can be calculated analytically for a given input PD from equ. (5.1) in the s-domain. Subsequently the value of the G-function is obtained by equ. (5.10) for the σ-domain.

The situation for the convolution in the σ-domain is displayed in Figure 5.1. The kernel function h is centered on zero, whereas the G-curve is centered on the $\tilde{\varphi}$ peaks. The σ-range corresponding to the actual Δp-curve in Figure 3.2, i.e., time t ranging from 1 to 700 s, is indicated with a solid G-curve. One can see that the G-curve can practically be measured in only a limited σ-range. Here a calculated time-range from 1 to 700 s is shown. Although calculation would be possible for any time range the deconvolution method should be developed for experimental data, also the computed input is limited to a practically measurable range.

Following [24] a qualitative analysis of the convolution situation, displayed in Figure 5.1, shows that the kernel function h changes slowly in the σ-domain in comparison with the analytical $\tilde{\varphi}$. Thus during the convolution of h with $\tilde{\varphi}$ fast changes with respect to σ in $\tilde{\varphi}$ are simply smoothed out by the broad kernel. This makes the convolution quite stable against fast changes. However, since the fast nuances in $\tilde{\varphi}$ are smoothed out quickly, information about them
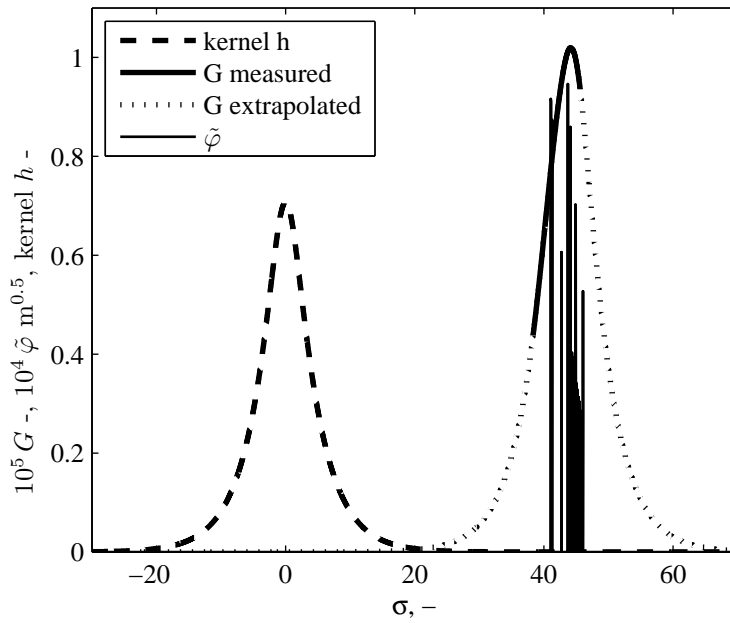
Figure 5.1: Convolution situation for the test data (Figures 3.1 & 3.2). The ordinate values are differently scaled for each curve, so the curves can be displayed in one chart.

is lost in the convoluted curve. In the more practical problem of deconvolution, that is tackled in section 5.3.5, fast changes of $\tilde{\varphi}$ are thus unidentifiable.

5.3.3 Convolution situation in the frequency domain

In a quantitative discussion on the different scales involving functions that are changing *quickly* compared to others, it is advantageous to actually look at the Fourier transformed functions in question, i.e., their power spectral densities. The power spectral density P at frequency f of a function h can be estimated by equ. (5.18) [23, sec. 13.4]. Here the asterix denotes the complex conjugate.

$$P_{\mathrm{h}}(f) = |\mathcal{F}[h](f)|^2 = \mathcal{F}[h](f) \cdot \mathcal{F}[h]^*(f) \tag{5.18}$$

The power spectral density describes how the power in a function is distributed over the frequency range. The definition of a power spectral density is not necessarily bound to power in the physical sense. By that concept the total variation in a function can be decomposed to the contributions at certain frequencies. The power spectral density values for a certain frequency are the contributions to the total signal's variance at that frequency.

In Figure 5.2 the power spectral densities of the functions in equ. (5.13) are displayed for positive frequencies f up to the Nyquist frequency f_{c}. All functions displayed are calculated analytically and thus they do not contain any noise except one stemming from machine precision limitations. Both the kernel h and G show a significant decrease of their power spectra at higher frequencies, i.e., high frequencies are not essential for describing these functions. This is in accordance with the observation in section 5.3.2, that the kernel as well as G are changing slowly over σ. However, the spectra of $\tilde{\varphi}$ is high on the full frequency range, which is due to the peaked structure of $\tilde{\varphi}$. The absolute values of the different spectra arise due to the absolute magnitude of the underlying functions and are not scaled in this plot.

When looking at the spectra of the kernel and G again, one observes a significant decrease in power of several decades until the spectra flatten with only some fluctuations. At the respective frequencies the power in these functions is almost negligible (double logarithmic chart), but the scatter and the flattening are resolved clearly. Since all the displayed curves stem from simulations, the noise arises from machine precision limitations only. For the G curve more computational operations were necessary resulting in a higher noise level than the explicit kernel function.

5.3.4 Convolution implementation

The convolution of a PD to a pressure drop curve is the typical filter simulation task. The PD is input and as such available. After calculating $\tilde{\varphi}$ and h at appropriate σ-points, as outlined above, the FFT is applied on both, the corresponding FFT coefficients are multiplied and the inverse FFT is applied to the result. The obtained G function is transformed into a Δp-function. Results
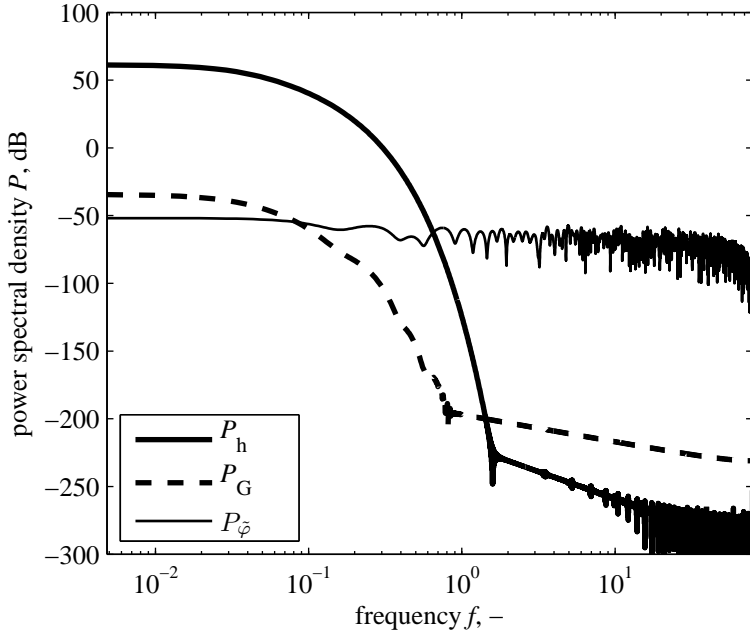
Figure 5.2: Power spectral densities of the functions involved in convolution.

of convolution are omitted here, since they would just lead to the starting point already displayed in Fig. 3.2.

Convolution of a PD is mainly used here to check the suitability of the chosen σ-domain for eventual deconvolution. However, the explicit calculation of equ. (5.1) for an equally good resolved φ-function as in the convolution version has a time complexity $O[m^2]$, with m again being the number of nodes in the PD discretization. From the convolution result the time t can be calculated from an integration of equ. (2.26) which is only linearly complex, i.e., $O[n]$ with n again being the number of measurements.

The convolution requires only the number of operations for an (actually 3) FFTs and the explicit evaluation of the integral transform equ. (5.1) is omitted. Thus the governing time complexity is – depending on the actually used FFT algorithm – around $O[N \ln(N)]$, which is, for the same accuracy, lower than $O[n^2]$ as found above. Nevertheless, the number of nodes required to sufficiently represent a PD is much less. In section 4.1 $m = 30$ nodes are used. Thus the CPU time saving remains small. In practice an acceleration factor of up to 10 is observed when using the FFT-convolution on the σ-domain with $N = 2^{15}$ nodes, instead of the conventional numerical integration on $m = 30$ and $n = 2^{15}$ to obtain the same accuracy. Of course, a reduction of the number of nodes n to a reasonable value, leads to reduced CPU-time for the conventional integration.

Eventually the use of the FFT-convolution might be unattractive in terms of time complexity and especially coding effort.

5.3.5 Deconvolution implementation

Deconvolution is reduced to a pointwise division in the frequency domain, which is the major benefit from using Fourier transformations:

$$\tilde{\varphi}(f) = \mathcal{F}^{-1}\left[\frac{\mathcal{F}[G](f)}{\mathcal{F}[h](f)}\right] \qquad (5.19)$$

Unfortunately deconvolution usually cannot be applied directly because the convoluted function G is, in practice severely, affected by noise. Even the computed functions in Figure 5.2 show at some point a significant noise level.

In the division in equ. (5.19) at a certain frequency f an only slight uncertainty in the numerator, i.e., the Fourier transform $\mathcal{F}[G](f)$, can be amplified enormously by a comparably small value in the denominator, i.e., the Fourier transform of the kernel $\mathcal{F}[h](f)$. The power spectrum of the kernel reaches low levels at frequencies that are far lower than the Nyquist frequency (see also Figure 5.2). Even the kernel is affected by numerical noise. Thus a small error of G will be amplified enormously when reaching higher frequencies. Also in the case of calculated data used here, deconvolution fails to give any useful results when directly applied to the data displayed in Figure 3.2.

However, this problem can be tackled by appropriately filtering the data in the frequency domain. Following the approach outlined in detail in [23, sec. 13.3] one can design a second order optimal filter, a so called Wiener filter. A filter function $B(f)$ is chosen in a way to minimize the square error difference between the (unknown) true function and the deconvoluted one. The filter is incorporated in equ. (5.19), which leads to:

$$\tilde{\varphi}(f) = \mathcal{F}^{-1}\left[\frac{B(f) \cdot \mathcal{F}[G](f)}{\mathcal{F}[h](f)}\right] \qquad (5.20)$$

The determination of the filter function requires a model for the power spectrum of noise affecting G which is denoted as P_{noise}. From minimization (cf. [23]) one obtains a second order optimal filter:

$$B(f) = \frac{P_{\text{G}}(f) - P_{\text{noise}}(f)}{P_{\text{G}}(f)} \qquad (5.21)$$

The filter is thus the power spectral density of the estimated true input over the power spectral density of the actual input. When, e.g. the power spectrum of the noise has the same magnitude as the actual input signal, the filter function becomes zero, i.e., the input and noise cannot be discriminated.

The noise model can often be determined directly from the spectral density of the signal in Figure 5.2. Presumably the noise in P_{G} begins when the spectrum levels out and becomes linear in the double logarithmic chart. Thus a power law noise model is chosen. Figure 5.3 shows the new situation with the noise model

and the resulting filter. At the point where the filter is not displayed any longer it is set to zero, i.e., it cannot be displayed on the decibel axis. Once the filter becomes zero at a certain frequency, because of the noise exceeding the actual signal, it is kept zero for all higher frequencies, even though the power spectral density of the signal may exceed the noise model because of fluctuations.
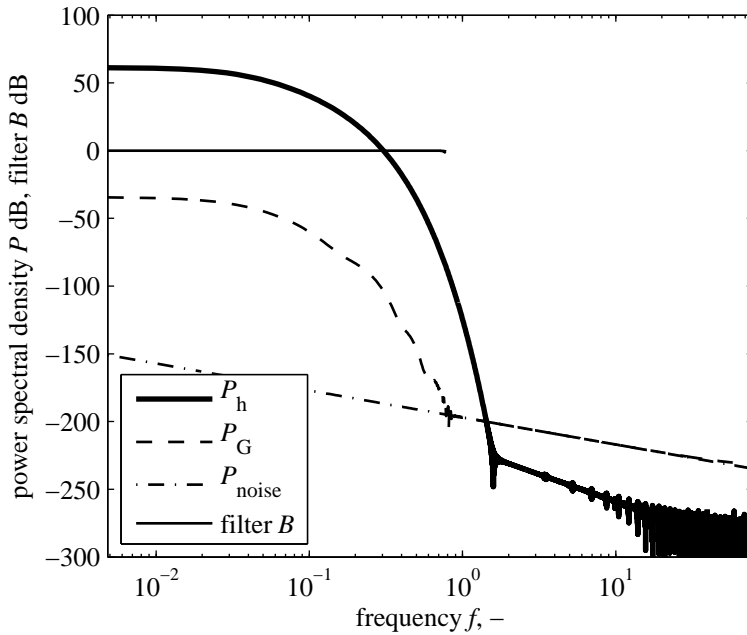

Figure 5.3: Power spectral densities with noise model for G and the Wiener filter B.

The $\tilde{\varphi}$-curve calculated by equ. (5.20) contains some noise on the entire σ-range, even when high frequencies are eliminated. During the transformation to φ and further to φ' this noise is amplified for small σ values. Thus a total cut-off in the σ-domain is used, that sets the $\tilde{\varphi}$ function to zero outside a certain range from the function centroid. In section 5.3.6 this cut-off is discussed more thoroughly.

The result of the deconvolution with the described filter is displayed in Figure 5.4. Compared to the stepped function of the analytical PD and the one obtained by optimization the deconvoluted curve is smoother, which is a result from filtering high frequencies. The Wiener filter imposes a fairly sharp cutoff and only frequencies in the signal lower than that cutoff can be resolved.
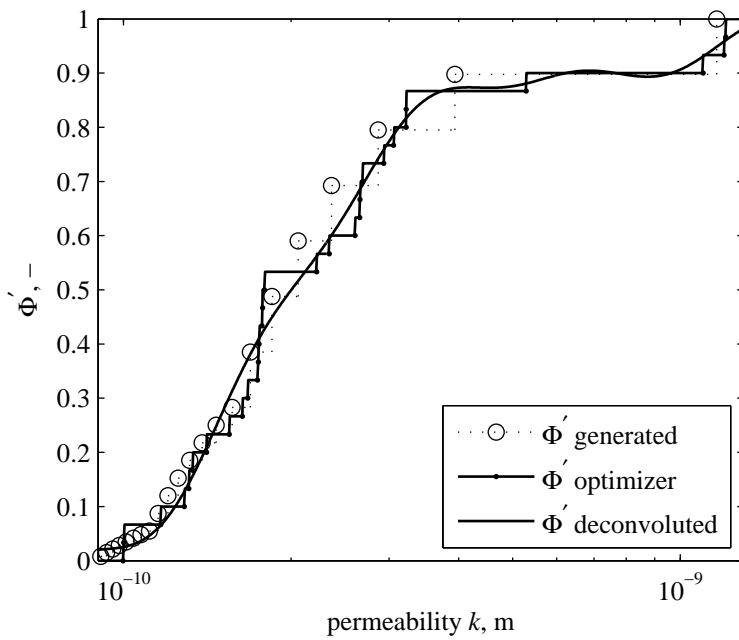
Figure 5.4: The result of the deconvolution on the calculated data is displayed together with the analytically generated and the optimized PD.

5.3.6   Error estimation in deconvolution

The error in the φ and φ' curves can be traced back to the actual deconvolution. The Wiener filter results, as stated, from a least squares minimization of the unknown true function to the approximated result. For the error estimation both the resolved frequencies and the magnitude of the error are taken into consideration.

It is assumed that the error affecting the $\tilde{\varphi}$-function occurs irrespective of the actual σ. The error ε_σ is affecting the $\tilde{\varphi}$-function according to equ. (5.22) on the full σ-range.

$$\tilde{\varphi}(\xi) = \tilde{\varphi}_{\text{true}}(\xi) \pm \varepsilon_\sigma \tag{5.22}$$

Transforming the $\tilde{\varphi}$-function to φ requires a switch from the σ to the s-domain following equ. (5.11). Consequently, also the error ε_σ must be transformed, giving ε_s affecting φ:

$$\varepsilon_s(u) = \varepsilon_\sigma \, u^{-\frac{3}{4}} \tag{5.23}$$

Further the error in φ' in the k-domain (cf. appendix A.1) gives an error ε_k :

$$\varepsilon_k(k) = \varepsilon_\sigma \, 2k^{-\frac{3}{2}} \tag{5.24}$$

Because of these transformations the originally constant error ε_σ affects the resulting distributions depending on the actual value of s and k, respectively. One can see that the error is amplified for small k-values (see Figure 5.6). Practically this unwanted amplification was countered by just setting $\tilde{\varphi}$ to zero on a part of the σ-domain, i.e., truncating the function to a certain range around the function centroid.

The actual value of the error in ε_σ is not known from the deconvolution and/or noise model directly. In Figure 5.5 the deconvoluted function $\tilde{\varphi}$ is displayed. The bold curve around the function centroid is the remaining region after truncation. In the remaining function range one can see oscillations which stem from the ground noise level of the deconvoluted function. From the oscilations seen in the figure the error magnitude is determined to $\varepsilon_\sigma = 3 \cdot 10^{-7} \mathrm{m}^{\frac{1}{2}}$

The error ε_σ is quite small around the function centroid compared to the function values there. Trivially both ε_s and ε_k become infinite for any ε_σ-value for small values of u and k, respectively. A visual comparison of the deconvoluted function φ' and the error ε_k accociated with it, is given in Figure 5.6. In the most relevant part of the PD, i.e. where the density $\tilde{\varphi}$ in Figure 5.5 exceeds the error level, ranging from around $k = 10^{-10}$ to 10^{-9} m in the k-domain the error is, of course, small. The strongly growing error which eventually exceeds the actual function for smaller k-values can be clearly seen, too.

However, the resulting PD is mostly represented as a cumulative distribution. Thus the cumulative error should also be looked at. The integral errors over the entire s- and k-domain are infinite, which is problematic. This can be seen
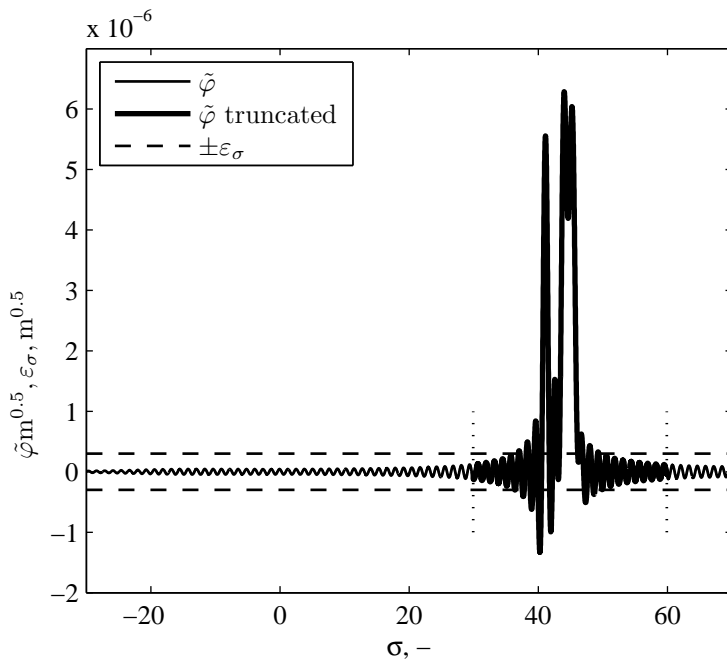
Figure 5.5: Deconvoluted function $\tilde{\varphi}$. The bold section indicates the remaining region after truncation. This region is also indicated on the σ-axis by the dotted lines. The level of the error ε_σ is displayed, too.
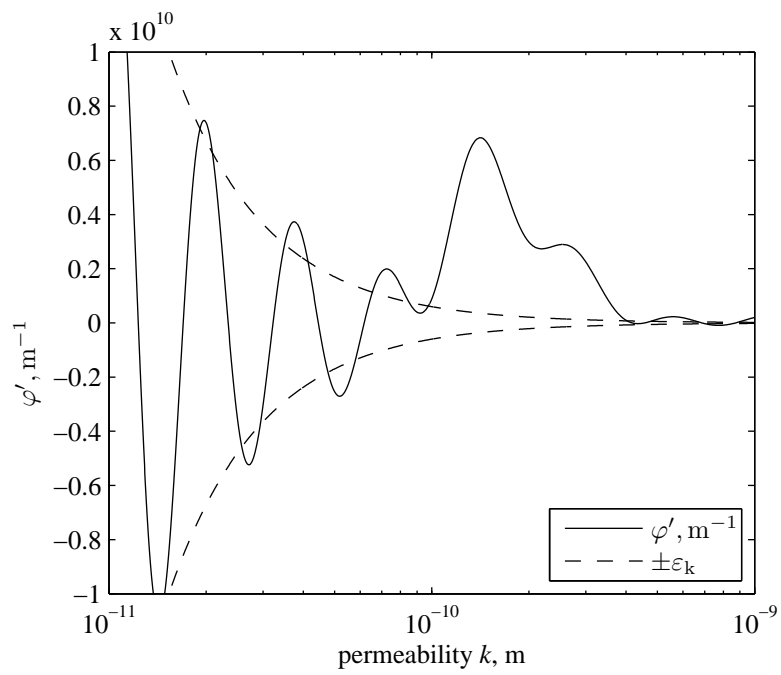
Figure 5.6: Deconvoluted PD density function φ' together with its error.

by calculating the cumulative distributions Φ and Φ' from their densities which leads to the improper integrals:

$$\int_0^\infty \varepsilon_s(u)\mathrm{d}u = \varepsilon_\sigma \int_0^\infty u^{-\frac{3}{4}}\mathrm{d}u = \infty$$

$$\int_0^\infty \varepsilon_k(k)\mathrm{d}k = 2\varepsilon_\sigma \int_0^\infty k^{-\frac{3}{2}}\mathrm{d}k = \infty$$

However, the integrals giving the integral errors $E_s(u) = \int_0^u \varepsilon_s \mathrm{d}u$ and $E_k(u) = \int_k^\infty \varepsilon_k \mathrm{d}k$ converge to finite values:

$$E_s(u) = \varepsilon_\sigma \int_0^u u^{-\frac{3}{4}}\mathrm{d}u = 4\varepsilon_\sigma u^{\frac{1}{4}} \tag{5.25}$$

$$E_k(k) = 2\varepsilon_\sigma \int_k^\infty k^{-\frac{3}{2}}\mathrm{d}u = 4\varepsilon_\sigma k^{-\frac{1}{2}} \tag{5.26}$$

The resulting cumulative PD is displayed in Figure 5.7 together with the integral error. Note that this error estimation is particularly pessimistic due to the integration of original fluctuations in both plus and minus directions without allowing for a compensating effect. This compensating effect can be seen in the comparison between Figures 5.6 and 5.7 when concentrating on small k-values: In Figure 5.6 the fluctuation are occasionally even exceeding the error, whereas in the cumulative function Figure 5.7 the fluctuations are compensated for, but the error without compensation becomes large.

However, the branches of the cumulative distributions Φ and Φ' for high u and small k values are unknown, since any small, but non-zero error will become infinite on these branches. Nevertheless, the error in the cumulative distributions for small u and high k-values, respectively, are finite. Note that the cumulative error for u approaching equ. (5.25) is finite, although the corresponding density error is infinite equ. (5.23).

In other words, the PD for permeabilities towards zero is intrinsically uncertain, but in the relevant range of k the error is moderate.

In a next step the frequency resolution is looked at. The cutoff frequency $f = f_\sigma$ for the σ-domain can be defined at e.g. a filter value $B(f_\sigma) = 0.5$, which is used hereafter. This cutoff frequency is constant for the entire σ-domain. For the data presented in Figure 5.3 one finds $f_\sigma = 0.78$. However, converting the frequency via a first order Taylor approximation into the s-domain gives:

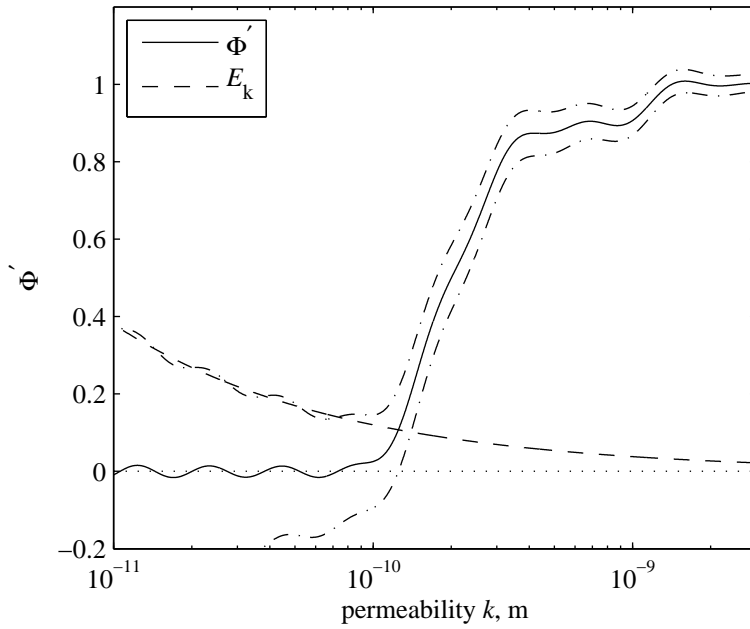$$f_s(u) = f_\sigma \frac{1}{\mathrm{e}^\sigma} = \frac{f_\sigma}{u} \tag{5.27}$$

Figure 5.7: Deconvoluted cumulative PD Φ' together with its error E_k displayed as dashed line. The dash dotted lines depict the error band around the distribution, i.e., $\Phi' \pm E_k$.

and further into the k-domain:

$$f_k(k) = f_s \frac{1}{0.5s^{-1.5}} = f_\sigma \frac{1}{0.5s^{-0.5}} = \frac{2f_\sigma}{k} \qquad (5.28)$$

One must note that because of symmetry reasons (positive-negative frequency) the minus of the Taylor approximation in equ. (5.28) is omitted. This equation means that for small permeabilities k the φ' distribution can be resolved at higher frequencies than for higher permeabilities. However, the error in magnitude according to equs. (5.24) and cumulatively (5.26) is increasing when k decreases.

Oscillations with the actual cut-off frequency f_σ can be observed in the off-centroid regions in Figure 5.5. These are, of course, also reflected in Figures 5.6 and 5.7 with the correspondingly adjusted frequency f_k. On the logarithmically scaled k-axis oscillations appear of course at a constant frequency.

5.3.7 Experimental pressure drop data

So far the pressure drop data itself used for deconvolution is not affected by a measurement error. Although it is demonstrated that even the small numerical noise can have devastating effects on deconvolution if not treated with a filter, the experimental noise practically encountered is orders of magnitude higher.

In addition the data is practically only available for a limited time range, as indicated already in Figure 5.1. There the bold continuous line for G indicates the range where actually measured pressure drop values are available. To make things even worse the data is discretely sampled usually with a constant sample time. The basic FFT, however, only accepts input data at equal spacing, not in the time but σ-domain.

In order to be able to apply the FFT to experimental data some additional processing steps are required. It is assumed that the experimental data starts at time $t = 1\,\text{s}$, since this overcomes the problem of singularity for $s = 0 \to \sigma = -\infty$. Subsequently the pressure drop Δp for s-values corresponding to $t < 1\,\text{s}$ is taken constant, similarly to the explanation in section 3.2.4. Since the pressure drop does not change measurably within the first second of filtration, this extrapolation does not add any additional error which would exceed the measurement noise.

For large times and consequently large s-values the pressure drop will increase linearly. That is also the assumption for the extrapolation to large s-values, i.e., the tangent on the measured data (here the last $100\,\text{s}$) is used to determine a linear pressure drop increased. This extrapolation, however, adds additional information and must in every single case be questioned concerning its applicability.

In the time range, where actually measured pressure drop data is available, the values of G are obtained on equidistant nodes in the σ-domain by interpolation. Because of the already significant noise in the pressure drop signal, interpolation does not add significant error itself. Practically the interpolation is found to be even advantageous, since it smoothes out the frequency effects

of the exponential sample intervals in the σ-domain, thus simplifying filtering data in the frequency domain.

The calculation scheme suggested here is applied on data presented by [25]. The convolution situation in the σ-domain is depicted together with the deconvolution result in Figure 5.8. The corresponding power spectra are shown in Figure 5.9. The spectrum of the kernel is, of course, not altered from Figure 5.2, but in the spectrum of the *G*-function the noise level is clearly much higher. Thus the noise model is giving generally higher values. Also the Wiener filter *B* is shown in Figure 5.9 and here the transition from 1 to 0 is not as sharp as in Figure 5.2, thus a continuous decrease in the value can be seen.

The amplitude error is found from a plot similar to Figure 5.6 to be $\varepsilon_\sigma = 2 \cdot 10^{-6}\,\mathrm{m}^{\frac{1}{2}}$.
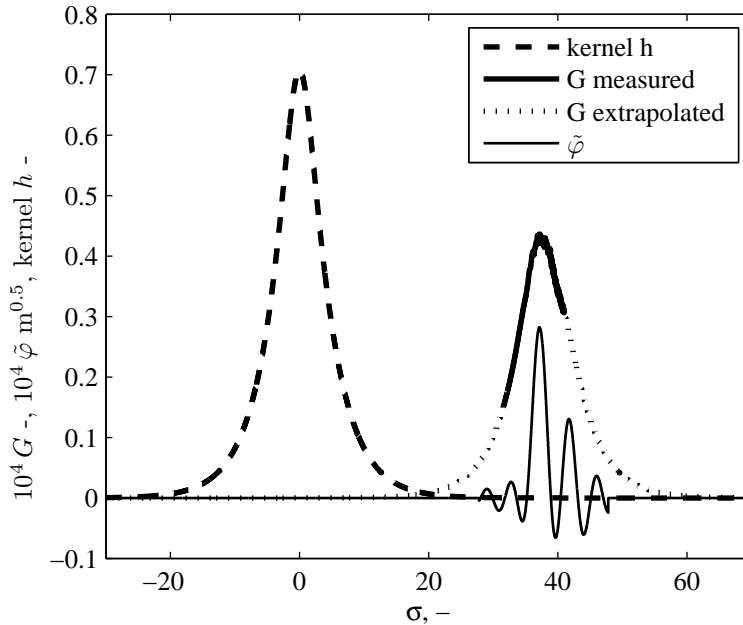

Figure 5.8: Deconvolution situation for experimental data in the σ-domain.

In Figure 5.10 the result of deconvolution is displayed. The deconvoluted PD shows hardly any jump when compared to the distribution obtained by optimization. This arises from the relatively low cut-off frequency $f_\sigma = 0.26$ for the given problem, i.e., higher frequencies than that cannot be resolved. However, the PD obtained by deconvolution is equally suitable for describing a pressure drop increase ramp which is displayed in Figure 5.11. The deconvoluted PD, however, exhibits significant oscillations and a significant integral error for small *k*-values which reaches even in the negative range being physically meaningless.
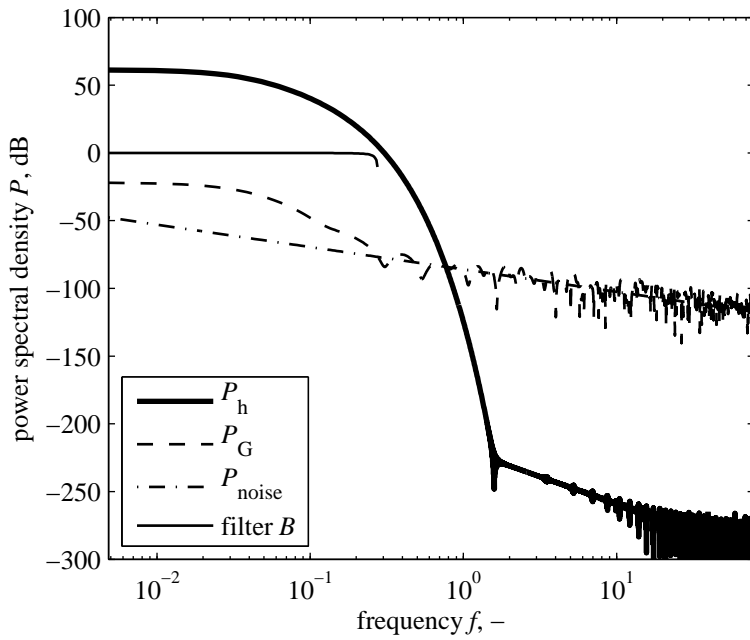
Figure 5.9: Power spectral densities for the deconvolution situation from experimental data.
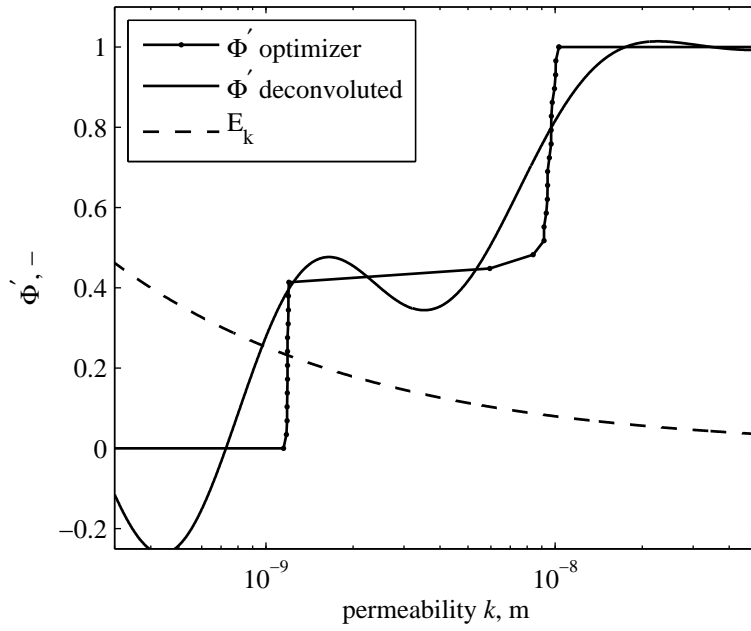
Figure 5.10: PD from experimental data obtained by deconvolution. In addition the corresponding PD determined by optimization and the integrated error E_k are displayed.
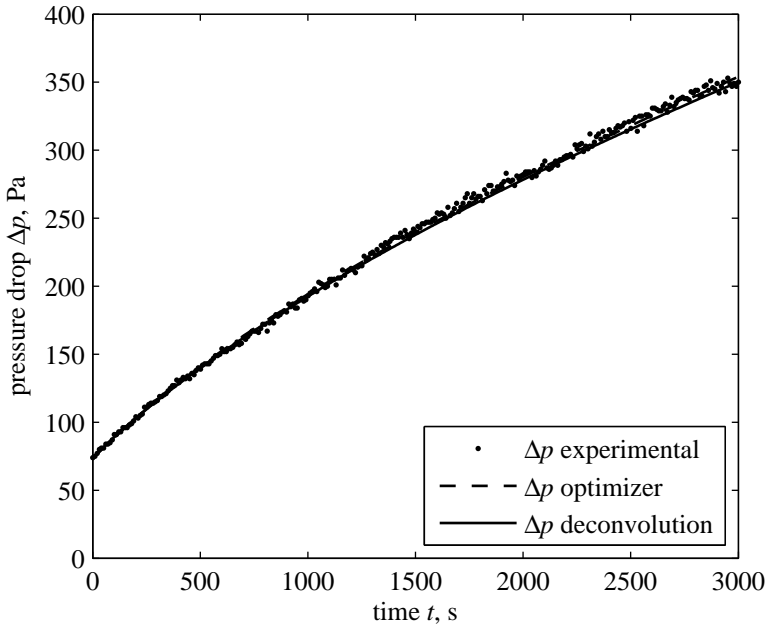
Figure 5.11: Pressure drop increase from experimental run day 1 presented by [25]. The simulated pressure drop curves from the optimized PD and the deconvoluted one are displayed. A slight deviation of the deconvoluted PD must be attributed to the linear extrapolation of the pressure drop curve, when calculating the G function for big s-values.

5.4   Discussion and conclusions

In the preceding sections the convolution integral version of the PD-method is introduced and applied. A PD can be obtained from pressure drop data by deconvolution using FFT. The deconvolution method is orders of magnitude faster than finding a PD by global optimization and allows for error estimation of the result. The error estimation is given as amplitude oscillations and a cut-off frequency.

The probably biggest disadvantage of the PD-method via deconvolution is, that it requires more assumptions on the raw data than the optimization, because of extra- and interpolation. In addition the filter design requires additional information, i.e., a noise model. The implementation effort is bigger and the subsequent possibility for implementation errors is higher in the deconvolution version. A PD from convolution is, in principal, more flexible than one obtained by optimization, since an optimizer allows only for a very limited number of nodes for the PD. However, the deconvolution does not give perfectly consistent distribution results, since oscillations in the results can lead to negative density functions.

The deconvolution is attempted on simulated data from a PD determined by optimizations (results are not displayed in detail here). In this case the deconvolution version can give a measure on the certainty of the PD determined by optimization. The pressure drop increase can be copied within very narrow limits by deconvolution and error bounds on the deconvoluted PD can be obtained. The PD from optimization is for the attempted case clearly within the error bounds. Thus the simplicity of optimization and the error estimation capabilities of deconvolution can be combined. Such an improvement can possibly be achieved by determining an estimate for a PD from deconvolution which is eventually refined by optimization.

The deconvolution version of the PD-method is applied and its suitability to obtain a PD is shown. More assumptions are necessary to be able to apply the deconvolution version compared to finding the PD by optimization. The latter is significantly simpler in application, but computationally more expensive. The most practical form of the PD-method may make use of optimization because of its simplicity and robustness, and eventually when an error estimation is required a deconvolution might be performed.

Chapter 6

Application

This chapter shows exemplarily applications of the PD-method. It is divided into two main sections: The determination of a PD of the filter medium itself and a PD due to industrial filter operation with incomplete filter cleaning.

6.1 Inhomogeneous filter media

The characterization of filter media by the PD-method requires pressure drop data of the filtration on the initially clean filter medium, henceforth termed *ramp test*, as input. Such data can be acquired in e.g. filter test stands, laboratory filter plants or even pilot and production scale plants. According to the findings from chapter 4 the obtained pressure drop profile can be transformed into a corresponding PD.

To determine the PD of the filter medium itself it must be ensured that the filter medium is clean at the beginning of filtration. Any filter cake present could add to the PD of the filter medium and will thus corrupt the PD of the filter medium.

To extract most information from such a PD it is desirable to know most operating parameters and, of course, the filter model presumptions must be fulfilled.

The extent to which the requirements of cleanliness and ascertained operating parameters are accomplishable depends largely on the filtration facility that is used to determine the pressure drop curve.

Kavouras and Krammer [20] are using a pilot scale filter and assume that the filter is carrying no cake any longer, when the pressure drop at a certain gas flow remains at a constant level despite continuous filter cleaning. However, it cannot be verified externally that the filter medium does not carry any cake at this stage. Saleem [26] has the possibility to actually verify the existence or lack of cake patches by stereo optical cake thickness measurements.

For practical reasons the clean filter state, used further on, willl be defined in accordance with the definition used by [20]. The clean filter state is thus

reached when further filter cleaning does not have any further influence on the pressure drop level. This is also the most practical definition, since it reflects the state of cleanliness achievable by the chosen filter cleaning method.

The way of obtaining the pressure drop increase that is required to determined the PD depends on the actual facility used. In laboratory plants it is generally possible to start gas flow and dust feed in sequence. The subsequent pressure drop increase is used as input for the PD-method. The experimental procedure may have to differ and is discussed in the respective section.

6.1.1   Filter media test stands

Usually it is easier to assure defined condition in a laboratory scale and also instrumentation is most comprehensive there. Existing filter test rigs do not require any modification of the setup or instrumentation and thus even existing data from past experiments can be used for evaluation with the PD-method.

A typical example of a commonly used test stand is the VDI 3926 [12] stand which comes in two modifications Type 1 and Type 2. The filter medium sample to be examined is a square with a total filtration area $A_{tot} = 144\,cm^2$. Thus the isolated effect of cake filtration on that sample is simulated. Any possible influence of the filter medium's installation as e.g. a bag in a baghouse with a possibly uneven dust distribution and/or dust settling, i.e., some dust is settling directly and not even reaching the filter medium, is eliminated.

In Figure 6.1 the pressure drop data recorded in a VDI 3429 Type 1 test stand is displayed together with its corresponding simulated pressure drop curve from the filter model. The pressure drop increase during filter testing of a clean cloth sample is depicted. The filter medium used is a polyimide needle felt on a polyester supporting scrim. The test dust used is the alumina monohydrate powder Pural SB. The agreement between the simulated and experimental pressure drop curve is excellent. That is not especially surprising, since the underlying PD is determined via simple optimization with a fixed distribution discretization (cf. section 4.1.1) from the experimental pressure drop data.

The parameter p_c is calculated from the design of the filter test rig and the measured volume flow $\dot{V} = 2.77\,m^3 \cdot h^{-1}$ which is constant within 0.5% during the test run. The gas viscosity is taken from air as $\eta_g = 18 \cdot 10^{-6} Pa \cdot s$.

The calculation of the t_c parameter requires the dust concentration $c_{sol} = 5\,g \cdot m^{-3}$ in addition, but is not as straightforward because of the unknown specific cake resistance α_m. Since the pressure drop ramp test is not continued beyond the time range displayed in Figure 6.1, this value cannot be directly extracted from the final asymptote of the pressure drop curve. Therefore the PD-method is executed with a roughly overestimated t_c value. In Figure 6.2 the corresponding PD is displayed as solid line with dot-markers.

A small part of the filter area ($< 10\,\%$) is found to have a high permeability. The remaining filter area is exhibiting a significantly lower, but rather homogeneous permeability. This part can be seen as nearly vertical line in Figure 6.2. The area exhibiting an even lower permeability than the homogeneous area is discussed below with respect to the model parameters chosen.
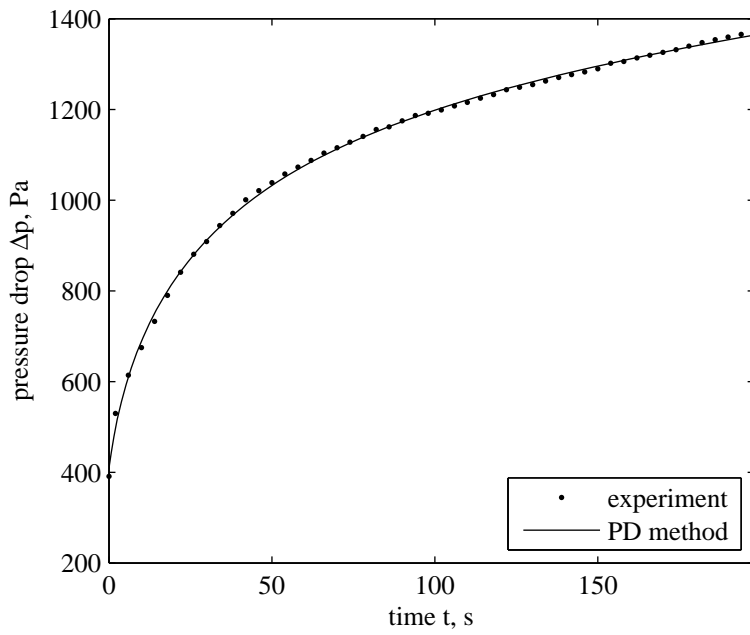
Figure 6.1: Experimental pressure drop curve of a filter medium test on a VDI 3429 Type 1 test stand.
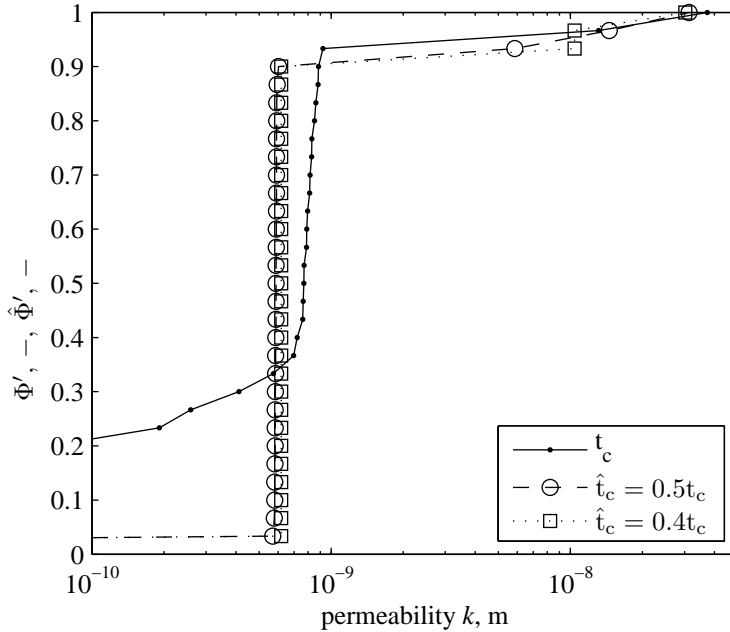
Figure 6.2: PD distributions determined for different parameters t_c.

Since the parameter t_c is estimated from the data it must be considered uncertain. According to the considerations in section 4.2 this will result in a scaled PD. The information contained in this scaled PD is equivalent to the PD that would be obtained with the *correct*, but unknown, parameter. To investigate the sensitivity of the parameter t_c on the obtained PD, two alternative PDs, which are determined for correspondingly lower $\hat{t}_c$-values, are displayed in Figure 6.2.

The quality of the fit in terms of pressure drop agreement is almost the same for all the displayed curves. The original PD with t_c finds part of the filter area at very low permeability towards zero. One should recall that a large value for the parameter t_c corresponds to a low specific cake resistance. All the other parmeters appearing in the definition of t_c equ. (2.23) are measured or known from design specifications of the test stand. Thus a PD is found that does not use a part of the filter area for filtration at all which is expressed by a rather low permeability in the lower left corner of Figure 6.3.

Using the parameter $\hat{t}_c = 0.5t_c$ instead of t_c corresponds a doubling of the actual specific cake resistance given that the other parameters remain the same. In order to mirror the experimental pressure drop curve equally well, a larger fraction of the filter area must be used. In fact this PD uses the full filter area for the parameter $\hat{t}_c$ with a non-zero permeability.
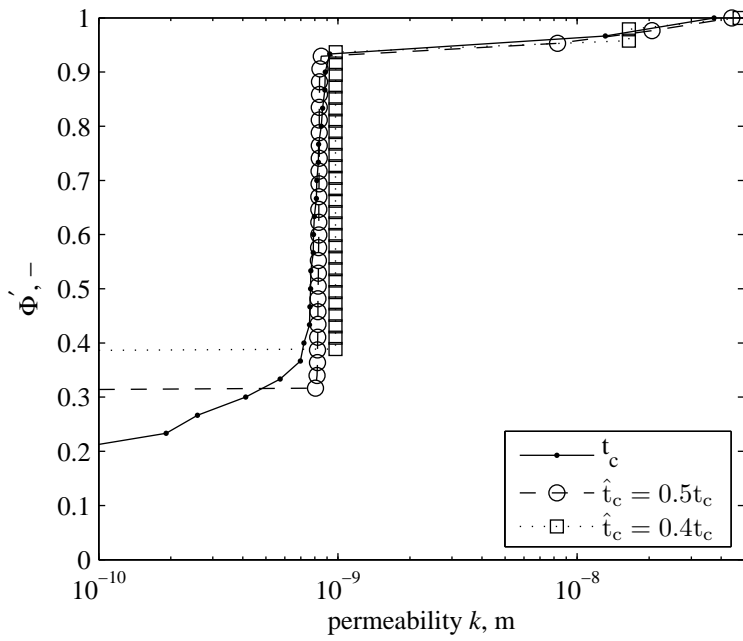
Figure 6.3: PD distributions determined for different parameters t_c. Curves determined for a paramter $\hat{t}_c$ scaled for comparability to the parameter t_c.

The model parameters are different for the curves in Figure 6.2. To ensure comparability of the PDs determined for $\hat{t}_c$-values these are transformed to the value of the parameter t_c according to the transformation outlined in section 4.2. In Figure 6.3 the distribution functions with $\hat{t}_c = 0.5\,t_c$ is rescaled to the parameter t_c and are thereby comparable to the curve determined with the t_c-value. According to equ. (4.11) the scaling factor for the cumulative distribution axis is $\sqrt{\frac{\hat{t}_c}{t_c}} = \sqrt{0.5} \approx 0.71$. Thus at least $30\,\%$ of the filter area must have zero permeability, which is reflected in the corresponding PD in Figure 6.3, which intersects the ordinate axis at this value. Nevertheless, the remaining $70\,\%$ are used. Good agreement between the original PD and the PD for $\hat{t}_c = 0.5 t_c$ is observed for these higher permeability values. At low permeability values the PD is anyway highly uncertain according to the findings in section 5.3.6.

When decreasing the parameter $\hat{t}_c$ even further to $\hat{t}_c = 0.4 t_c$ the PD makes use of the entire filter area too (see Figure 6.2), i.e., there are no parts of the filter area with zero permeablity. In Figure 6.3 this means, of course, a non-zero PD for $\sqrt{0.4} \approx 63\%$ of the filter area. However, one observes a shift of the large step in the distribution around $k = 10^{-9}\,\mathrm{m}$ towards bigger permeability values. This might indicate that the parameter $\hat{t}_c$ chosen is too low, since the permeability shifts towards higher values to compensate for a higher specific cake resistance. However, the quality of the obtained fit does not worsen, which must be mainly attributed to a relatively better resolution of the PD at high permeability values. Since the PD for relatively lower $\hat{t}_c$ values is scaled to cover only a part of the distribution axis Φ', the resolution on this part is higher for the same number of nodes.

Reversing the train of thoughts leading to the error estimation from section 5.3.6 one finds that the pressure drop is, of course, most influenced by deviations of the PD at high permeability values. Thus apparently a small advantage in the resolution of these can compensate for a shortcoming in capturing of small permeability values.

The filter test stands are designed to provide best intercomparability between results determined at different test stands. Thus comparable/reproducible results between different experimental runs and different test stands are expected. However, for the determination of a PD this also entails the greatest shortcoming: The test dust is standardized and differs thereby naturally from the dust to be encountered by the filter medium in the application. The PD, however, is depending on the actual dust and extrapolation from the test dust to the actual dust is not a priori possible.

6.1.2 Laboratory scale filter plants

The next step is to investigate laboratory scale filter plants that resemble industrial scale plants in the basic construction and operation. They are, however, smaller and commonly only designed for investigation of various filtration features. Also here operational parameters are usually well defined and known and also the instrumentation of such plants is good. One advantage of such

plants is the regeneration mode which closely resembles the regeneration in industrial plants. Also the operation of laboratory filter plants with the same dust as industrial plants is advantageous, since it overcomes the problems of dust depending PDs.

During this work mainly data gathered by the plants presented by [26] and [25] are used. The former plant is designed for optical cake thickness measurements and henceforth identified as *plant #1*. The latter plant is used to study reactive gas cleaning and is hereafter termed *plant #2*. Both filter plants consist of a dust supply unit that disperses a certain mass flow of dust in air which is sucked through the filter plant. The gas volume flow after the filter is recorded and controlled to a certain set value via a frequency controlled fan. Experiments were conducted with both plants having installed three filter bags which are pervaded by the dust laden gas from the outside to the inside. In order to support filter bags they are mounted on wire cages. Dust particles are retained at the filter bag's outer surface. Due to the dust which is accumulating on the filter bags forming a filter cake the overall permeability of the filter decreases. As the fan keeps the gas volume flow approximately constant the pressure difference over the filter rises. The filter is regenerated either after a certain pressure difference over the filter is reached or after a certain time interval for filtration has elapsed. Filter regeneration is carried out by a reverse air jet pulse. Each filter bag can be regenerated separately. The layout of both plants is according to the basic scheme (see Figure 1.1). The plants, however, differ in the actual specification and scale. Table 6.1 gives an overview of these specifications.

Plant	A_{tot}	$\dot{m}_c$	η_{g}	α_{m}	$\dot{V}$
#	m^2	$\text{kg} \cdot \text{s}^{-1}$	Pa s	$\text{m} \cdot \text{kg}^{-1}$	$\text{m}^3 \cdot \text{h}^{-1}$
1	2.04	$8.4\ 10^{-4}$	$1.8\ 10^{-5}$	$6.67\ 10^9$	240
2	0.53	$1.5\ 10^{-5}$	$2.0\ 10^{-5}$	-	40

Table 6.1: Specifications of laboratory scale filter plants

Only the online measurements of pressure drop over the filter and gas volume flow are used in this work. The measuring locations are shown in the flowchart (see Figure 1.1) indicated by PDC for pressure difference and FC for flow. The dust concentration is calculated according to:

$$c_{\text{sol}} = \frac{\dot{m}_{\text{c}}}{\dot{V}} \tag{6.1}$$

The total dust mass $\dot{m}_{\text{c}}$ conveyed to the filter is set by the dust dosing equipment.

Figure 6.4 shows the start up of filter plant #1 as ramp test. The filter medium is thoroughly cleaned at the beginning of this experimental run and thus does not carry any filter cake. The vertical dashed line indicates the point in time when the dust dosing equipment is activated. Subsequently one observes an increase in pressure difference.

During the pre-experimental phase of this plant special emphasis was put on the quality of data recording of transient pressure drop and volume flow data. In

addition the gas flow control loop which consists of an orifice flow measurement
and a frequency controlled fan was optimized to achieve fast transient perfor-
mance, thereby minimizing the effect of sudden pressure drop changes on the
gas volume flow as encountered during filter cleaning. However, the controlled
gas volume flow changes slightly due the response time of the control loop. To
account for a not perfectly constant gas volume flow the measured pressure drop
is corrected to a single set volume flow according to equ. (6.2).

$$\Delta p = \Delta p_{\exp} \frac{\dot{V}}{\dot{V}_{\exp}} \tag{6.2}$$

For the application of the PD-method this correction enables the direct use of
the constant volume flow model section 2.4. However, from equ. (2.19) it is clear
that only a fraction of the pressure drop and volume flow is relevant. Equ. (6.2)
is merely contracting this fraction into the single variable Δp for the ease of
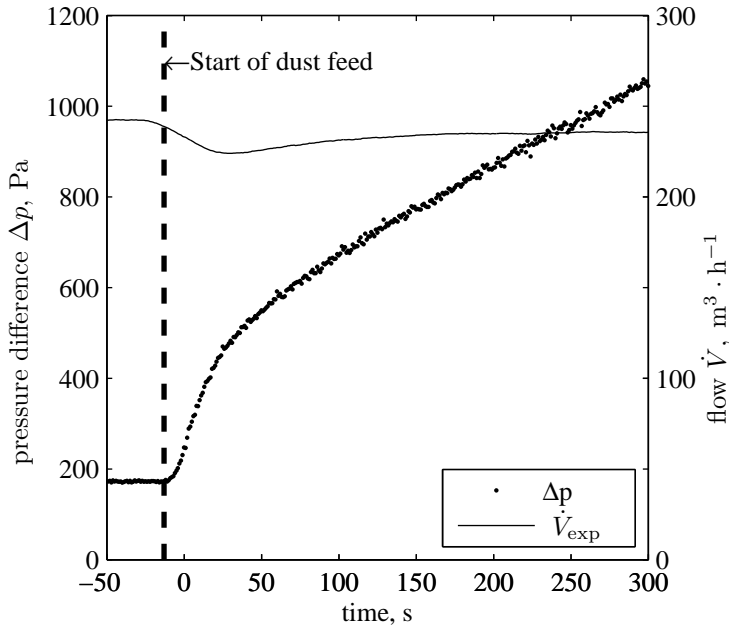further treatment.

Figure 6.4: Experimental pressure drop profile in the experimental plant #1.
The pressure drop is corrected for the flow variation according to equ. (6.2).

The pressure drop curve has a positive curvature for the short period of 15-
20 seconds after dust dosing started. During this period the dust concentration
in the filter housing is increasing until it reaches a constant value. The filter
plant is equipped with an optical measurement system, i.e., a glass window
is installed in the filter housing and the increase of dust concentration can

be observed qualitatively. Also the average gas residence time in the filter housing is in the observed range of time. The filter housing contains a raw gas volume of approximately $0.8 \, \text{m}^3$ which leads to an average residence time of $12 \, \text{s}$ at the operation point displayed. Assuming infinite backmixing in the filter housing, which is justified given the turbulence observed in the filter housing, $80 \, \%$ of the final dust concentration is reached after approximately $19 \, \text{s}$. More interestingly the curvature of the pressure drop curve changes when a constant dust concentration in the housing is reached. A pronounced concave curved pressure drop profile can be observed.

Finally the transient pressure drop increases linearly, which can be explained by a practically equalized permeability profile over the filter. This entails homogenous flow and an isotropic cake builds up homogeneously. The slope of the transient pressure drop asymptote can directly be used to obtain the specific cake resistance α_{m} by combining equs. (2.4) and (2.8) for an equalized permeability, i.e., no dependency on filter location A has to be considered:

$$\alpha_{\text{m}} = \frac{1}{\eta_{\text{g}} \, c_{\text{sol}}} \left(\frac{A_{\text{tot}}}{\dot{V}} \right)^2 \lim_{t \to \infty} \frac{\text{d}\Delta p}{\text{d}t} \qquad (6.3)$$

For practical use one cannot employ the limit but should restrict time t to sufficiently large numbers, i.e., where the pressure increase is linear within the error of measurement.

The PD corresponding to the pressure drop ramp from Figure 6.4 is displayed in Figure 6.5. The integral mean value can be displayed in addition. Note that in this figure the abscissa is linearly scaled and thus the area on the left hand side of the PD and the mean value curves are equal.

The basic shape of the PD found resembles the PD found in the filter test rig in section 6.1.1 with a significant step in the PD, whereas a small part of the area exhibits a high permeability.

In filtration plant #2 filter cloth condition experiments with reactive dust are carried out. Details to this test series can be found in [25]. The basic features are similar to the filtration plant #1 presented already. The different plant specifications are given in Table 6.1. The specific cake resistance value is not reported there, because several different values are determined corresponding to each filter start-up.

The aim of the experiments is to study the conditioning of filter media at an elevated temperature of $140 \, ℃$ over time. The sample dust used is CaO and $Ca(OH)_2$ respectively, which is suspended in a simulated flue gas atmosphere containing H_2O and CO_2. These compounds are especially reactive towards CaO forming reaction products such as $Ca(OH)_2$ and $CaCO_3$. Since the reaction products have a significantly higher molar volume than CaO a mechanical expansion of the reacting particles is expected. In the flue gas atmosphere most residence time is provided whilst the particles are deposited on the filter medium, i.e., in the filter cake. During the conditioning period some particles might even penetrate inside the filter medium and react there. A mechanical growth of the particles there can lead to pore blocking, rendering normal filtration impossible. In order to minimize the possible particle penetration with
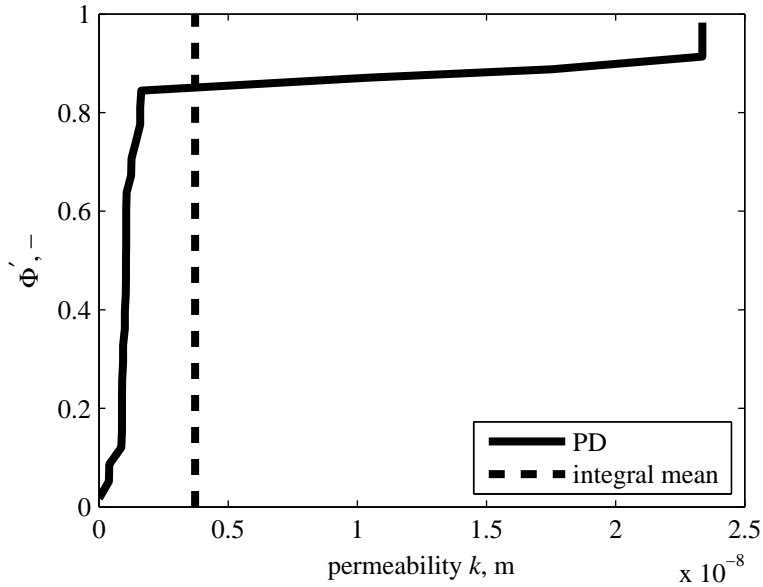
Figure 6.5: PD determined for a ramp test in the filtration plant #1

CaO particles a pre-conditioning is carried out with $Ca(OH)_2$ which is intended to fill easily penetrable voids in the filter medium and thereby preventing CaO to penetrate into these voids in the subsequent conditioning period.

For the experimental simulation of the possibly slow hydration and carbonation reaction 120h filtration experiments are conducted with an initially virgin cloth. Once every day filtration is stopped, the filter is thoroughly cleaned with the pulse jet system to determine the cloth permeability. Subsequently ramp tests on the clean filter cloth are performed. In Figure 6.6 the PDs determined from these ramp tests are displayed for a conditioning test with CaO dust on a certain cloth.

The PD of the filter cloth changes dramatically in the course of the conditioning period. On the first experimental day a step in the PD at about 50 % of the filter is observed with again a high and low permeability level. In the course of cloth conditioning this step shifts upwards and a relatively smaller area with a high permeability remains. The actual permeability values on these steps interestingly remain similar.

From this data the characteristics proposed in section 3.2 can be calculated and are shown in Figure 6.7. According to the expectations the initial pressure drop value Δp_0 is increasing over the conditioning period reflecting the decreasing integral resistance of the filter cloth. Eventually the initial pressure drop is approaching a constant level.
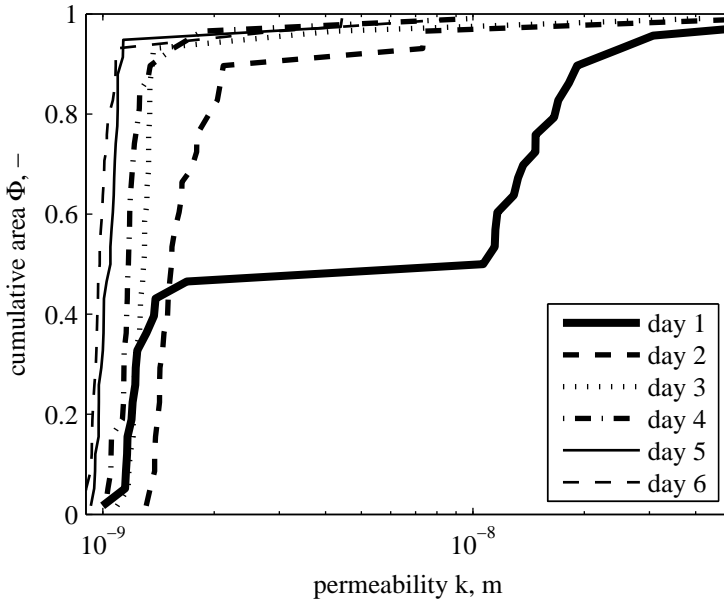
Figure 6.6: PD determined for a ramp test in the filtration plant #2

The asymptotic pressure drop offset on the ordinate $\Delta\tilde{p}_0$ is always above Δp_0. The broad PD on the first experimental day is reflected in a fairly large difference between Δp_0 and $\Delta\tilde{p}_0$. This span is thereafter reducing slightly.

The initial pressure drop slope augmentation κ_s is significantly increasing during the experimental period. This is a result of the increasingly skewed PDs as the condition period proceeds[1]. Practically that means that the pressure drop initially increases very fast, with a factor up to 13 from linear. Thus the pressure drop curve is approaching the asymptote quickly. In this situation the filtration behavior resembles more a homogeneous cloth with the initial pressure drop $\Delta\tilde{p}_0$. The actual initial pressure drop value Δp_0 is not really significant for the filter performance.

6.1.3 Pilot and industrial scale plants

The pressure drop data from bigger filtration plants is in principle similar to the data gathered in laboratory scale. However, there the filtration unit is part of a process which imposes external influence on the filter operation. Operational parameters such as gas volume flow, dust concentration, dust properties et cetera are determined by the process operation and can hardly be set directly.

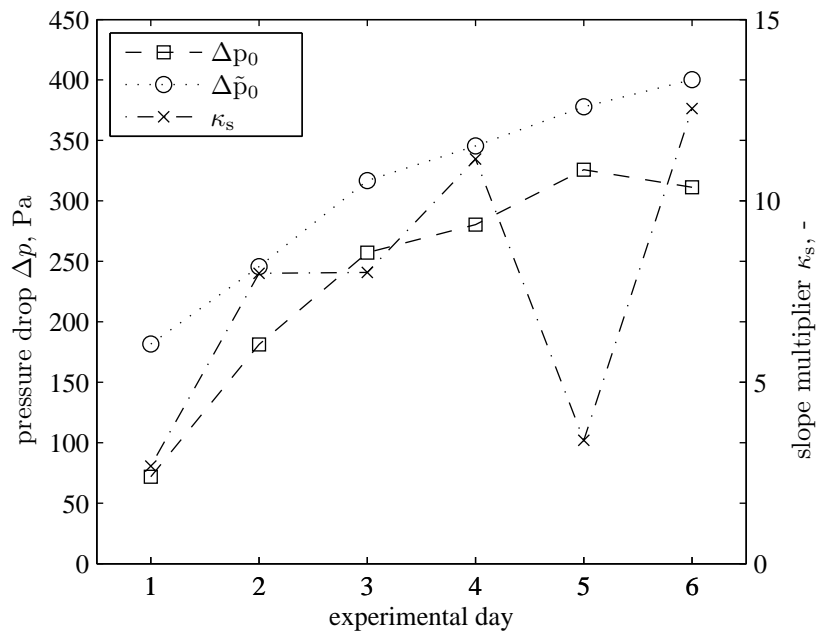[1]Note that the skewness of a distribution is described by its third order moment.

Figure 6.7: The characteristic values of the PDs versus the experimental period: initial pressure drop, asymptotic ordinate intersection and pressure drop slope multiplier.

Also in laboratory scale tests feed back of periodic filter cleaning on the gas volume flow is observed. This intrinsically semi-continuous filter operation can feed back into the otherwise continuous plant operation. In turn back coupling on the filter operation, as described by [27] for a pilot scale plant, can be observed. E.g. a changing dust mass flow violates the assumption of the PD-method. Thus special care must be taken when using pressure drop data from industrial plants. Additionally, industrial plants are often equipped with limited instrumentation, which makes it even difficult to recognize such a violation. Nevertheless, when detailed information about the changes in dust mass flow are available a corresponding correction, i.e., an appropriate time scaling, may be applied and the PD-method can eventually be applied.

The study presented by [28] makes use of the PD-method to characterize the filtration behavior while changing dust properties including the dust mass flow. Measurements are made in an industrial scale bag filter plant which is cleaning the off-gas of a cement plant. The bag filter is retrofitted after an electrostatic precipitator (ESP) and enhancing the dust collection efficiency to meet emission standards. During ordinary plant operation most dust is removed by the ESP and only a rather small dust concentration is reaching the bag filter.

The experimental parameter is the impact of the ESP on bag filter operation. The plant is operated with the ESP in operation and with the ESP switched off. In Figure 6.8 the recorded measurement signals of volume flow and pressure drop are shown for the experiment with the ESP in operation. Compared to the laboratory data presented in the earlier section the data quality is clearly worse, with much noise in the pressure drop signal. Initially the normal operation of the filter is shown. At about $7000\,\text{s}$ the filter is extensively cleaned until no further reduction of the pressure drop can be observed. Since dust is continuously reaching the bags, some cake will always be present on the bags as cleaning the entire filter once, i.e. pulsing every row once, takes about 90 seconds. However, according to the definition above the filter is considered sufficiently clean thereafter. Then the pressure drop is allowed to build up without further filter cleaning. This ramp is used to determine a PD.

In this plant the information on the amount of dust reaching the filter bags is not available and thus the dust concentration is unknown for both ESP in operation and ESP switched off. This is overcome by determining the entire parameter t_c from the linear part of the pressure drop ramps directly, instead of just determining α_m as described in section 6.1.2. Of course two different t_c values for the operation with and without ESP must be determined. To extract more interpretable information from these values the definition equ. (2.23) can be used to calculate the product $\alpha_m \cdot c_{sol}$, since the volume flow $\dot{V}$ and the filter area A_{tot} are known.

Figure 6.9 shows two PDs determined for the pressure drop ramp discussed above and a corresponding ramp where the ESP is not in operation. This result clearly shows the dependency of the PD on the dust properties. The filter setup and plant operation remain unaltered during these tests. Only the amount of dust and probably also its properties, such as the particle size distribution,
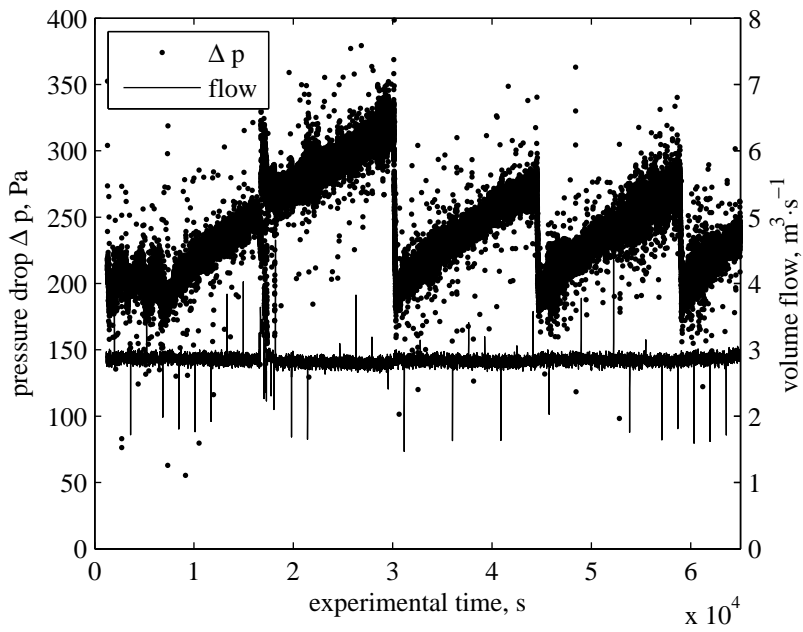
Figure 6.8: Pressure drop and volume flow measurements in an industrial bag filter plant with an upstream ESP in operation.

change when the ESP is switched off. In turn the filtration behavior on the same cloth is altered.

Generally the PD with the ESP in operation is spread over a wider range of permeability values, i.e., a broader distribution is found. After the ESP only the fines reach the bag filter, and fine particles pose the greater challenge to the bag filter, than a coarser fraction [29]. The parameter t_c, which differs by almost a factor 100 between the two runs, accounts for the possible change of the specific cake resistance and the absolute difference in dust mass.
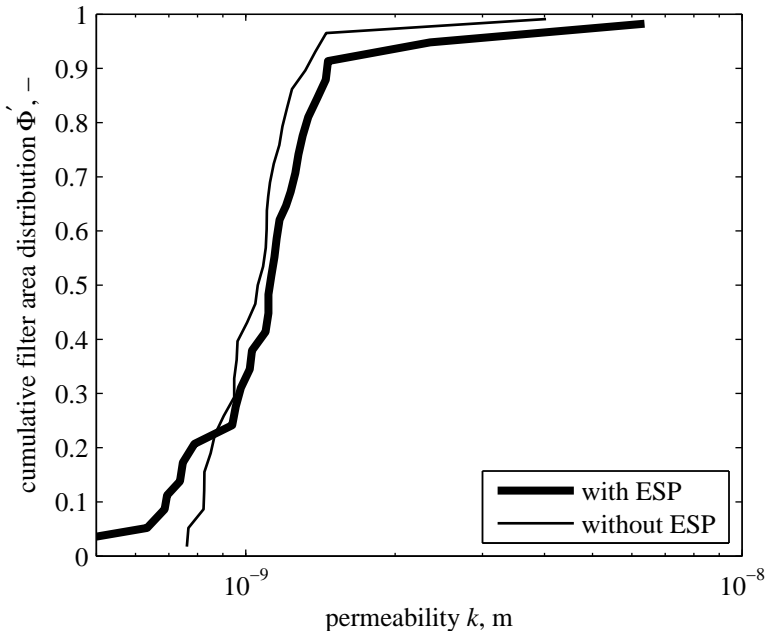
Figure 6.9: PDs determined for the filter operation with and without the ESP in operation.

In Figure 6.10 a comparsion is displayed between the calculated pressure drop cuves generated by the two PDs from Figure 6.9 using the t_c-value determined the operation with the ESP on. The initial pressure drop rise caused by the more pronounced PD with the ESP in operation is clearly visible. After that initial increase the pressure drop curves converge towards a the same slope of the final asymptote, since t_c is the same for both curves.

6.2 PDs from filter operation

In section 6.1 the determination of a PD of the clean filter medium itself is addressed. However, a filter can exhibit an inhomogeneous PD also because of

Figure 6.10: Calcuated pressure drop profiles determined from the PDs with and without ESP in operation using the same t_c-value.
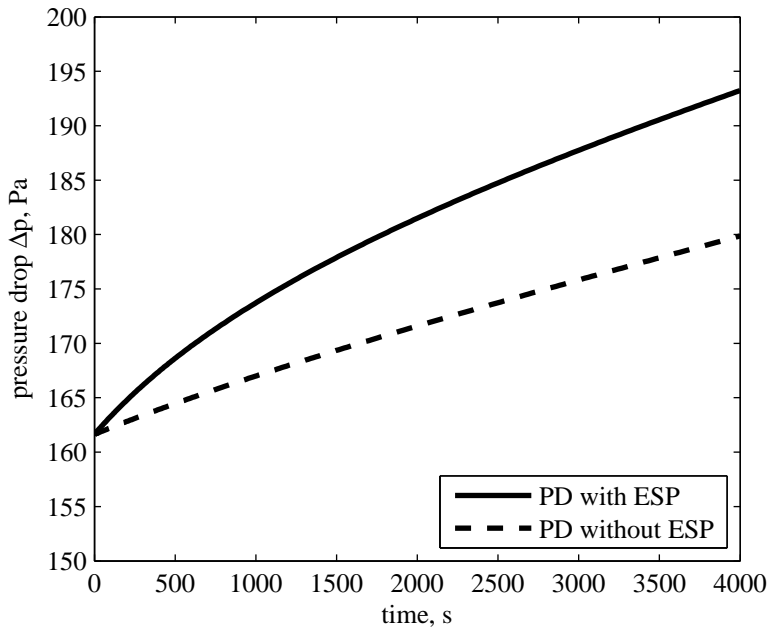
an uneven residual cake distribution. Residual cake refers to filter cake present on the filter cloth at the beginning of filtration. Such cake originates from incomplete filter cleaning.

Kavouras and Krammer [20] give an extensive literature overview on reasons and applications for such incomplete cleaning. Two reasons are reported leading to a residual filter cake. On the one hand the filter cake might not be removed entirely from a filter medium that is exposed to regenerative action. E.g. Humphries and Madden [30] and Seville et al. [16] describe this phenomenon termed patchy cleaning. It refers to filter cake that is partially completely removed from the filter medium, but patches stay unchanged on the filter medium despite a cleaning action. Duo et al. [17], Ju et al. [18], and Dittler et al. [31] focus mainly on patchy cleaning of the filter medium for their pressure drop simulations. Also Kavouras and Krammer [20] consider patchy cleaning for the simulation of filter pressure drop.

On the other hand only a part of the filter area is exposed to a cleaning action at one time in industrial filters. Typically one filter compartment or one filter bag row is cleaned at once, whereas the remaining filter area is unaffected. This easily conceivable mechanism also leads to an uneven distribution of filter cake over the filter area. Kavouras and Krammer [20] discriminate between patchy cleaning and sequenced filter cleaning as reasons for incomplete cleaning for filter simulation. Duo et al. [17] only mention the possibility for an inhomogeneous cake distribution due to sequenced filter cleaning.

However, the effect on filtration when residual dust cake is present can be described in the same framework as an inhomogeneous filter medium. Filter areas carrying residual cake patches have a lower permeability than clean filter area or area carrying a thinner residual cake. The filter medium and the residual cake as entity have a distributed permeabilty, which is corresponding to the cake distribution. The filter model and PD-method can therefore be directly applied to this type of problem too. The models presented by Duo et al. [17] and Kavouras and Krammer [20] are shown to be embraced by the filter model presented in section 2. Under certain provisions concerning cake compressibility also the model of Ju et al. [18] is captured. This equivalence of the models is based on the same approach with a 1-dimensional flow description and the correspondingly identical governing equations. In line with the literature models the PD stems only from a residual cake distribution. The filter cloth is, as in the literature, homogeneous itself and is thus not contributing to the PD.

6.2.1 Patchy cleaning

In this section patchy cleaning is looked at separately, i.e., without any influence from segmented filter cleaning. During semi-continuous filter operation several cake generations are present on the filter cloth. In Figure 6.11 such patchy cleaning is depicted for data from the model by Kavouras and Krammer[20]. On the ordinate axis the cumulative area distribution is shown. In the left most part the fractional area distribution of the cake area load is displayed. The situation immediately after cleaning is depicted. Generation 1 in the uppermost

part of the figure represents the clean filter cloth, i.e., the part of cloth from which cake was successfully removed. The generation 2 area depicted below is carrying the residual cake which was not removed at cleaning. The cake area load corresponds to the filtration on the clean filter cloth for one filtration cycle. The area carrying generation 2 is smaller than the cleaned area generation 1, because a part the filter cake from generation 1 is removed at cleaning, and thereby becomes generation 1 again in a new cycle. Generation 3 stems from the part of generation 2 where cake is not removed at cleaning. During one filtration cycle additional cake builds up onto the already present generation 2 cake, thereby forming generation 3. Kavouras and Krammer[20] outline this mechanism in detail.

By considering the filter cleaning mechanism one finds that the cake building up on the generation 1 spot will reach the cake thickness of generation 2 during one filtration cycle. Upon filter cleaning, part of this cake will be removed, whereas the rest stays on the cloth unchanged, thereby forming generation 2. In other words the thickness of cake generation 1 before cleaning equals the cake thickness of generation 2 after cleaning. This applies correspondingly to all generations.

According to the notation of the filter model from chapter 2 the cake thickness in terms of cake area load is corresponding to a certain permeability k according to equs. (2.2) and (2.3). The filter cloth permeability is constant. Hence the cake area load can be converted into the permeability which is displayed in the center of Figure 6.11. Please note that further on in this chapter the nomenclature refers to k as the overall permeability of cake and cloth, whereas k_0 denotes the initial permeability. This is necessary to be consistent with the nomenclature for the filter model presented in chapter 2. In the case of patchy cleaning the initial permeability comprises of contributions of both, filter cloth and filter cake. For a consistent nomenclature the initial filter cake must be included in the initial permeability k_0. However, as in the chapters before this index 0 is omitted, since PDs are only displayed for the initial permeability.

Periodic filter operation at period one implies that the pressure drop curve between two subsequent cleaning actions is identical for all cycles. This, however, corresponds to a certain change in filter state s defined by equ. (2.12) which is only depending upon the pressure drop. For periodic filtration a filter state s_{cyc} shall be defined as the filter state change during one cycle, i.e., evaluation of equ. (2.12) for one cycle. This filter state change applies of course to all filter generations. In the rightmost chart in Figure 6.11 the abbreviation $k^{-2} = u$ is depicted. The steps between the separate generations have the same height, which results from equ. (2.13) governing the permeability evolution. The height of the steps is s_{cyc} which is shown in the figure for the generations 2-4.

Hence by knowing the area distribution of the cake patches and s_{cyc} the distribution of cake on the various generations is analytically known. The permeability at the beginning of filtration for each generation can be easily calculated according to

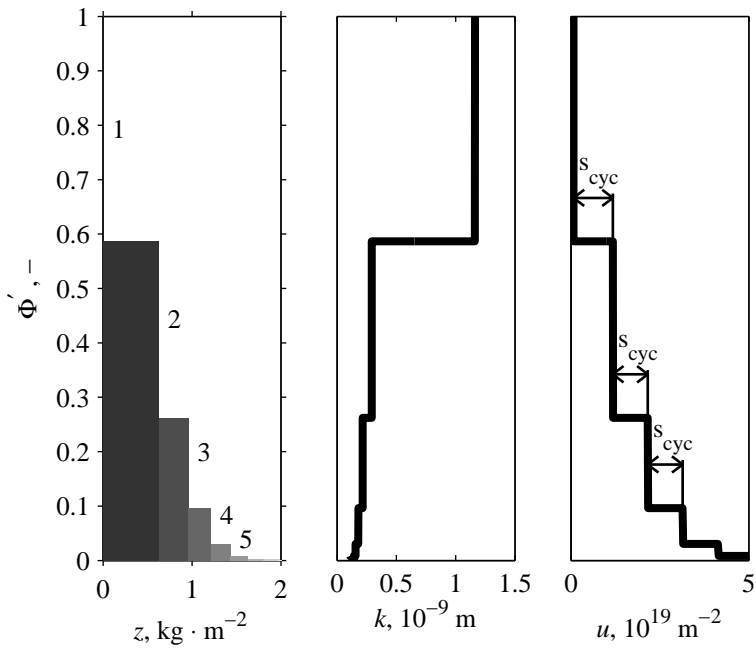$$k_i = \left[k_0^{-2} + s_{cyc} \cdot (i - 1) \right]^{-\frac{1}{2}} \tag{6.4}$$

Figure 6.11: Patchy cleaning on a homogeneous cloth with 10 cake generations calculated, but the generations 6-10 cannot be discriminated clearly, because they cover an almost negligible part of the filter area. Left: cake area load z, center: permeability k, right: $k^{-2} = u$.

The constant cloth permeability is denoted k_0 and i is the index for the cake generation. Generation 1 is without cake. Thus it trivially has the permeability k_0.

The filter state change s_cyc can be determined from the filter operation mode. This only requires a line search of the respective filter state s_cyc. E.g. for constant flow filtration with a maxium pressure drop control the corresponding s_cyc value can be determined from equ. (2.24). Filtration at constant cycle time requires a line search in equ. (2.31). The corresponding equations for constant pressure filtration are equs. (2.21) and (2.20), respectively.

For the filter model the filter area $\mathrm{A_{tot}}$ is divided into areas A_i carrying a cake generation i. The density PD function can thus be written as

$$\varphi'(k) = \frac{1}{\mathrm{A_{tot}}} \sum_i A_i \delta\left(k - k_i\right) \qquad (6.5)$$

whereas δ denotes the Dirac delta function. The cumulative distribution can be obtained by integrating equ. (6.5).

For the determination of the generation area distribution different approaches have been in used. Kavouras and Krammer [32] use a parametric distribution of filter cake to account for the inhomogeneously deposited filter cake. The main aim of that work is to simulate the bag filter as a gas-solid reactor, and therefore the history of the solid dust is of interest. In later work they, however, replace that parametric cake distribution by a mechanistic cleaning implementation outlined below. The direct parametric implementation straightforwardly gives the A_i values.

Duo et al. [17] model patchy cleaning as the complete removal of the filter cake from the a constant area fraction of the filter medium. This fraction is independent of the cake load.

However, studies such as DeRavin et al. [33] suggest a dependency of the actually cleaned area fraction upon the filter cake area load, arguing that the dislocation forces acting on the cake when the filter is cleaned depend on the cake mass. Ju et al. [18] and Kavouras and Krammer [20] incorporate such a relation for filter simulation. They assume that the fraction of cake removed is a function of the actual cake area load for each generation.

For such a cake area load dependent cleaning function $f(k)$, which is denoting the fraction of removed cake, one can recursively describe the area evolution as:

$$A_{i+1} = (1 - f(k_{i+1}))A_i \qquad i = 1, 2, \ldots \qquad (6.6)$$

The first cake generation is present on the accumulated cleaned area originating from all cake generations:

$$A_1 = \sum_j f(k_{i+1})A_i \qquad (6.7)$$

Note that the cleaning fraction depends on the initial thickness of the generation $i + 1$, which is the thickness before cleaning of the generation i. The cleaning

function is written here to depend on the overall permeability k, which directly corresponds to the cake area load. For the model used by Duo et al.[17] the relation is even simpler, since the cleaning function f is constant and does not depend on the cake thickness.

6.2.2 Segmented filter cleaning

During segmented filter cleaning the filter is divided into several sections, that are cleaned in sequence. This leads also to different areas of the filter carrying cakes of different thicknesses. For the isolated discussion of segmented filter cleaning the cloth is again assumed to be homogeneous and patchy cleaning is not considered either.

During periodic operation the pressure drop profile is identical between two subsequent cleaning actions. This is of course only true when it is always the same filter area which is cleaned, which implies that usually the segments are of equal size in terms of filter area and that any cleaning action the same number of segments is being pulsed.

For a filter divided into p equal segments it takes p cycles before a certain segment is cleaned again. Using the above definition of the filter state change per cycle s_{cyc}, the total filter state change on a segment between two cleaning actions on that very segment is $p \cdot s_{\mathrm{cyc}}$. The permeabilities after cleaning on the various filter sections can be calculated as:

$$k_j = \left[k_0^{-2} + s_{\mathrm{cyc}} \cdot (j-1) \right]^{-\frac{1}{2}} \qquad j = 1 \ldots p \tag{6.8}$$

Thus the PD for segmented filter cleaning in periodic operations with the definition of the permeability k_j according to equ. (6.8):

$$\varphi'(k) = \frac{1}{p} \sum_j \delta\left(k - k_j\right) \tag{6.9}$$

The main advantage of the proposed analytic filter model compared to the literature models cited, is the analytic time integration. Hence the need to numerically integrate coupled differential equations [20] or a single differential equation [17] is replaced by a simple line search procedure. In addition the PD caused by patchy cleaning and/or segmented cleaning during periodic operation is obtained analytically. This PD corresponds directly to the cake generations mentioned in literature.

Ju et al. [18] use a constant pressure model and also determine the area distribution for periodic filtration analytically. They do, however, not give an analytic expression for the time integration and hence the cake thickness distribution.

6.3   Combined effects: filter medium – filter operation

An inhomogeneous cloth, patchy cleaning, and segmented filter cleaning might occur all together. E.g. Kavouras and Krammer [20] use a model mirroring both effects, patchy cleaning and segmented cleaning. The PD corresponding to their model for periodic operation when one segment is pulsed at once is given by:

$$\varphi'(k) = \frac{1}{A_{\text{tot}}} \sum_j \sum_i A_{j,i} \cdot \delta \left[k - \left(k_0^{-2} + [(j-1) + (i-1) \cdot p] \cdot s_{\text{cyc}} \right)^{-\frac{1}{2}} \right] \quad (6.10)$$

For segmented cleaning the PD of the filter cloth replaces the constant cloth permeability on cleaned area. This PD of the filter medium as tackled in section 6.1 should be denoted $\varphi'_{\text{cloth}}(k)$. When cake builds up on an inhomogeneous cloth, the cake build up for every segment is uneven. Therefore the entire PD of the filter cloth must be shifted for each segment, instead of just the integral cloth permeability as in equ. (6.8). These combined effects are captured by equ. (6.11).

$$\varphi'(k) = \frac{1}{p} \sum_i \varphi'_{\text{cloth}} \left[\left(k^{-2} - (i-1) \cdot s_{\text{cyc}} \right)^{-\frac{1}{2}} \right] \quad (6.11)$$

The combined consideration of patchy cleaning and a PD on the filter cloth leads to a possible interdependency of the separate effects. Patchy cleaning is reported to depend on cake thickness. During cake build up on an inhomogeneous cloth, cake builds up unevenly as shown earlier. Hence, the cleaning effectiveness might depend upon the cloth PD. The cleaned fraction per cleaning action can thus vary depending on the filter cloth. In addition the cleaned cloth area has a different PD than the entire filter. This can, of course, be mirrored by the present filter model. However, an actual cleaning model is required to describe the evolving PD. Under the assumption that patchy cleaning does not depend on filter cake thickness the closed form PD evolving during periodic operation is analogue to equ. (6.11).

6.4   Pressure drop data from semi-continuously operating filters

Hitherto, only pressure drop profiles, that clearly show a negative curvature, have been used to apply the PD-method, i.e., either ramp tests or clearly resolveable filter cycles were required to determine a PD. However, in industrial plants it is frequently impossible to carry out ramp tests, since a plant startup requires the simultaneous startup of all unit operation and defined conditions for the filter startup cannot be provided. In addition, the semi-continuous operation does not clearly resolve the filtration and cleaning cycles. Frequently cleaning

pulses are carried out in quite short succession to keep the pressure drop level within narrow limits. From a process control point of view, small filter pressure drop variations are certainly favorable, because they generally prevent negative feedback from excessively fluctuating plants as described in [27].

6.4.1 Raw pressure drop data - data quality

Figure 6.12 the pressure drop pattern of a cement plant filter is displayed over slightly more than an hour. This industrial filter consists of 8 filter sections that are cleaned in sequence. Each section consists of 5 bag rows and the total filter area of the plant is $A_{tot} \approx 700 \, m^2$. A pressure drop measurement is installed across the entire filter and across one specific filter section. The filter is operated within a narrow pressure drop band between the start to the end of a filtration cycle. In Figure 6.13 only the first 15 minutes of the filter operation are
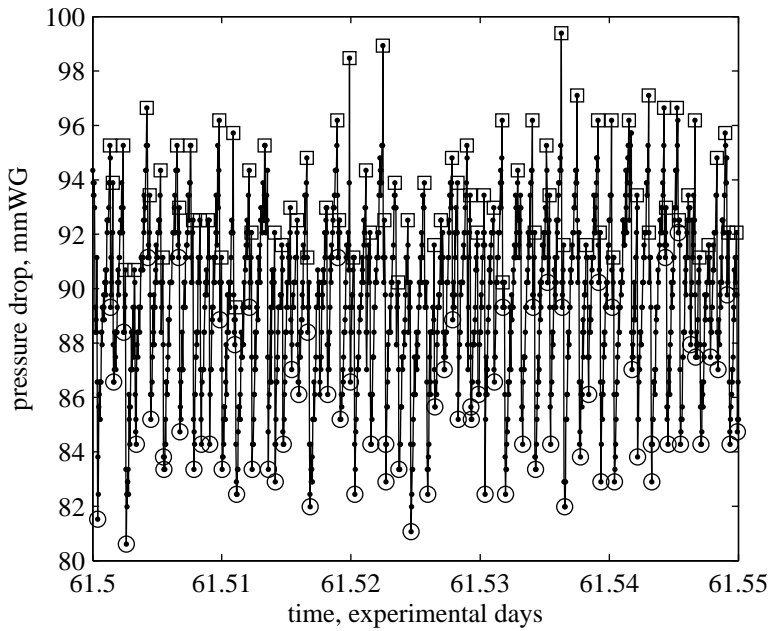
Figure 6.12: Pressure drop across a filter section for the semi-continuous operation in a cement plant filter. The minima and maxima of separated filter cycles are highlighted by circles and squares, respectively.

displayed. Both, the pressure drop signal across the filter segment and across the entire filter including inlet and outlet are displayed. The pressure drop across the filter is higher, but is closely resembling the pattern of the pressure drop across the section. In this figure the cleaning cycles can be distinguished

from each other. Typically only one to two segments of the filter are cleaned at
the end of a filtration cycle.

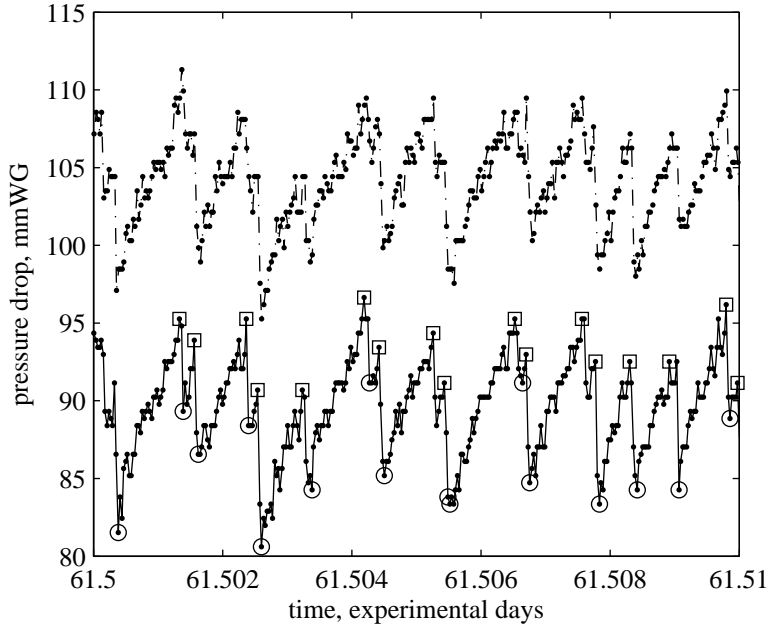Figure 6.13: Enlargement of beginning of Figure 6.12. In addition the pressure
drop measurement across the entire filter is displayed.

The resolution of the measurement setup is fairly coarse at 0.5 mmWG. The
latter is illustrated in the histogram Figure 6.14. The pressure drop axis is
divided into small bins of equal size and the number of actual pressure drop
measurements in each bin is counted. It is found that in the measured pressure
drop range spanning from 77.86 mmWG to 104.88 mmWG only 61 actually dif-
ferent values are recoded, which must be attributed to a coarse digital resolution
of the measurement signal. The recorded values do not show a smooth distri-
bution over the non-empty bins either, but approximately every second bin is
populated with only about one third measurements than neighboring bins. The
reason for this apparent artifact is not known, but it can be speculated that the
coarse digital resolution is not even, i.e., the actual bin widths are possibly not
equal.

6.4.2   Idealized number distribution of pressure drop sam-
ples

The resulting pressure drop increases during one cycle as depicted in Figure 6.13
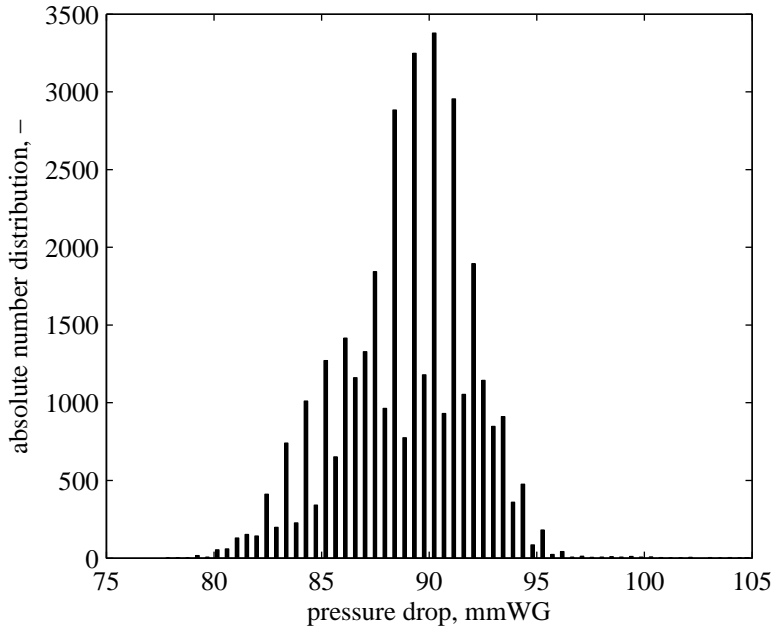cannot be used directly to apply the PD-method, since the fluctuations are

Figure 6.14: Histogram of the pressure drop measurement points for one day.

significant, partly due to the coarse resolution. Moreover only a very limited number of points, i.e., 10-30 per cycle, are recorded. However, the distribution of the pressure drop points is looked at closer to extract further information from the pressure drop profile.

To illustrate this concept an idealized periodic filter operation as depicted in Figure 6.15 is considered initially. The depicted filtration cycles repeat themselves identically in terms of pressure drop. Typically one measured points on this pressure drop pattern. Under the assumptions that

- the filter regeneration does not consume a significant amount of time compared to the filtration time, i.e., is negligible in the pressure drop plot, and

- that the actual pressure drop measurements are taken at a constant sample rate

the cumulative number distribution of the discrete pressure drop measurements, which can stretch over many cycles, is an estimator for the underlying pressure drop increase during each cycle.

To illustrate this statement, the number density distribution of the measurement time t must be considered, which is termed $q_t(t)$. Since the sample time is equal the density function of time distribution of the measurements $q_t(t)$ must be constant, i.e., all sample times are equally likely. This density can then be
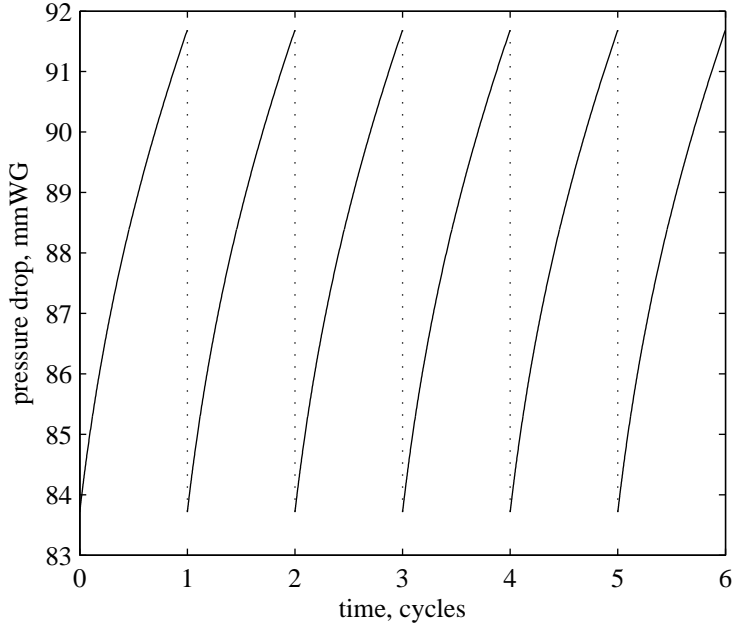
Figure 6.15: Schematic periodic filter operation.

converted into the pressure drop density function $q_{\Delta p}(\Delta p)$ by considering the mapping of the time axis via the pressure drop curve $\Delta p(t)$. Any time interval $[t, t + \mathrm{d}t]$ is mapped on the pressure drop axis onto $[\Delta p, \Delta p + \mathrm{d}(\Delta p)]$ which is described by:

$$q_{\Delta p}\mathrm{d}(\Delta p) = q_t\mathrm{d}t \tag{6.12}$$

Integrating via the pressure drop Δp gives:

$$\int_{\Delta p_{\mathrm{low}}}^{\Delta p} q_{\Delta p}\mathrm{d}(\Delta p) = q_t t(\Delta p) \tag{6.13}$$

The function $t(\Delta p)$ is the inverse function to the pressure drop relation $\Delta p(t)$. The integration limit Δp_{low} is the lowest measured pressure drop value and is chosen, because the inverse function, of course, does not exist for lower pressure drop values. The LHS of equ. (6.13) is the cumulative distribution function $Q_{\Delta p}$:

$$Q_{\Delta p}(\Delta p) = \int_{\Delta p_{\mathrm{low}}}^{\Delta p} q_{\Delta p}\mathrm{d}(\Delta p) \tag{6.14}$$

This distribution can be estimated from the pressure drop values of the separate measurements using e.g. a kernel density estimator for $q_{\Delta p}$. The time compo-

nent of the measurements is not used and thus any pressure drop measurement irrespective of the cycle might be used, i.e., the benefit of the method is, of course, that many pressure drop cycles can be used as input to determine $Q_{\Delta p}$. However, the time scaling of pressure drop function $t(\Delta p)$ cannot be determined from this method. I.e., the proportionally constant q_t which is scaling the time axis cannot be determined inherently from the scheme outlined above. For the example given in Figure 6.15 the scaling would be $q_t \equiv 1$ to scale the pressure drop increase on exactly one cycle time. Practically the scaling with an actual (mean) cycle time t_{cyc} is useful.

From Figure 6.15 it is clear that the inverse function $t(\Delta p)$ does not exist unambiguously for the entire time axis, but just for one cycle and the singularity at the filter regeneration is not considered. Since the cleaning duration is required to be insignificant, it is assumed that he pressure drop measurements during cleaning do not significantly affect the estimated distribution.

6.4.3 Varying cycle times and acyclic pressure drop patterns

In section 6.4.2 it is assumed that the pressure drop cycles repeat themselves identically in terms of pressure drop. Unfortunately, this is not always a justified assumption, as only a glance at e.g. Figure 6.13 reveals. The actual duration of a pressure drop cycle is varying and not constant and also the lower and upper pressure drop values fluctuate. Such behavior might arise from influence of other unit operation in the plant, variations of filter operating parameters, errors in the pressure drop measurement and consequently inaccuracies in filter control.

To be able to account for such variations a correction is introduced for the pressure drop span of a single filter cycle. It is assumed that all recorded filter cycles have in principal the same underlying pressure drop increase, but only different parts of that increase are actually recorded. Which part of a certain filter cycle is recorded, is determined from the minimum and the maximum pressure drop value of a specific cycle.

The situation for varying the minimum pressure drop value is shown schematically in Figure 6.16. The underlying pressure drop curve is shown as dashed curve from time -1 to 0. The actually available pressure drop consists of 4 numbered cycles of respective parts of the underlying pressure drop curve, which are starting from different lower pressure drop values. The cycle durations vary correspondingly. Directly applying the density estimation scheme outlined in the section above fails, because the different starting points of the cycles will influence the distribution of the pressure drop measurements. E.g., in Figure 6.16 all four cycles are available to be recorded at pressure drop levels above 87 mmWG, but only three cycles are available between 85 mmWG and 87 mmWG. To give pressure drop values in this range the same weight as above 87 mmWG the pressure drop density distribution $q_{\Delta p}$ in this range must be weighted by $\frac{4}{3}$. From 84 mmWG to 85 mmWG only one of four cycles is available which must be weighted with a factor 4. Such weighting is, of course, at the expense of

accuracy, and practically only the pressure drop range that is recorded in many
cycles can be used further. An analogue discussion applies to varying maximal
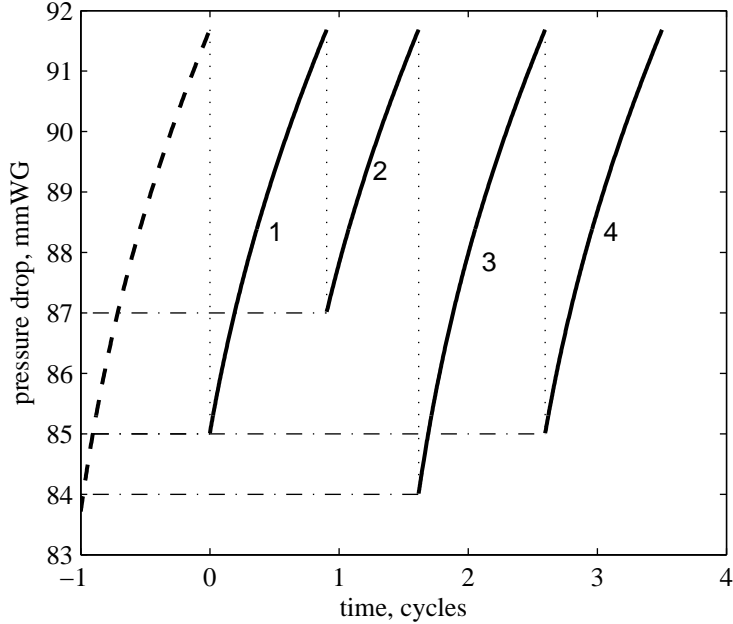pressure drop levels.

Figure 6.16: Schematic pressure drop cycles with varying minimum values.

In a more general notation the actual parts which are recorded of each filtra-
tion cycle can be accounted for by another distribution function: The number
distribution of the minima and maxima. These distributions can be estimated
from the minimum and maximum pressure drop values determined above. The
cumulative number distribution of the minima is termed $\Theta_{\min}$. Dividing the
density $q_{\Delta p}$ by the cumulative number distribution of the minima yields the
correction described above for the simple example. For the maxima the situa-
tion is analogue, but here the density for pressure drop levels above a certain
value must be amplified. This correction can be summarized as:

$$\hat{q}_{\Delta p} = \frac{1}{\Theta_{\min}} \cdot \frac{1}{1 - \Theta_{\max}} \cdot q_{\Delta p} \tag{6.15}$$

Practically additional information on the minima and maxima of the recorded
pressure drop cycles is required. In Figure 6.13 these values are marked by cir-
cles and squares, respectively. The actual division of the pressure drop data into
cycles is done by a simple pattern recognition routing, which, naturally, is not
perfectly able to determine each filtration cycle correctly. This must be consid-

ered as error. External information on filter cleaning, e.g. from the cleaning system, is not available for the presented dataset, but could also be used.

The situation for the recorded pressure drop data (see Figure 6.12) is depicted in Figure 6.17. The density estimate obtained from raw pressure drop data is shown as bold dashed curve and corresponds directly to the histogram Figure 6.14. The uneven distribution between neighboring columns in the histogram is reflected by oscillations observed in the kernel density estimate $q_{\Delta p}$. The cumulative distributions of the minima is depicted as thin dotted curve. Unfortunately, the oscillations in the density estimate $q_{\Delta p}$ are amplified where the correction requires a stronger weighting, i.e., towards the tails of this distribution. This is, of course, to be expected, since relatively fewer pressure drop cycles were recorded, which actually cover that limited range and thus less input information is available. The actual estimate of the underlying pressure
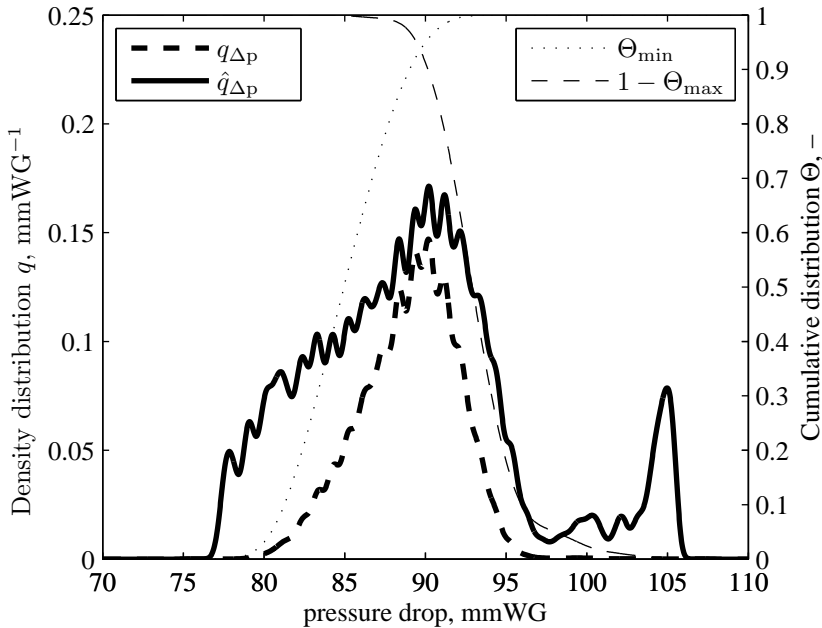
Figure 6.17: Estimated density number distribution (bold, dashed) and corrected density (bold, solid). Cumulative pressure drop minima/maxima distributions.

drop increase is the cumulative distribution $Q_{\Delta p}$. By scaling the corresponding density to $\hat{q}_{\Delta p}$ the scaling of the density is lost, and the integral over the corrected density is bigger than one. This, however, only affects the scaling of the cumulative distribution which is proportional to the time and time information is anyway not conveyed in this distribution form. It must be reintroduced as discussed in section 6.4.4.

6.4.4   Rescaling to a characteristic cycle

The density displayed in Figure 6.17 represents the corrected shape of the underlying pressure drop curve. However, the density does not contain any information on the time scaling. Of course, the non-zero part of the density spans the entire pressure drop band where measurements are available.

A characteristic reference filter pressure drop cycle is defined. The pressure drop of this reference cycle is spanning from the mean pressure drop minimum $\Delta p_{\min}$ to the mean pressure drop maximum $\Delta p_{\max}$. The duration of this reference cycle is the mean cycle time. The mean minima and maxima are calculated from their respective number distributions according to:)

$$\Delta p_{\min} = \int\limits_{0}^{\infty} \Delta p \, \mathrm{d} \left(\Theta_{\min}(\Delta p) \right) \tag{6.16}$$

$$\Delta p_{\max} = \int\limits_{0}^{\infty} \Delta p \, \mathrm{d} \left(\Theta_{\max}(\Delta p) \right) \tag{6.17}$$

The parts of the corrected density $\hat{q}_{\Delta p}$ lying outside the interval $[\Delta p_{\min}, \Delta p_{\max}]$ are disregarded for the determination of the characteristic filter cycle. Thereby, the large error inherent to the tails of $\hat{q}_{\Delta p}$ does not affect the resulting pressure drop distribution.

Since the PD-method is applicable to any part of a pressure drop curve this truncation of the characteristic cycle does not impede the application of the PD-method. Although the error will, of course, become bigger.

In Figure 6.18 two characteristic filter cycles determined by the outlined routine are shown. The solid curve corresponds to the data underlying the Figures 6.12 to 6.17. The characteristic part of the cycle is depicted as bold line and the truncated tails are thin lines. Towards the end of the cycle a turning point in the pressure drop is observed. Probably this turning point must be attributed to an insufficient correction of the pressure drop maxima. The distribution $\Theta_{\max}$ is quite wide and a perfect correction is apparently not achieved.

In addition to the data discussed in this section another characteristic cycle is displayed as a dashed curve. This characteristic cycle is determined from data, which is recorded on the same filter plant after the filter bags were replaced with new ones. The same routine is applied as outlined above on recordings of semi-continuous pressure drop data for 24 h. Preceding the evaluated period, the new filter bags were in operation for about 30 h. The cloth during the evaluated period is hence not directly comparable to virgin filter media.

The maximum pressure drop level of the two characteristic cycles are about the same. Since the filter is cleaned upon reaching a certain pressure drop level this must be expected. However, the cycle time with new filter bags is significantly longer and the operating pressure drop span is also increasing. Thereby a more clearly defined cycle structure in the raw data is present and the error
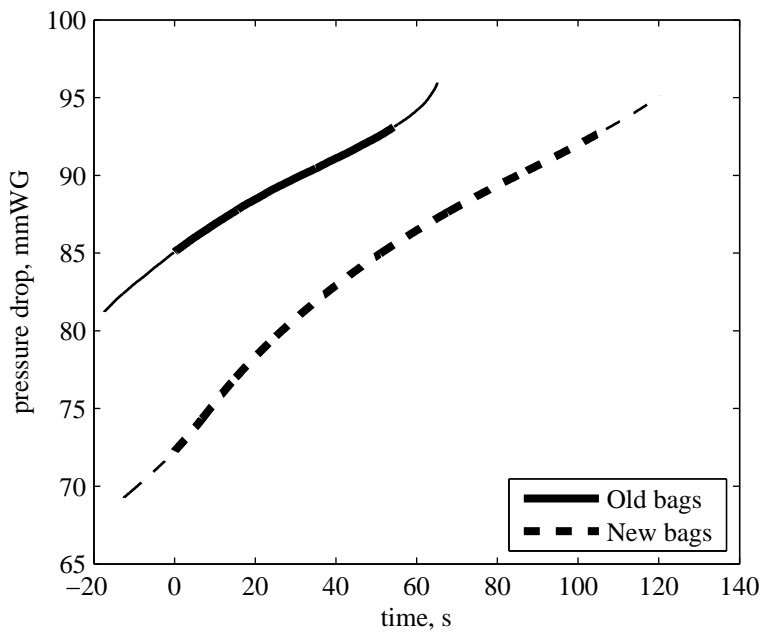
Figure 6.18: Characteristic pressure drop profiles.

towards the tails of the pressure drop distribution is decreasing, since relatively fewer points are close to the beginning or the end of a single cycle (when compared with the total available pressure drop measurements). In Figure 6.18 this fact is articulated by the truncated tails, which continue the characteristic curve. In addition, these truncated tails are relatively short because the distributions of minima an maxima, Θ_{min} and Θ_{max}, are narrower. The latter must be attributed to a more regular pressure drop pattern.

6.4.5   Application of the PD-method

On the pressure drop data displayed in Figure 6.18 the PD-method can be applied directly. It is, of course, not possible to carry out a dedicated ramp test for these characteristic cycles to determine an accurate specific filter cake resistance value. Instead the slope of the final asymptote is estimated from the available curves in Figure 6.18. In Figure 6.19 the corresponding PDs are shown.
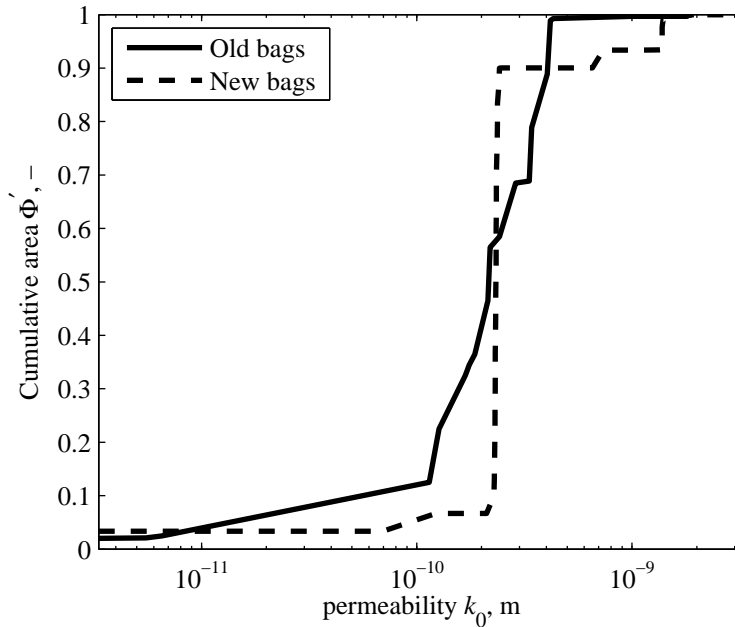
Figure 6.19: PDs determined from characteristic pressure drop cycles

At first the filter parameters affecting the model parameters p_c and t_c are ignored and a PD $\hat{\Phi}$ is estimated with $\hat{p}_c = 1$ and the fraction $\frac{\hat{p}_c}{t_c}$ equal to the estimated slope the final asymptote. This facilitates the data processing for the estimation, since varying operating points of the filter can be disregarded. In addition, the permeability is scaled by a factor of about 10^7, which enhances

the numerical performance. (Results displayed in Figure 6.19 do not include this factor and thus Φ' is plotted versus k_0.)

The characteristic pressure drop profiles are typically very well defined with a large number of underlying pressure drop measurements. Because of this averaging over a large number of cycles also statistical variations from measurement errors are largely compensated for. In other words, the characteristic pressure drop curves present a very nuanced pressure drop profile, that is hardly obtainable from a single pressure drop increase. During the estimation of PDs via optimization it turned out that an even better fit could be obtained when more than 30 nodes are used for the discretization of the PD. Therefore the PDs in Figure 6.19 are estimated using a simple adaptive mesh routine. Initially, a PD is estimated on a fixed discretization using 30 nodes as in section 4.1.1. This optimization step is terminated, when no significant further improvement of the resulting PD is possible. The gradient of this intermediate result is calculated and the node at where the gradient is a maximum is replaced by 5 evenly distributed, new nodes, which get the same permeability value assigned as the original node. Thereby the calculated pressure drop curve remains unaltered from the original result. Then another run of the same optimization routine is conducted with the refined PD. This run starts at the same target value where the first run ended, but because of the finer discretization, further tuning of the PD is possible and typically a better fit is obtained. Here, 10 successive optimization runs with refining steps in between are carried out.

The thereby obtained PDs are transformed according to the relations outlined in section 4.2 to actual parameters p_c and t_c by considering the constant slope of the asymptote:

$$\frac{p_c}{t_c} = \frac{\hat{p}_c}{\hat{t}_c} \tag{6.18}$$

From equ. (4.11) it can be seen that condition equ. (6.18) leaves the distribution axis unaltered and only a scaling on the permeability axes occurs.

The PDs in Figure 6.19 characterizes the filter in semi-continuous operation. Thus the combined effects of the filter cloth and the sequenced cleaning are included in the PDs. Since the PDs are determined for a characteristic filter cycle, the initial permeability k_0 represents the filter condition after cleaning at the start of the filtration cycle. The clear step at $\Phi' \approx 0.9$ for the new filter cloth (dashed line) is caused by the newly cleaned filter fraction. The filter fraction carrying residual cake is hardly discernible on the rest of the filter area. The old filter cloth shows a continuously decreasing permeability distribution with a much less dominant step at high permeabilities. The old cloth even exhibits a higher permeability than the new one for a fairly large area fraction. This can be explained by the higher cleaning frequency which is in effect for the old cloth. The cycle time for the old cloth is about half the cycle time for the new cloth (see Figure 6.18). In order to keep the old filter cloth operating below the maximum pressure drop level, where cleaning is initiated, it is cleaned more often. Thereby a continuous filter cake distribution evolves, which is reflected by the continuous decrease in permeability in Figure 6.19. On the new cloth, however, cleaning of

only one segment suffices to reduce the pressure drop further than for the old cloth. The high permeability on this cleaned segment of new cloth reduces the pressure drop to a significantly lower $\Delta p_{\min}$ value for the new cloth, than for the old one (Figure 6.18). The remaining, i.e., not recently cleaned, filter area carries a substantial amount of filter cake, since the longer cycle times between cleaning steps entail a higher cake mass. Thereby the PD for the remaining filter area is not pronounced.

Due to the setup of the filter with 8 sections which are cleaned separately, one expects a distribution of cake generations as outlined in section 6.2.2. However, it is not possible to resolve the expected filter cake distribution from pressure drop data. If such a filter cake distribution exists, it does not significantly contribute to the shape of the pressure drop profile and therefore cannot be identified by the PD-method.

Figure 6.19 shows a clear distinction between the two PDs. Similarly to the results shown in Figure 6.6 the newer filter media is found to have a more pronounced step in the PD. The older filter bags exhibit a relatively high permeability only on a very small part of the filter area ($< 2\,\%$). However, extreme caution must be applied when quantitatively comparing these curves, since in the characteristic cycles the influence of the industrial cleaning of separate filter segments, as described above, is lumped into the PD.

Chapter 7

Solid distribution

7.1 Introduction

Filter operation is affected by inhomogeneities with respect to the filter medium and/or the filter cake, which is discussed in the preceding chapters. At the beginning of filtration inhomogeneities that can be attributed to the filter medium and/or a residual filter cake, can be tackled with the PD-method. The model on which the PD-method is based on, however, assumes a clear mechanistical cake build up with an even solid loading, i.e., the dust concentration in the fluid is a non-distributed constant and irrespective of time. Nevertheless, an uneven solid distribution might arise due to an uneven dust concentration in the filter housing. In this chapter a modified version of the filter model is presented that can account for an uneven distribution of the solid in the fluid.

7.2 Solid distribution model

The filter models basic equs. (2.1) to (2.4) are used unaltered. To account for the uneven solid distribution the mechanistical cake build up equ. (2.5) is modified to:

$$\frac{\mathrm{d}z(t, A)}{\mathrm{d}t} = c_{\mathrm{sol}}(t, A)\, v(t, A) \tag{7.1}$$

The only formal difference between the original equation is the allowance for a varying solid concentration on both time t and filter location A. A combination of equs. (2.2) and (7.1) gives:

$$\frac{\mathrm{d}\left(\frac{1}{k_c(t, A)}\right)}{\mathrm{d}t} = \alpha_{\mathrm{m}}\, c_{\mathrm{sol}}(t, A)\, v(t, A) \tag{7.2}$$

The time dependency is introduced to satisfy solid mass flow continuity. As a model assumption the solid mass flow and the total volume flow to the filter

should remain constant. In the case of a constant solid concentration the gas volume flow continuity automatically satisfies the solid continuity. However, the distribution of the solid concentration over the filter leads to an accordingly changing filtration velocity, and do thereby not satisfy the solid continuity per se. The solid concentration is therefore be split into a separable term:

$$c_{\text{sol}}(t, A) = \bar{c}_{\text{sol}} \, \zeta(A) \, \xi(t) \tag{7.3}$$

Here the term $\zeta(A)$ is the actual solid distribution over the filter location and $\xi(t)$ is the correction factor that must be determined to ensue a constant solid flow onto the filter.

The combination of equs. (7.2), (2.4), and (7.3) yields analogous to equ. (2.10):

$$-\frac{\mathrm{d}k(t, A)}{k^3(t, A)} = \frac{\alpha_{\text{m}} \, \bar{c}_{\text{sol}}}{\eta_{\text{g}}} \zeta(A)\xi(t)\Delta p(t)\mathrm{d}t \tag{7.4}$$

The integration of the separated equ. (7.4) gives:

$$k^{-2}(t, A) - k_0^{-2}(A) = \frac{2\,\alpha_{\text{m}}\,\bar{c}_{\text{sol}}}{\eta_{\text{g}}}\zeta(A)\int\limits_0^t \xi(t)\Delta p(t)\mathrm{d}t \tag{7.5}$$

The slightly adjusted abbreviation for filter state s is introduced again as:

$$s = \frac{2\,\alpha_{\text{m}}\,\bar{c}_{\text{sol}}}{\eta_{\text{g}}} \int\limits_0^t \xi(t)\Delta p(t)\mathrm{d}t \tag{7.6}$$

Integration of equ. (2.4) over the filter area employing equs. (7.5) and (7.6) gives corresponding to equ. (2.15):

$$\frac{\eta_{\text{g}} \cdot \dot{V}(t)}{\Delta p(t)} = \int\limits_{A=0}^{A_{\text{tot}}} (k_0^{-2}(A) + s(t)\zeta(A))^{-\frac{1}{2}}\mathrm{d}A \tag{7.7}$$

In the following the cloth resistance k_0, and according to definition (2.16) the corresponding u, are regarded as constant. A combined dependency of the filter area of both, the solid concentration and the cloth resistance leads to a 2-dimensional distribution.

The dimensionless filter area A can again be replaced by a normalized distribution function:

$$\Psi(\zeta) \equiv \frac{A}{A_{\text{tot}}} \tag{7.8}$$

and the integral transform equ. (7.9) can be rewritten in the same fashion as equ. (2.19):

$$\frac{\eta_{\text{g}} \cdot \dot{V}}{A_{\text{tot}}\Delta p} = \int\limits_0^\infty (u + s\,\zeta)^{-\frac{1}{2}}\mathrm{d}\Psi(\zeta) \tag{7.9}$$

The solid distribution model is only used for constant flow filtration and thus the governing equations for constant pressure are not outlined here. For constant flow filtration the abbreviations p_c and t_c, defined in sec. 2.4 by equs. (2.22) and (2.23), respectively, are used. The pressure drop transformation reads to:

$$\frac{p_c}{\Delta p} = \int\limits_0^\infty (u + s\,\zeta)^{-\frac{1}{2}} d\Psi(\zeta) \tag{7.10}$$

The closing condition originates from the analogous calculations explained in section 2.4 and it has the corresponding form:

$$t = t_c \int\limits_0^\infty \left[(u + s\,\zeta)^{\frac{1}{2}} - u^{\frac{1}{2}} \right] d\Psi(\zeta) \tag{7.11}$$

Note that the closing condition does not explicitly depend on the time variant correction factor ξ introduced in equ. (7.3). However, this correction factor can be calculated from the definition of s equ. (7.6) in comparison with equ. (7.11) via derivation:

$$\xi = \frac{\int\limits_0^\infty (u + s\,\zeta)^{-\frac{1}{2}} d\Psi(\zeta)}{\int\limits_0^\infty (u + s\,\zeta)^{-\frac{1}{2}} \zeta\, d\Psi(\zeta)} \tag{7.12}$$

7.3 Properties of the solid distribution model

Characteristic values of a solid concentration distribution can be determined, which correspond to the explanations in sec. 3.2. The initial pressure drop value without filter cake Δp_0 is obtained by:

$$\Delta p_0 = \frac{p_c}{k_0} = p_c \sqrt{u} \tag{7.13}$$

The slope of the pressure drop curve for the modified model can be calulated according to equ. (3.6). This differential can be evaluated using the expressions for the solid distribution model equs. (7.10) and (7.11):

$$\frac{d\Delta p}{dt} = \frac{p_c}{t_c} \frac{\int\limits_0^\infty (u + s\zeta)^{-\frac{3}{2}} \zeta\, d\Psi(\zeta)}{\left[\int\limits_0^\infty (u + s\zeta)^{-\frac{1}{2}} d\Psi(\zeta) \right]^2 \int\limits_0^\infty (u + s\zeta)^{-\frac{1}{2}} \zeta\, d\Psi(\zeta)} \tag{7.14}$$

For $s = 0$ the evaluation of equ. (7.14) yields $\frac{p_c}{t_c}$, i.e., the starting tangent of a homogeneous filter.

The asymptote of the pressure drop curve can be obtained similarly to section 3.2.3. However, in the present case neither the slope nor the ordinate offset

of the asymptote are known. The slope is obtained by evaluating equ. (7.14) for $t \to \infty$, i.e., $s \to \infty$:

$$\lim_{s \to \infty} \frac{d\Delta p}{dt} = \frac{p_c}{t_c} \frac{1}{\int\limits_0^\infty \zeta^{-\frac{1}{2}} d\Psi(\zeta) \int\limits_0^\infty \zeta^{\frac{1}{2}} d\Psi(\zeta)} \tag{7.15}$$

The factor describing the deviation from the homogenous filter only depends on moments of the solid distribution Ψ and is abbreviated as:

$$\gamma \equiv \frac{1}{\int\limits_0^\infty \zeta^{-\frac{1}{2}} d\Psi(\zeta) \int\limits_0^\infty \zeta^{\frac{1}{2}} d\Psi(\zeta)} \tag{7.16}$$

With this asymptotic slope the ordinate offset is calculated according to:

$$\Delta \tilde{p}_0 = \lim_{t \to \infty} \left(\Delta p - \frac{p_c}{t_c} \gamma \cdot t \right) \tag{7.17}$$

Surprisingly the evaluation of equ. (7.17), which is analogue to the computation in section 3.2.3, shows that $\Delta \tilde{p}_0$ is related to the initial pressure drop value Δp_0 via the same factor γ, applying to the slope:

$$\Delta \tilde{p}_0 = \gamma \, \Delta p_0 \tag{7.18}$$

and thus the analytical equation of the asymptote reads:

$$\Delta p = \gamma \left(\frac{p_c}{t_c} t + \frac{p_c}{k_0} \right) \tag{7.19}$$

The initial tangent of the pressure drop curve for a solid distribution on the filter coincides with the linear pressure drop increase on a homogeneously challenged filter. The final asymptote is derived from that initial tangent by a single scaling factor γ, which in turn is depending only on moments of the solid distribution.

7.4 Results of a two area model

To illustrate the effect of a solid distribution a two area model is used. The model is easy to be implemented and can be regarded as an extreme case of a distribution. Moreover experimental pressure drop data under a proven solid distribution is lacking, and thus one can only resort to analytic models for the discussion.

A two area model can be very simply obtained with the following density function $\psi = d\Psi/d\zeta$ consisting of two Dirac Delta functions:

$$\psi(\zeta) = \beta\delta(\zeta - 1) + (1 - \beta)\delta(\zeta - \alpha) \tag{7.20}$$

Here δ denotes the Dirac Delta function, β the area ratio ($\beta = 0.5$ means equally large areas), and α is the solid excess in comparison to 1. I.e. on the area fraction $(1 - \beta)$ of the filter the solid concentration is α times the concentration on the area fraction β. For the parameters the range is for the area distribution naturally $\beta \in [0, 1]$ and for the solid distribution parameter it may be confined to $\alpha \in [0, 1]$ without loss of generality. This is explained by the definition of the solid distribution in equ. (7.3), where a correction factor ξ is foreseen to keep the solid mass flow constant at a time. When one requires an $\tilde{\alpha}$-value being larger than one, then an equivalent model exists with parameters $\alpha = \tilde{\alpha}^{-1}$ and also an inverted area distribution $\beta = 1 - \tilde{\beta}$. However, the correction factor ξ will be different to ensure the same mass flow, and thus the s values will differ as well. This two area function represents an extreme case of inhomogeneity for all functions $\psi(\zeta)$ that are zero for $\zeta \notin [\alpha, 1]$.

The pressure drop curve can be given parametrically dependent on s. A closed form expression $\Delta p(t)$ is not obtained as straight forwardly.

$$\Delta p(s) = \frac{p_\text{c}}{\frac{\beta}{\sqrt{u+s}} + \frac{1-\beta}{\sqrt{u+s\alpha}}} \tag{7.21}$$

$$t(s) = t_\text{c} \left[\beta\sqrt{u+s} + (1-\beta)\sqrt{u+s\alpha} - \sqrt{u} \right] \tag{7.22}$$

The asymptotical factor γ can also be given analytically:

$$\gamma = \frac{1}{\left(\beta + (1-\beta)\frac{1}{\sqrt{\alpha}} \right) \left(\beta + (1-\beta)\sqrt{\alpha} \right)} \tag{7.23}$$

For the asymptotical factor it can be shown that for a constant α equ. (7.23) becomes a minimum for $\beta = \frac{1}{2}$, i.e., the extreme case in terms of inhomogeneity for a two area filter is the case of equally large areas. The location of the minimum is irrespective from α itself. For this extreme case the γ value depends only on α:

$$\gamma_\text{min} = \frac{4\sqrt{\alpha}}{(1 + \sqrt{\alpha})^2} \tag{7.24}$$

In Figure 7.1 the pressure drop increases for a two area model distribution with $\alpha = 0.2$ and $\beta = 0.5$ is shown. The asymptotical pressure drop increase is clearly diverging from the homogeneous filter. The inhomogeneous solid distribution leads to a relatively slower simulated pressure drop increase. Interestingly the pressure drop curve appears to be linear, although the solid distribution is highly inhomogeneous.

The initial phase of filtration is of special interest and in Figure 7.2 this part is enlarged. One can see that the simulated pressure drop increase has the same initial level as the perfectly homogeneous curve. Additionally the initial tangent also coincides with the homogeneous filter. However, immediately after the start of filtration the homogeneous filter continues its linear pressure drop increase, whereas the simulated inhomogeneous filter exhibits a lower slope of the
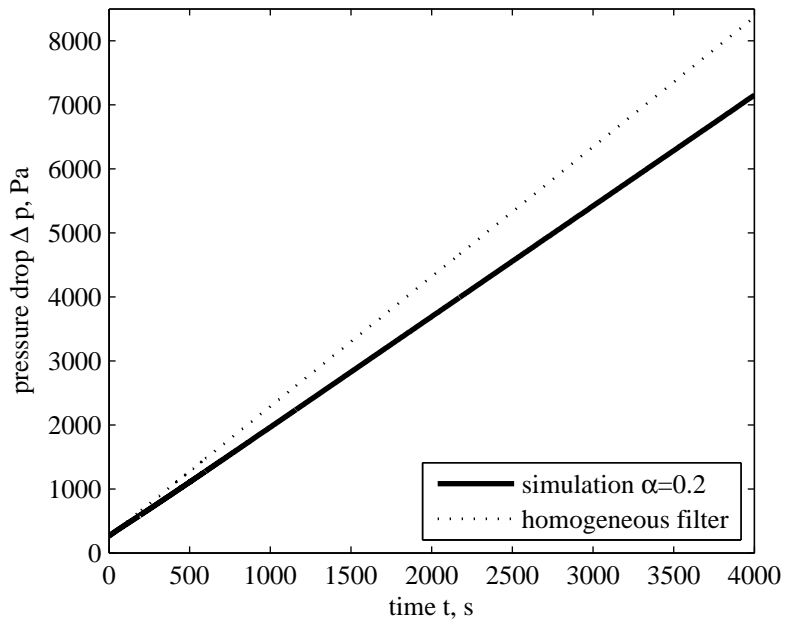
Figure 7.1: Simulated pressure drop curve of the two area solid concentration distribution model. In addition the pressure drop increase of a perfectly homogeneous filter is shown.

pressure drop curve and starts to approach its asymptote from above. Thereby the simulated pressure drop curve is changing its curvature from negative to positive. Most remarkable, however, are the slight differences between the sim-
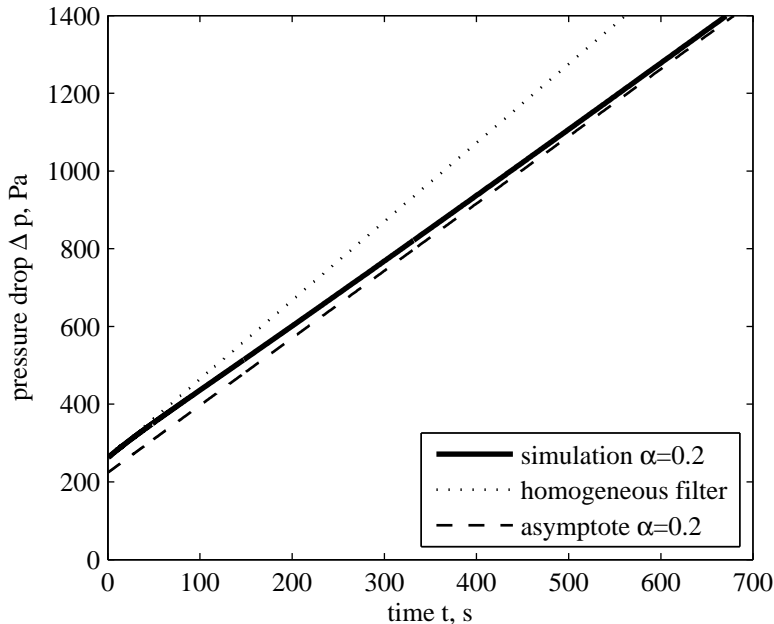

Figure 7.2: Magnification of Figure 7.1. In addition the asymptote of the simulated pressure drop curve is shown.

ulated pressure drop curve and the homogeneous one. The only discrimination from experimental data that could possibly be found is the difference of the asymptotical slope. However, the specific cake resistance value is frequently determined from exactly this slope, and thus a possible distribution of the solid cannot be detected unless independent measurements of the solid distribution were available. A determination from the curvature of the pressure drop curve seems impossible because of the only slight variations, which could not easily be resolved in experiments. But the simulated inhomogeneous distribution is very significant, given that half of the filter area receives a 5-fold dust loading. Slighter variations would be even more difficult to resolve from pressure drop data. In Figure 7.3 the minimal γ-value is displayed to illustrate this aspect. One can see, that a 10% change of the asymptote's slope requires an $\alpha \approx 0.25 - 0.3$. Such strong inhomogeneous distributions are hardly to be expected in real filters.
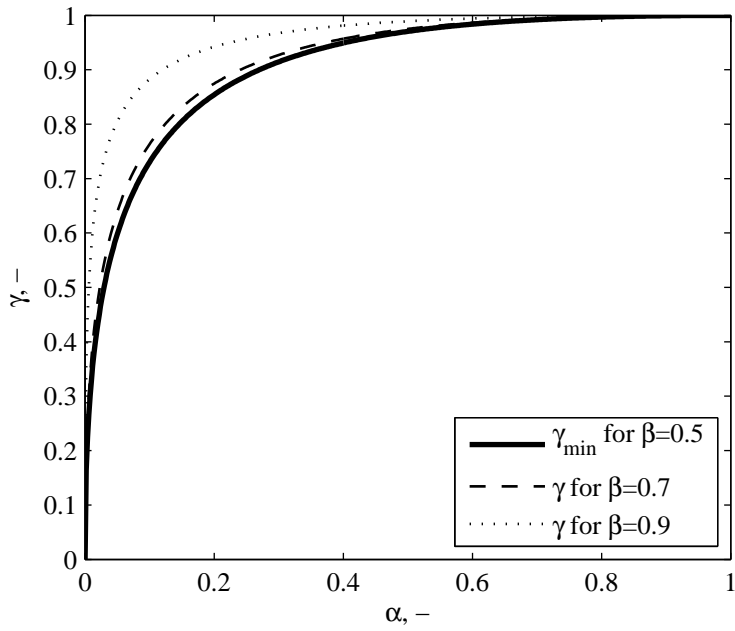
Figure 7.3: γ-values as a function of the solid distribution coefficient α for certain parameters β including $\gamma_{\min}$ for $\beta = 0.5$.

Chapter 8

Conclusions and outlook

In this work an analytical filter model is developed based upon governing equations commonly used for filter modeling. The focus of this model lies in the simulation of cake filtration on inhomogeneous filters with respect to the filter medium and cake distribution for incompressible cakes. It is shown that this filter model fully includes previous model concepts targeting towards the description of industrial filter operation. Because of its analyticity it is possible to make clear statements on invertibility of the model, which is used to develop and justify the PD-method. This method can be used to determine the PD of a filter from commonly available pressure drop data. An error estimation is outlined for the PD-method.

8.1   Filter media characterization

The PD-method is applied to filter media characterization. PD of filter media are determined from various filter equipments. It is shown that even apparently clean filter media can exhibit a PD, which has not been explicitly reported in the literature. Depending on the PD the filtration behavior of the filter medium is assessed in the industrial filter application. With the same integral filter media permeability and the same dust cake properties a filter medium exhibiting a less pronounced PD is performing superior over a filter medium with a strong PD in terms of operating pressure drop level and/or cycle time.

The PD-method can be easily applied to filter media testing experiments. The effects affecting the filtration dynamics of a filter media sample are captured more completely by a PD, than by today's reporting standards. The expected filtration performance of a certain cloth is closely related to these dynamics.

The analytic filter model is a prerequisite to determine a PD of filter media. Since for optimization routines frequent function calls are required, it would not have been practically possible to determine a PD when the model is carried out as numerical integration, since the long execution times of the numerical integration impede the pratical application.

It is shown that for a certain pressure drop curve variations of the model parameters lead only to a scaling of the PD. All the scaled PDs contain basically the same information. Thus parameter variations or error in parameters do not affect the PD-method's determination of a PD, making the PD-method rather robust against uncertain parameters. In fact this makes the applicability of the PD-method widely independent from the actual availability of parameters, when absolute values are not mandatorily required. This feature opens up possibilities for intercomparison of PDs in applications with intrinsically high uncertainties in parameters as encountered in most practical applications. However, certain parameter variations can lead to unphysical PDs. In turn errors in parameters might not be detected by the PD-method.

Characteristics of a pressure drop increase describing the initial tangent and final asymptote are identified and analytically derived from moments of a PD. They are readily available from a full PD. These characteristics or moments of a PD are a compact and easily comparable form of reporting the key dynamics conveyed by a full PD.

The pressure drop of a filter in operation is increased by a PD. While a homogeneous filter would give a linear pressure drop increase, which can be predicted using classical theory, a filter exhibiting a PD is operating along a curved pressure drop profile. For long filtration durations the actual filter pressure drop is approximated well by the final asymptote. In addition this is the prediction of filter operation with more caution, since the asymptote always give higher pressure drop values, than the actual pressure drop. For filter design it is advantageous to use the final asymptote rather than the ideal homogeneous behavior from classical theory. Thereby one takes into account the increased pressure drop due to a PD, but at the same time one can resort oneself to the simplicity of a linear pressure drop increase. This is accomplished by using the asymptotic pressure drop ordinate offset, rather than the initial pressure drop. Otherwise the classical theory can remain unaltered.

The PD of one cloth-dust combination may change over time due to long-term filtration effects, i.e., so called filter ageing. Thus the filtration characteristics of such a combination can change significantly during the life time of the filter medium. This must also be expected during a life cycle of an industrial filter bag, although to date no long term filtration monitoring with the PD-method is available. In industrial plants filter bags are frequently not changed all together, but only a few bags at a time. Thus a possible change of filtration performance of some bags over time cannot be retraced individually by the PD-method during plant operation. An assembly of bags used parallel for filtration always appear as an entity to the PD-method and the PD of some bags cannot be isolated.

8.2   Industrial filter operation

It is shown that the filter model presented also includes the generation models used in literature. Except for the model of Ju et al.[18], where the part with

compressible cake is not captured by the proposed filter model, all models found in literature are fully represented by the proposed model.

The presented model can of course be used to simulate a filter dynamically, which is enhanced by the analytic time integration. Thus the need for numerically solving differential equations is omitted, and the simulations speed up by orders of magnitude. The strength of this model, which distinguishes it from the dynamic models, is the fact that for periodic filtration the PD from filter operation can be given analytically, without simulating the full transient pressure drop curves of the filter.

With the PD-method any PD should be identifiable unambiguously. However, error consideration shows that it is not possible to identify a PD for more than about two cake generations, not even considering segmented cleaning. The numerical problem becomes highly ill defined. This argumentation is equally valid for the parameter estimations for cake generation models reported in the literature. Since the basic model structure is the same for all models including the PD-methods, the inverse problem posed by parameter identification is equally ill defined for the models in literature. However, due to the parametric approach in literature the number of possible PDs is limited. Under the assumption that the chosen mechanistic model is valid, a parameter identification might be possible. However, agreement between the model and the actual data must not be interpreted as verification of the mechanistic approach. Other PDs that are not captured by the mechanistic models are probably equally or better suitable to describe experimental data. The problems of identifying filter operation worsen, when a PD of the filter medium itself is superimposed to the PD stemming from filter operation. Admittedly this problem is not tackled in the literature. The error estimation in this work suggests error bounds, that let a separable identification of superimposed PDs appear impossible. Even the direct problem of only identifying a PD is already difficult to handle.

8.3 Solid distribution

The filter model is adapted to cover the case of inhomogeneous solid distribution in the filter. Characteristic values of the pressure drop curve can be derived analogous to the PD-method. The analytically obtained pressure drop asymptote is related to the pressure drop for a homogeneous solid distribution by only one scaling factor.

Model simulations with this adapted model are carried out for a highly inhomogeneous solid distribution on two model areas. The pressure drop increase is not significantly distinguished from a linear increase, although its slope is significantly different from the homogeneous filter. The inhomogeneous solid distribution is barely reflected in the curvature of the pressure drop curve, even in this sample case where its quite significant. Consequently, the mere presence of a solid distribution on a filter can hardly be detected from pressure drop data even if solid distribution is pronounced.

However, the determination of filtration parameters is affected if a solid distribution is present. Typically the cake resistance parameter is extracted from the slope of the pressure drop asymptote. However, this slope is altered for filtration with a solid distribution present, although the underlying model parameters remain unaltered. This might also add to the difficulties of reproducing parameters, especially the cake resistance, in laboratory experiments. However, the fluctuation of the cake resistance parameter actually observed may often be larger than the change explainable by a moderate solid distribution.

A combination of a PD of the filter media and a solid concentration distribution is feasible. The corresponding model, however, becomes complex. Since the separate identification problems of a PD and a solid distribution are difficult, one will hardly be able to identify parameters from pressure drop data for the combined model. In addition a cross correlation of the PD and the solid distribution is possible, i.e., the two distributions might not be independent from each other. However, a combined and dependent PD and solid distribution may obscure the otherwise clear effects of the PD, which in turn is erroneously identified or rendered unidentifiable.

8.4   Further work and potential

Independent determination of a PD: Speaking of a PD determined from pressure drop data, of course the question arises of independently determining a corresponding distribution directly from an analysis of the filter medium. A possibility for accomplishing such an independent measurement is a highly resolved velocity profile measurement as schematically depicted in Figure 2.1. Assuming that the permeability of a filter medium is a result of viscous flow through pores of the medium an average pore diameter of about $40\,\mu$m is obtained for a typical commercial bag filter medium, assuming a negligible porosity effect accelerating the flow through the filter medium.

However, this pathway appears unfeasible, since CFD simulations clearly show that the maximum gas velocity of a single pore of this diameter is reduced to about only a third after only $300\,\mu$m after the pore. Since this is approximately the surface roughness of the textile filter medium, high resolution measurement so close to the surface are not possible. Especially the identification of small local differences in the gas velocities are not feasible.

Experimental methods considered were particle imaging velocimetry and Laser Doppler anemometry. Both methods require tracer-particles in the fluid and therefore only an upstream measurement could be performed. However, since the filter medium will retain the particles the flow will be altered in the course of the measurement.

Another possible approach is based on an integral measurement of the flow through the filter medium locally resolved. A possible way to accomplish such a measurement is via the reaction of a reactive layer on the filter medium with a gas. The filter medium must be coated with a thin layer of a reactive substance and then at a certain pressure drop gas containing a reactive compound is

conveyed through the filter medium. The reaction between the layer and the gas should preferentially be fast, so reaction kinetics need not to be accounted for. Then the conversion of the solid layer with the gas must be evaluated locally resolved by e.g. electron microscopy with diffractive scanning for the reaction product. The distribution of the reaction product corresponds to the flow distribution and thereby the PD.

A suitable pair of reactive compounds must be found. The combination potassium iodate and sulfur dioxide, as used in gas detection tubes, was considered. It must be possible to coat the filter medium with a thin layer of the solid reagent. This is typically a challenging task, because the small pore and fiber structure prevent the fibers from wetting.

Evaluation of filter medium tests: The evaluation routines of filter medium tests in standardized equipment (VDI-3926, [12]) include the monitoring of the filtration cycle duration, the weight increase of the filter sample, the development of the pressure drop after cleaning and the clean gas concentration. In addition, the guideline states that: *It is also possible to derive quality characteristics of the filter media from [...] the course of the pressure drop loss curves.* Certainly, trained filter test operators are able to deduct information from the shape of the pressure drop curves intuitively. The PD-method can quantitatively derive information from such curves, which is supposedly most relevant for industrial application of the filter (when compared to the hitherto practiced data evaluation routine). The generally poor predictability of a filter medium's performance in its industrial application must to some extent be attributed to the neglecting of any inhomogeneity of the filter media. Especially, the laboratory scale testing of filter media with the very dust used eventually in the industrial application is encouraged in combination with an evaluation incorporating the PD-method.

Continuous filter plant monitoring: In section 6.3 a routine is proposed that can be incorporated into filter process control systems. In addition to the commonly available information on pressure drop and occasionally cleaning frequency, a characteristic pressure drop profile can be used for monitoring the condition of the filter cloth, possibly together with an evaluation by the PD method. Gradual and/or discontinuous changes of the filter medium could be detected and measures, e.g. the replacement of filter bags, can be taken on a factual basis of the operation performance instead of just operational time or the impression of the plant operator.

Bibliography

[1] R. H. Perry, D. W. Green, and J. O. Maloney, editors. *Perry's chemical engineers handbook*. Mc-Graw-Hill, Singapore, 7 edition, 1997.

[2] C. Tien. *Introduction to cake filtration - Analyses, experiments and applications*. Elsevier, Amsterdam, 2006.

[3] H. Darcy. *Les fontaines publiques de la ville de Dijon. Exposition et affiliation des principes à suivre et des formules à employer dans les questions de distribution d'eau*. Dalmont, Paris, 1856.

[4] J. Bear. *Dynamics of fluids in porous media*. Environmental Science Series. American Elsevier Publishing Company, New York, 1972.

[5] F. Löffler, H. Dietrich, and W. Flatt. *Dust Collection with Bag Filters and Envelope Filters*. Fried. Vieweg & Sohn, Braunschweig, Germany, 1988.

[6] J. Kozeny. Über die kapillare Leitung des Wassers im Boden. *Sitz. Ber. Akad. Wiss. Wien. Math. Nat. (Abt. IIa)*, 136a:271–306, 1927.

[7] A. Dittler and G. Kasper. Simulation of operational behaviour of patchily regenerated, rigid gas cleaning filter media. *Chemical Engineering and Processing*, 38:321–327, 1999.

[8] J. Dufrêche, M. Prat, P. Schmitz, and J. D. Sherwood. On the apparent permeability of a porous layer backed by a perforated plate. *Chemical Engineering Science*, 57:2933–2944, 2002.

[9] E. Schmidt. Experimental investigations into the compression of dust cakes deposited on filter media. *Filtration and Separation*, pages 789–793, September 1995.

[10] E. Schmidt. Theoretical investigations into the compression of dust cakes deposited on filter media. *Filtration and Separation*, pages 365–368, May 1997.

[11] H. Leubner and U. Riebel. Einfluss der Oberflächenbeschaffenheit des Filtermediums auf den spezifischen Staubkuchenwiderstand. *Chemie Ingenieur Technik*, 73:1320–1323, 2001.

[12] VDI-3926: Testing of filter media for cleanable filters. VDI-guideline, Beuth Verlag GmbH, Berlin, December 1994.

[13] C.-C. Chen, W.-Y. Chen, S.-H. Huang, W.-Y. Lin, Y.-M. Kuo, and F.-T. Jeng. Experimental study on the loading characteristics of needlefelt filters with micrometer-sized monodisperse aerosols. *Aerosol Science and Technology*, 34:262–273, 2001.

[14] D. Koch, J. Seville, and R. Clift. Dust cake detachment from gas filters. *Powder Technology*, 86:21–29, 1996.

[15] W. Peukert and C. Wadenpohl. Industrial separation of fine particles with difficult dust properties. *Powder Technology*, 118:136–148, 2001.

[16] J. Seville, W. Cheung, and R. Clift. A patchy cleaning interpretation of dust cake release from non-woven fabrics. *Filtration & Separation*, 26:187–190, 1989.

[17] W. Duo, N. Kirkby, J. Seville, and R. Clift. Patchy cleaning of rigid gas filters – I. A probabilistic model. *Chemical Engineering Science*, 52(1):141–151, 1997.

[18] J. Ju, M. S. Chiu, and C. Tien. A model for pulse jet fabric filters. *J. Air Waste Management Association*, 50:600–612, 2000.

[19] A. Kavouras. *The filter cake of jet pulsed filters as a fixed bed reactor for SO_2 and HCl scrubbing.* Ph.D. thesis, Graz University of Technology, 2002.

[20] A. Kavouras and G. Krammer. Deriving cake detachment versus cake area load in a jet pulsed filter by a mechanistic model. *Powder Technology*, 133:134–146, 2003.

[21] I. I. Hirschman and D. V. Widder. *The convolution transform.* Princeton University Press, Princeton, New Jersey, 1955.

[22] R. A. Horn and C. R. Johnson. *Matrix analysis.* Cambridge University Press, New York, 1985.

[23] W. H. Press. *Numerical recipes in C : the art of scientific computing.* Cambridge University Press. John Wiley & Sons, Cambridge, 2nd edition, 1987.

[24] A. F. Jones and D. L. Misell. The problem of error in deconvolution. *J. Phys. A: Gen. Phys.*, 3:462–472, 1970.

[25] M. Koch, M. Saleem, P. Pucher, and G. Krammer. Conditioning of filter bags with reactive CaO and $CaOH_2$ dust in flue gas. In *Proceedings of the International Conference & Exhibition for Filtration and Separation Technology, FILTECH*, pages II–42–II–49. Wiesbaden, Germany, 27 February - 1 March 2007.

[26] M. Saleem. *Experimental study of gas cleaning with jet-pulsed bag filter.* Ph.D. thesis, Graz University of Technology, 2007.

[27] M. Koch and G. Krammer. Feedback of a semi-continuous bag filter unit in a continuous process operation. In *Proceedings of the 7th World Congress of Chemical Engineering.* Glasgow, July 11-14, 2005.

[28] C. V. Rasmussen, M. Koch, and G. Krammer. Large scale bag filtration enhanced by electrostatics. In *Proceedings of the 10th Nordic Filtration Symposium.* Trondheim, Norway, 4-5 September 2006.

[29] E. Schmidt. Simulation of three-dimensional dust structures via particle trajectory calculations for cake-forming filtration. *Powder Technology*, 86(1):113–117, 1996.

[30] W. Humphries and J. Madden. Fabric filtration for coal-fired boilers: Dust dislodgement in pulse jeg filters. *Filtration & Separation*, (January/February):40–44, 1983.

[31] A. Dittler, M. F. Ferer, P. Mathur, P. Djuranovix, G. Kasper, and D. H. Smith. Patchy cleaning of rigid gas filters – transient regeneration phenomena comparison of modelling to experiment. *Powder Technology*, 124:55–66, 2002.

[32] A. Kavouras and G. Krammer. Distribution of age, thickness and gas velocity in the cake of jet pulsed filters: application and validation of a generations filter model. *Chemical Engineering Science*, 58:223–238, 2002.

[33] M. DeRavin, W. Humphries, and R. Postle. A model for the performance of a pulse jet filter. *Filtration and Separation*, pages 201–207, May/June 1988.

[34] H. Kestelman. *Modern theories of integration.* Dover Publications, New York, 2 edition, 1960.

Appendix A

Mathematical handling of PDs

A.1 Conversion between PDs depending on k and u

For an application of the convolution notation it is helpful to write the distribution as a function of u in the s-domain instead of the plain permeability k in the k-*domain*. However, interpretation might usefully be done using the permeability k itself. The distributions with k as the variable is denoted by a prime, e.g. $\varphi'(k)$ is the PD density depending on the permeability k.

For the cumulative distribution the conversion is trivial since the type of the distributed property (filter area) is not changed. Since the assignment equ. (2.16) $u \equiv k^{-2}$ is changing the ordering of the independent variable, i.e., when k is ordered ascending, u is descending and vice versa, the cumulative distribution functions are complementary to each other:

$$\Phi'(k) = 1 - \Phi(u) = 1 - \Phi(k^{-2}) \tag{A.1}$$

For the distribution density the conversion is obtained from equ. (A.1) by differentiation.

$$\begin{aligned}
\frac{\mathrm{d}\Phi'(k)}{\mathrm{d}k} &= \frac{\mathrm{d}\left(1 - \Phi(u)\right)}{\mathrm{d}k} \\
\varphi'(k) &= -\frac{\mathrm{d}\Phi(u)}{\mathrm{d}u} \cdot \frac{\mathrm{d}u}{\mathrm{d}k} \\
\varphi'(k) &= -\varphi(u) \cdot (-2)k^{-3} \\
\varphi'(k) &= 2k^{-3}\varphi(u) \\
\varphi'(k) &= 2k^{-3}\varphi(k^{-2})
\end{aligned} \tag{A.2}$$

A.2   Moments of a PD

Moments of the PD are defined directly only for the distribution depending on the permeability $\Phi'(k)$.

$$\mu_r = \int\limits_0^\infty k^r \mathrm{d}\Phi'(k) \tag{A.3}$$

By expressing the cumulative distribution $\Phi'(k)$ by $\Phi(u)$ according to equ. (A.1) and replacing k by u as defined in equ. (2.16) one obtains equ. (3.3) already introduced in chapter 3:

$$\mu_r \equiv \int\limits_0^\infty u^{-\frac{r}{2}} \mathrm{d}\Phi(u) \tag{3.3}$$

because of:

$$\int\limits_{k=0}^\infty k^r \mathrm{d}\Phi'(k) = \int\limits_{k=0}^\infty \left(u^{-\frac{1}{2}}\right)^r \mathrm{d}\left(1 - \Phi(k^{-2})\right) = \int\limits_{u=\infty}^0 u^{-\frac{r}{2}}(-1)\mathrm{d}\Phi(u) = \int\limits_{u=0}^\infty u^{-\frac{r}{2}} \mathrm{d}\Phi(u)$$

A.3   Riemann-Stieljes integral

In chapter 2 the PD is introduced with the cumulative distribution function $\Phi(u)$. This function is used in integtals similar to equ. (2.19) as a so called Riemann-Stieljes integral of the general form in this work:

$$\int\limits_0^\infty g(u)\mathrm{d}\Phi(u) \tag{A.4}$$

This type of integral type is easily converted to a Riemann integral. The derivation of the cumulative PD gives the density function of the PD:

$$\varphi(u) = \frac{\mathrm{d}\Phi(u)}{\mathrm{d}u} \tag{A.5}$$

With this additional definiton equ. (A.4) can be converted to a Riemann integral:

$$\int\limits_0^\infty g(u)\varphi(u)\mathrm{d}u \tag{A.6}$$

The latter integral exists given certain conditions listed by Kestelman [34, chapter XI] are fulfilled. Most importantly $g(u)$ must be continuous (which is fulfilled for all integral kernels used in this work) and $\varphi(u)$ must be integrable in the Riemann sense over the full range (cf. [34, theorem 322]).

Formally the required Riemann integrability of $\varphi(u)$ function is not satisfied when Dirac-Delta functions are used and a rigorous treatment hereto would

call for a more advanced mathematical theory. However, practically the use
of peaked $\varphi(u)$ functions is unproblematic and this formal inconsistence may
be forgiven as it. Dirac-Delta functions may be approximated by very narrow
continuous functions and thereby turn into integrable functions.